A review on functional nanoarchitectonics nanocomposites based on octahedral metal atom clusters (Nb-6, Mo-6, Ta-6, W-6, Re-6): inorganic 0D and 2D powders and films

Ngan T.K. Nguyen, Clément Lebastard, Maxence Wilmet, Noée Dumait, Adèle Renaud, Stéphane Cordier, Naoki Ohashi, Tetsuo Uchikoshi, Fabien Grasset

Taylor & Francis
Taylor & Francis Group

Science and Technology of Advanced Materials

ISSN: (Print) (Online) Journal homepage: https://www.tandfonline.com/loi/tsta20

A review on functional nanoarchitectonics nanocomposites based on octahedral metal atom clusters (Nb_6, Mo_6, Ta_6, W_6, Re_6): inorganic 0D and 2D powders and films

Ngan T. K. Nguyen, Clément Lebastard, Maxence Wilmet, Noée Dumait, Adèle Renaud, Stéphane Cordier, Naoki Ohashi, Tetsuo Uchikoshi & Fabien Grasset

To cite this article: Ngan T. K. Nguyen, Clément Lebastard, Maxence Wilmet, Noée Dumait, Adèle Renaud, Stéphane Cordier, Naoki Ohashi, Tetsuo Uchikoshi & Fabien Grasset (2022): A review on functional nanoarchitectonics nanocomposites based on octahedral metal atom clusters (Nb_6, Mo_6, Ta_6, W_6, Re_6): inorganic 0D and 2D powders and films, Science and Technology of Advanced Materials, DOI: 10.1080/14686996.2022.2119101

To link to this article: https://doi.org/10.1080/14686996.2022.2119101

Accepted author version posted online: 01 Sep 2022.

Publisher: Taylor & Francis & The Author(s). Published by National Institute for Materials Science in partnership with Taylor & Francis Group.

Journal: *Science and Technology of Advanced Materials*

DOI: 10.1080/14686996.2022.2119101

A review on functional nanoarchitectonics nanocomposites based on octahedral metal atom clusters (Nb_6, Mo_6, Ta_6, W_6, Re_6): inorganic 0D and 2D powders and films.

Ngan T. K. Nguyen[1,2]*, Clément Lebastard[1,3]*, Maxence Wilmet[1,3,4], Noée Dumait[3], Adèle Renaud[3], Stéphane Cordier[3], Naoki Ohashi[1,5], Tetsuo Uchikoshi[1,5], Fabien Grasset[1,3]*

[1]CNRS-Saint Gobain-NIMS, IRL3629, Laboratory for Innovative Key Materials and Structures (LINK), National Institute for Materials Science (NIMS), 1-1 Namiki. 305-0044 Tsukuba, Japan
[2]International Center for Young Scientists, ICYS-Sengen, Global Networking Division, NIMS, Tsukuba, Japan.
[3]Univ Rennes, CNRS, ISCR, UMR6226, F-35000 Rennes, France
[4]Saint Gobain Research Paris, F-93300 Aubervilliers, France
[5]Research Center for Functional Materials, NIMS, 305-0047 Tsukuba, Japan
*Corresponding authors: E-mail: nguyen.thikimngan@nims.go.jp; lebastard.clementhugo@nims.go.jp; fabien.grasset@univ-rennes1.fr

Abstract:
This review is dedicated to various functional nanoarchitectonic nanocomposites based on molecular octahedral metal atom clusters (Nb_6, Mo_6, Ta_6, W_6, Re_6). Powder and film nanocomposites with two-dimensional, one-dimensional and zero dimensional morphologies are presented, as well as film matrixes from organic polymers to inorganic layered oxides. The high potential and synergetic effects of these nanocomposites for biotechnology applications, photovoltaic, solar control, catalytic, photonic and sensor applications is demonstrated. This review also provides a basic level of understanding how nanocomposites are characterized and processed using different technics and methods. The main objective of this review would be to provide guiding significance for the design of new high-performance nanocomposites based on transition metal atom clusters.

Keywords: Nanoarchitectonics, nanocomposites, octahedral metal atom clusters, coatings, thin films, EPD, NIR Blocker, solar technology, catalysis

1. Introduction

Today, the term “nanocomposite”, proposed by Blumstein in 1961, [1] describes generally a bi(or multi)phasic material where one of the phases, at least, presents a nanometric size. The definition and the choice of materials are very broad including metallic, ceramic or polymer compounds. [2-4] Indeed, the high flexibility of the composition and the complexity of the structure have allowed various kinds of nanocomposites to be developed, zero-dimensional (0D) (e.g., nanoparticles), one-dimensional (1D) (e.g., nanowires), two-dimensional (2D) (e.g., multilayered based film and coating composites), three-dimensional (3D) (e.g., mesoporous based composites) and the even more complex hierarchical 3D nanostructured networks. [5] In this review, this term will refer only to functional composite nanoarchitectures which represent a class of nanostructured entities that integrate dissimilar nanoscale inorganic octahedral metal cluster units in the frame of the nanoarchitectonics concept. [6-11] As one of the nanocomponents of the nanocomposites, the nanometer-sized metal atom clusters (MC) also called “nanoclusters or superatoms” (size < 2 nm), [12] which consist of less than a few dozens of metal atoms, were used to synthesize functional nanocomposites during the last decades. Indeed, metal nanoclusters are promising candidates for novel materials due to their size-specific properties arising from unique atomic packing and electronic structures. Most of the papers are dedicated to silver, platinum and gold nanoclusters for catalysis, optics, sensors or biotechnology. [13-28] In parallel to this commonly studied family of nanoclusters, nanocomposites based on molecular octahedral metal atom clusters (Nb_6, Mo_6, Ta_6, W_6, Re_6) units were developed more recently. [See reviews 29-36] Although less popular than noble metal nanoclusters or superatoms, these octahedral transition metal atom clusters, with general formulas $\{M_6L^i_8L^a_6\}^{n-/+}$ or $\{M_6L^i_{12}L^a_6\}^{n-/+}$, are well known for one century and are a part of the large family of the transition metal atom clusters compounds defined by Cotton. [37] The $[\{M_6L^i_8\}L^a_6]^{n-/+}$ nanosized cluster units are generally built up from an octahedral M_6 clusters with Mo, W or Re metals, whereas the $[\{M_6L^i_{12}\}L^a_6]^{n-/+}$ are based mainly on Nb or Ta metals. [38-41] These $[\{M_6L^i_8\}L^a_6]^{n-/+}$ and $[\{M_6L^i_{12}\}L^a_6]^{n-/+}$ cluster units are bonded to eight inner face-capping ligands or twelve face-capping ligands (L^i, i = inner, L = Cl, Br, I,

S, or Se) respectively, and both of them have six apical ligands (L^a, a = apical, L = F, Cl, Br, I, OH, CN, organic molecules...) located in terminal positions. These species can be isolated (at molecular level) or condensed by either ligands or metals in the solid-state compounds. [39-41] Depending on the degree of condensation and dimensionality of the metal atom clusters, these compounds present fascinating crystal structures and electronic properties as for instance superconductivity [42], thermoelectricity [43], intercalation/de-intercalation [44] or Mott insulating behaviors [45]. This review will focus only on molecular cluster compounds, in which cluster units are fully isolated in the crystal structures. For illustration, the molecular $[\{M_6L^i_8\}L^a_6]^{n-/+}$ (M = Mo, W, Re) and $[\{M_6L^i_{12}\}L^a_6]^{n-/+}$ (M = Nb, Ta) cluster units are represented in **Figure 1**.

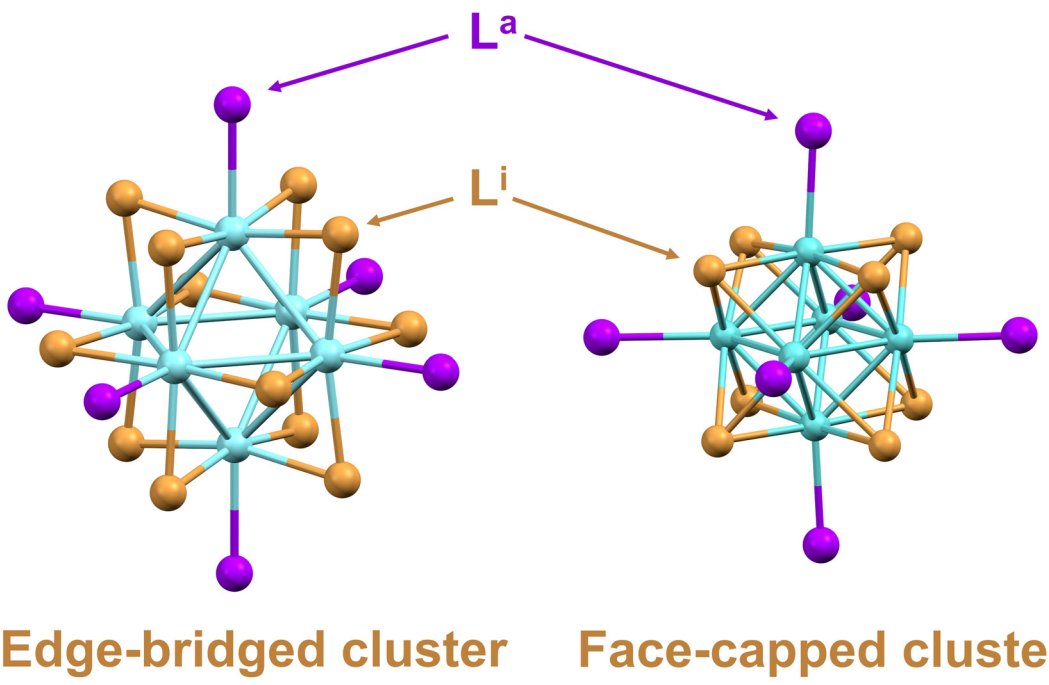

Figure 1: Schematic representation of $[\{M_6L^i_{12}\}L^a_6]^{n-/+}$ (M = Nb, Ta) and $[\{M_6L^i_8\}L^a_6]^{n-/+}$ (M = Mo, W, Re) molecular cluster units. Apical ligands (L^a) and inner ligands (L^i).

These molecular metal atom cluster units can be defined as a link between atom and nanoparticle. The solid-state compounds built-up from these units are characterized by insulating behavior combined with specific physical and chemical properties. Generally, the

molecular compounds based on non-interacting face-capped $[\{M_6L^i_8\}L^a_6]^{n-/+}$ cluster units (M = Mo, W, Re; L^i = halogen; L^a = halogens, organic molecules) are characterized by strong phosphorescence that ranges from red to near-IR (NIR) with a high quantum yield and long lifetime [44-52], whereas , the molecular compounds based on non-interacting edge-bridged $[\{M_6L^i_{12}\}L^a_6]^{n-/+}$ cluster units (M = Nb and Ta; X = halogen) are well known to be strong ultraviolet (UV) and NIR absorbers. [53,54] Several parameters influence the general properties of the cluster units: the nature of the metal, the nature of the ligands and the number of electrons involved in the metal–metal bonds, the so-called valence electron count or concentration (VEC). This review is not dedicated to the synthesis and properties of the octahedral metal atom clusters, for more specific details see these references. [39,40,55-67] These cluster units are prepared either by solid-state chemistry or by combined use of solid state and solution chemistries and associated with inorganic or organic counter cations in a large variety of molecular metal atom cluster compounds. [37-67] Actually, although prepared by solid-state chemistry processes, for instance the $Cs_2[\{Mo_6Br^i_8\}Br^a_6]$ clustered compounds can be resolubilized in many solvents until obtaining 1 nm objects in solution thanks to their molecular properties. [68] Indeed, one of the key points is the high solubilization of these molecular metal atom clusters compounds in various solvents and matrixes, which was an important parameter to provide very interesting building blocks with multifunctional properties (optical, magnetic, electronic, redox…) that can be further used for the design of a large variety, from hybrids (dendrimers, liquid crystals, polymers…) to all-inorganic, of functional nanocomposite materials and surface coatings during the last decades. [29-36, 68-220] Clearly, the number of publications about nanocomposites based on octahedral metal atom clusters has been increasing for the last 3 decades (started from less than 10 before 2000 to almost 100 between 2010 to 2019, and already 43 since the last two years). These nanocomposites based on these octahedral nanoclusters are already an emerging field in material science. They found applications in many important domains like energy, [91-108] catalysis, [94,109-119,217] biotechnology, [47,120-145] sensors, [75,80,142,146-153] and photonic (Figure 2). [89,154-171]

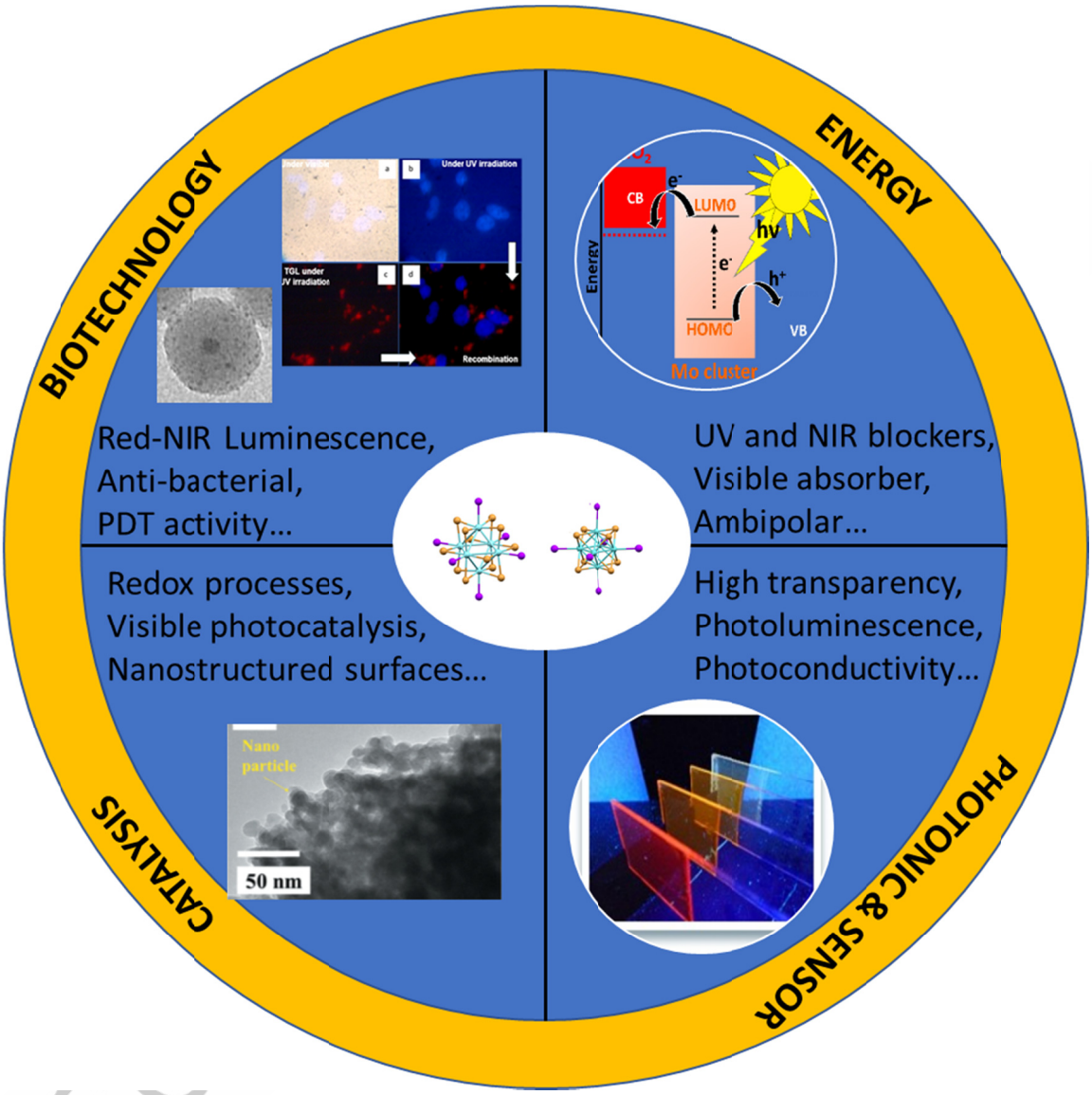

Figure 2: The illustration of the applications of $[\{Mo_6L^i_8\}^a_6]^{n-/+}$ and $[\{Ta_6L^i_{12}\}^a_6]^{n-/+}$ molecular cluster units.

Due to the remarkable properties of these octahedral metal atom clusters, a large number of studies are reported and this article will review only the inorganic powder (nanoparticles, 2D) and film nanocomposites. More specifically, the relationships between synthesis, properties and process of these inorganic powders and film nanocomposites will be

discussed and new trends will be emphasized:

-The electrophoretic deposition (EPD) process appears to be a new strategy to fabricate highly transparent, homogeneous and colored nanocomposite thin films and coatings,

-The clear potential of Mo_6 based nanocomposites for biotechnology applications as anti-bacterial or anti-cancer or as a new broadband emitter for photovoltaic (PV), photonic and sensor applications,

-The strong potential and synergetic effects of nanocomposites based on nanoclusters and layered 2D compounds for catalysis and photocatalysis applications,

-The reborn of Nb_6 and Ta_6 nanoclusters, which appeared recently as very interesting UV and NIR blockers for saving energy applications.

One of the objectives of this review would be to provide guiding significance for design of new high-performance nanocomposites based on transition metal atom clusters from the aspects of processing, characterization and applications.

2. Inorganic powder nanocomposites: 0D nanoparticles and layered materials

The idea of improving the properties of materials by combining at least two phases with different properties is not new and nanocomposites are found in nature or have been created by human long time ago. [221] As mentioned in the introduction, the diversity of the architectures to prepare nanocomposites is very large. Nevertheless, in the case of inorganic nanoparticles (0D) and layered (2D) material nanocomposites, the nanoclusters are mainly embedded into nanoparticles (often considered as the matrix) or deposited at the surface of nanocrystals or nanoparticles or 2D materials, depending on the targeted application. The high flexibility of the inorganic matrix's composition was also mentioned as an advantage for the synthesis of new nanocomposites, however, only few are still reported in the case of the 0D nanocomposites based on transition metal atom clusters. The main matrix used is SiO_2 and by far.

2.1 0D nanocomposites:

2.1.1 @SiO_2

It is necessary to mention that the first examples of SiO_2 nanocomposite based on transition metal atom clusters were related to bulk and not to 0D nanocomposites. For instance, at the end of the 80's, Newsham has shown that $[\{Mo_6Cl^i_{12}\}(OSi(CH_3)^a_3)_2]^{2-}$ can be encapsulated in a silica matrix prepared by sol-gel route in methanol. [71] In 1994, Robinson *et al.* studied the nature of the interaction between commercial silica gel and $[\{Mo_6Cl^i_8\}X^a_6]^{2-}$ ($X^a = SO_3CF_3$, Cl) cluster units in organic solvents and different pH conditions by a simple absorption process. [72] Both cluster units, $[\{Mo_6Cl^i_8\}X^a_6]^{2-}$ and $[\{Mo_6Cl^i_8\}(SO_3CF_3)^a_6]^{2-}$, were able to be strongly absorbed at the surface of the silica gel, which contains a high density of Si-OH groups. The authors concluded that clusters could be bound by either electrostatic or covalent interactions, which mainly depends, under the same conditions, on the apical ligand's properties. Indeed, the cluster units with the less substitutional labile apical ligands, in this specific case X^a= Cl, was not covalently attached to silica gel. In opposite, the SO_3CF_3- ligands, which could be readily replaced by solvent molecules for instance, presented the opportunity to coordinate the cluster to Si-O^- groups in basic condition or even adsorb the solvated cluster cation by ion exchange in acid condition. The problem of the apical ligands' substitution is a very important issue for preparing the nanocomposites and for controlling their properties and it will be discussed several times in the following sections. Nevertheless, the main result of these studies of bulk nanocomposites was that the integrity of the $\{Mo_6Cl^i_8\}^{4+}$ cluster core could be maintained in this heterogeneous environment, even in the case of exchange of apical ligands by other ions or solvent molecules. These results were very important for the first synthesis of 0D silica nanocomposites (noted @SiO_2) based on $[\{Mo_6Br^i_8\}X^a_6]^{2-}$ cluster units (X = Br, OH) in 2008 (Figure 3). [68] Grasset *et al.* reported the synthesis of red-NIR luminescent $[\{Mo_6X^i_8\}X^a_6]$@SiO_2 nanoparticles (X = Cl, Br, or I) via a water-in-oil (W/O) microemulsion process wherein the nanosized $[\{Mo_6Br^i_8\}X^a_6]^{2-}$ cluster units are homogeneously dispersed in high monodisperse silica nanoparticles (called homogeneous 0D nanocomposites) (Figure 4). Very shortly, the microemulsion is a thermodynamically stable dispersion of water droplets with a size about tens nanometers in oil phase, stabilized

at the interface by amphiphilic surfactant molecules. Those water droplets, also called inverted micelles, constitute a suitable confined reaction medium for the synthesis of a wide variety of well-defined functional 0D silica nanoparticles with controlled size and architectures. [30,32,222]

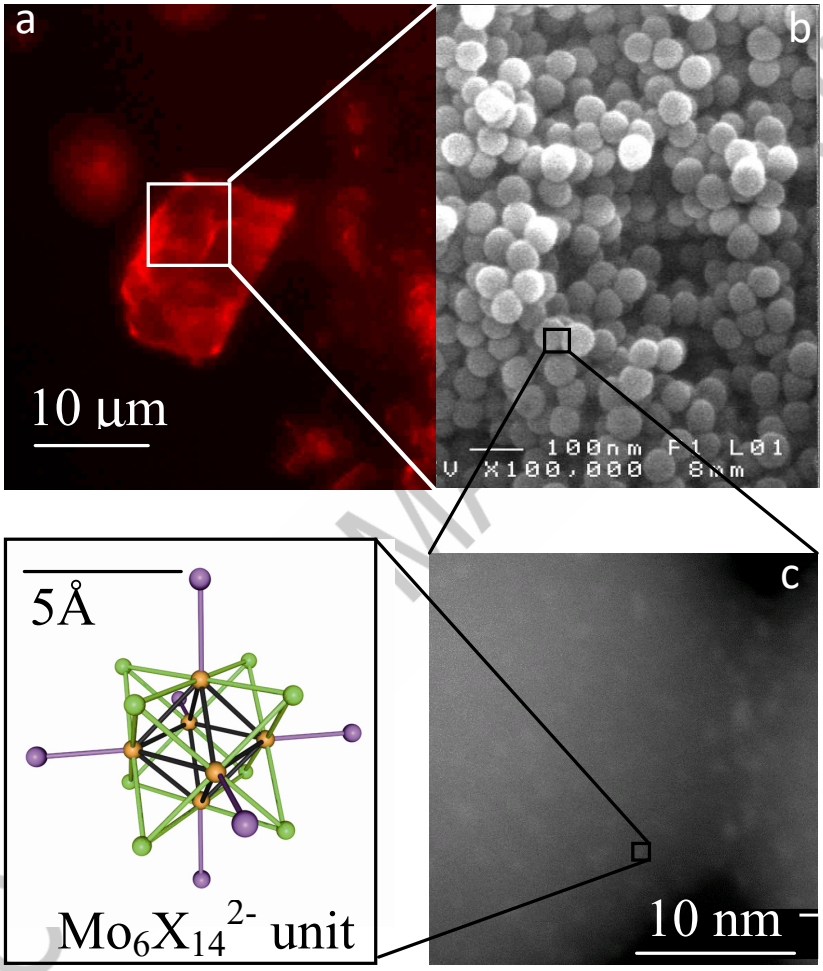

Figure 3: a) Optical microscopy image of $[\{Mo_6X^i_8\}X^a_6]@SiO_2$ (X = Cl, Br, I) nanocomposites (powder between two plates of glass under irradiation at λ_{exc} = 546 nm). b) Scanning electron microscope (SEM) images of $[\{Mo_6X^i_8\}X^a_6]@SiO_2$ 0D homogeneous nanocomposites. c) Z-contrast high-angle annular dark field scanning transmission electron microscopy (HAADF-STEM) mode image of two adjacent $[\{Mo_6X^i_8\}X^a_6]@SiO_2$ nanoparticles. Adapted from 68 with permission from Wiley.

This process is quite simple and highly reproducible for preparing multifunctional $@SiO_2$

nanocomposites with complex architectures with a diameter around 50 nm (Figure 4). The key point in this microemulsion process for embedding nanosized metal clusters in 0D silica nanocomposites is to obtain stable colloidal solutions containing highly dispersed nanoclusters to avoid their aggregation and precipitation before the encapsulation. [68]

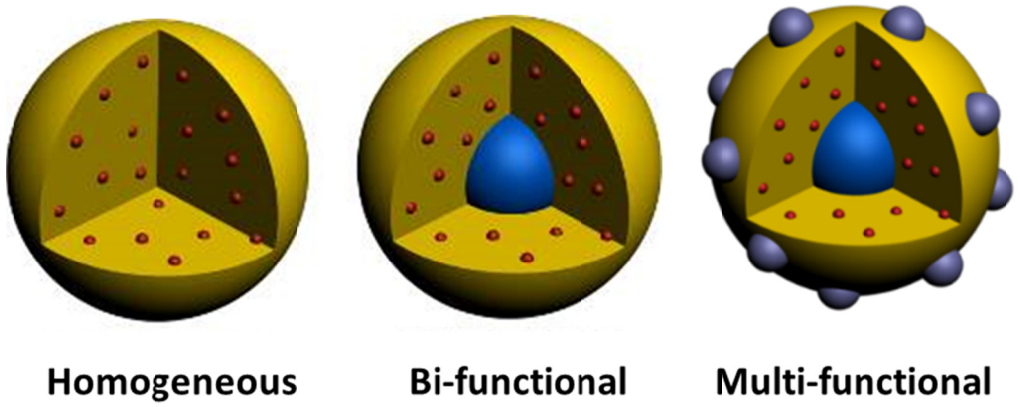

Figure 4: Multifunctional nanoparticles with complex architectures. Adapted from 32 with permission from Springer.

The microemulsion was prepared by adding acidic $Cs_2[\{Mo_6Br^i_8\}Br^a_6]$ (X = Cl, Br, I) colloidal water/ethanol solution to a Polyoxyethylene (4) lauryl ether/heptane mixture. Then, the precursor of silica nanoparticles, tetraethoxysilane (TEOS), was added to the microemulsion. The silica matrix was synthesized by increasing the pH inside the nanoreactors by adding an ammonia water solution, which catalyzes the TEOS condensation. The acidic solution, containing the Mo_6 nanoclusters, catalyzed first the hydrolysis of the monomeric species of TEOS, which consequently migrated into the nanoreactors for the condensation and formation of monodispersed @SiO_2 OD nanocomposites after 2-3 days. Aubert *et al.* have been confirmed that during the microemulsion process, the cluster units are losing a part of their Br apical ligands and counter cations. [120]. The Br ligands are replaced partially by OH groups that can form hydrogen bonds with the silanol groups of the silica and by OSi groups through a covalent bonding between the cluster units and the silica matrix.

One of the goals of the preparation of these first $[\{Mo_6X^i_8\}X^a_6]@SiO_2$ functional silica 0D nanocomposites was to prepare relevant candidates in theranostic applications (bioimaging, labelling, photodynamic therapy (PDT)…). Indeed, functional silica nanoparticles present a strong potential for biotechnologies for decades. [223-227] Silica constitutes a very good candidate as a matrix for the preparation of nanocomposites-based metal atom clusters thanks to its high chemical stability and biocompatibility. Silica can prevent the degradation of the cluster units' properties and, moreover, the surface of the SiO_2 matrix can easily be conjugated with various biomolecules and is water-soluble. Cytotoxicity is a very important issue for biotechnology applications, Aubert *et al.* showed that these $[\{Mo_6Br^i_8\}X^a_6]@SiO_2$ 0D nanocomposites (X = Br, OH, OSi) presented a dose effect but no time effect, and the cell toxicity became significant only for the fibroblastic cells and for the highest concentration (100 µg/mL). [120] More interestingly, the *in vitro* cytotoxicity in spheroid models, examined by the acid phosphatase assay, revealed that this 0D nanocomposites induced a strong oxidative stress to model cancer KB cell lines ((ATCC® CCL-17™) derived from a human epidermal mouth *carcinoma*. [130] In opposite, Cabello-Hurtado *et al.* showed that $[\{Mo_6Br^i_8\}X^a_6]@SiO_2$ have any phytotoxicity significant effect on plant cell growth and viability or photosynthetic efficiency on *Arabidopsis thaliana*. [125]

Since this first example of 0D $\{[\{Mo_6X^i_8\}X^a_6]@SiO_2$ (X = Cl, Br, or I) nanocomposites, some studies have been published on the synthesis of homogeneous functional silica nanocomposites based on transition metal atom cluster compounds. For the Mo_6, this process was successfully used with the highly red-NIR luminescent $(Bu_4N)_2[\{Mo_6I^i_8\}(NO_3)^a_6]$ [124,135,191] and $Cs_2[\{Mo_6I^i_8\}(C_2F_5COO)^a_6]$ [123] cluster compounds. In 2010, it was expanded to Re_6 cluster compounds by Aubert *et al.* [88] and then very recently by Khazieva *et al.* [142] Aubert *et al.* synthesized and characterized a new red-emitting @silica 0D nanocomposites based on $A_4[\{Re_6X^i_8\}X^a_6]$ metal atom clusters compounds (A = Cs or K, X^i = S or Se, and X^a = OH or CN) with an interesting changing in the chemical process. Indeed, to prevent the precipitation of the clusters due to the low pH, the microemulsions were prepared by adding ammonia to the polyoxyethylene (4) lauryl ether/heptane mixture prior to the aqueous cluster colloidal solution and prior to

TEOS, so both the hydrolysis and condensation steps in the silica synthesis were base-catalyzed. In 2018, the W/O micoemulsion process was extended to positively charged Ta_6 nanoclusters $[\{Ta_6Br^i_{12}\}(H_2O)^a_6]^{2+}$ by Chen *et al.* [199] This new step could be very attractive for biotechnology applications because interestingly, over the past several decades, hexanuclear tantalum bromide clusters have attracted considerable attention, in particular as a commercial tool for the phase determination of large biological assemblies by X-ray crystallography and as radiographic contrast agents [228-231].

In parallel to this homogeneous 0D SiO_2 nanocomposites, it is also possible to use the microemulsion process to prepare more complexes bi- or multifunctional @SiO_2 0D nanocomposites as presented in Figure 4. Compared to homogeneous 0D SiO_2 nanocomposites, complexes bi- or multifunctional @SiO_2 0D nanocomposites combine in the same nanoparticles several properties such as magnetism, photoluminescent and/or plasmonic. For instance, magnetic nanocomposites could be handleable and sensitive to radiofrequency signals. The first example of bi-functional @SiO_2 0D nanocomposites was done by Grasset *et al.* as early as 2008 by the controlled and nanostructured association of $[\{Mo_6Br^i_8\}Br^a_6]^{2-}$ cluster units and γ-Fe_2O_3 nanocrystals. [86] These bi-functional 0D nanocomposites exhibit silica nanoparticles with regular spherical shape of 50 nm in diameter and the γ-Fe_2O_3 nanocrystals (6 nm) are located at the center of the nanoparticles whilst the $[\{Mo_6Br^i_8\}Br^a_6]^{2-}$ cluster units are homogeneously dispersed around the magnetic core within the @SiO_2 matrix (Figure 5). The bi-functional character (magnetism and luminescence) of these nanocomposites has been evidenced by complementary technics. The effect of the applied magnetic field, concomitant to the red emission, was directly observed in an aqueous ethanolic solution by using an optical microscope under irradiation at λ_{exc} = 405 nm and an applied magnetic field (1.5 T). Very interestingly, the presence of γ-Fe_2O_3 as core does not affect the red luminescence properties of the cluster units, and an intense broad band with a maximum located at λ_{em} = 738 nm was observed as expected for the $[\{Mo_6Br^i_8\}Br^a_6]^{2-}$ cluster units. The zero field cooled-field cooled (ZFC-FC) magnetic behavior was typical of superparamagnetic ferrite nanocrystals dispersed in silica matrix. [232,233]

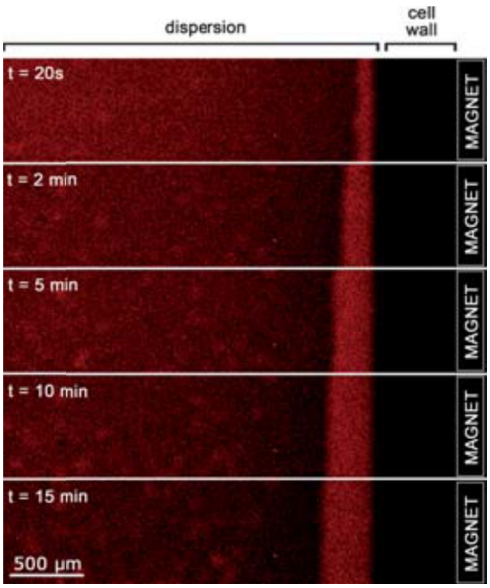

Figure 5. Optical microscope images using λ_{exc} = 405 nm of dispersed nanoparticles under a magnetic field (1.5 T) showing the growth of a nanoparticles layer along the wall of a cell as a function of time. Adapted from 86 with permission from the Royal Society of Chemistry.

In 2014, Nerambourg *et al.* improved this bi-functional nanocomposites by tuning the size of the magnetic nanocrystals (from 6 to 15 nm) and by preparing the first multifunctional nanocomposites (Figures 6a-f). [155] Indeed, gold nanoclusters (2 nm) were successfully generated on the surface of the $[[\{Mo_6X^i_8\}X^a_6]$-γ$Fe_2O_3]@SiO_2$ by the direct nucleation of gold ions immobilized on their surfaces under UV light (Figure 6g and 6h). The goal was to obtain a hybrid nanocomposite which possesses luminescent, magnetic and plasmonic properties.

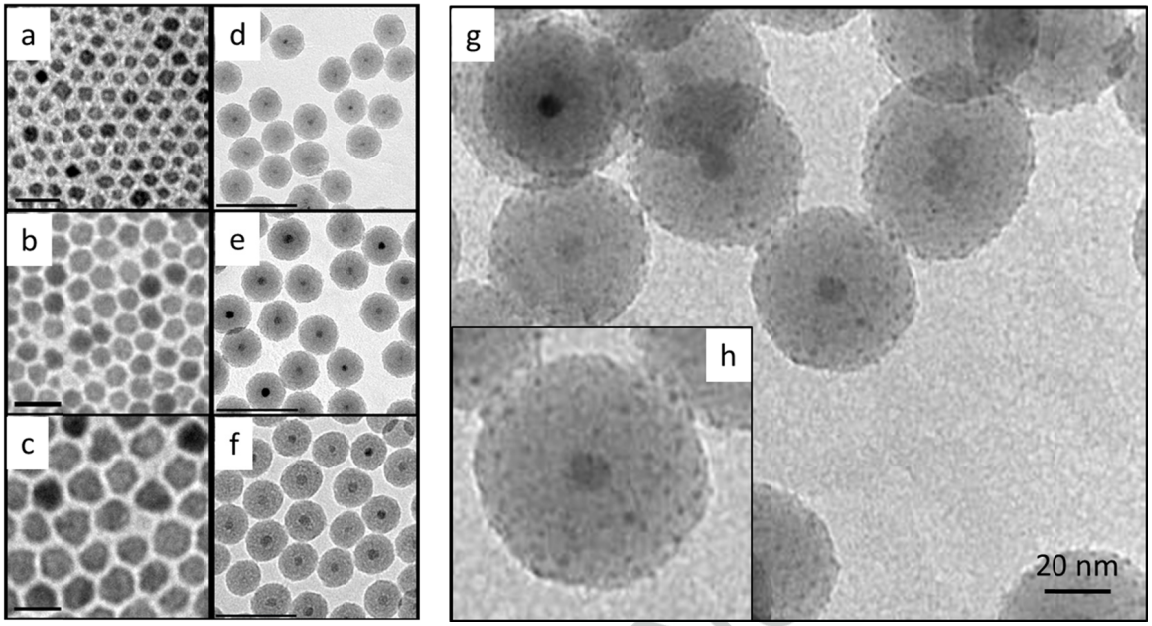

Figure 6. High resolution transmission electron microscopy (HRTEM) images of (a) 6 nm, (b) 10.5 nm, (c) 15 nm (scale bar = 20 nm) γFe_2O_3 nanoparticles and the corresponding d, e and f $[[\{Mo_6X^i_8\}X^a_6]\text{-}\gamma Fe_2O_3]@SiO_2$ 0D nanocomposites (scale bar = 100 nm). g) TEM image of $[[\{Mo_6X^i_8\}X^a_6]\text{-}\gamma Fe_2O_3]@SiO_2@Au$. h) zoom. Adapted from 155 with permission from Elsevier.

This strategy of multifunctional nanocomposites or decorated silica nanoparticles by nanoclusters was recently and nicely extended by Elistratova *et al.* and Fedorenko *et al.* [132,139] Elistratova *et al.* introduced a facile and very interesting synthetic route to embed phosphorescent $[\{Mo_6I^i_8\}I^a_6]^{2-}$ and $[\{Mo_6I^i_8\}(CH_3COO)^a_6]^{2-}$ cluster units onto amino-decorated silica nanoparticles prepared by microemulsion.

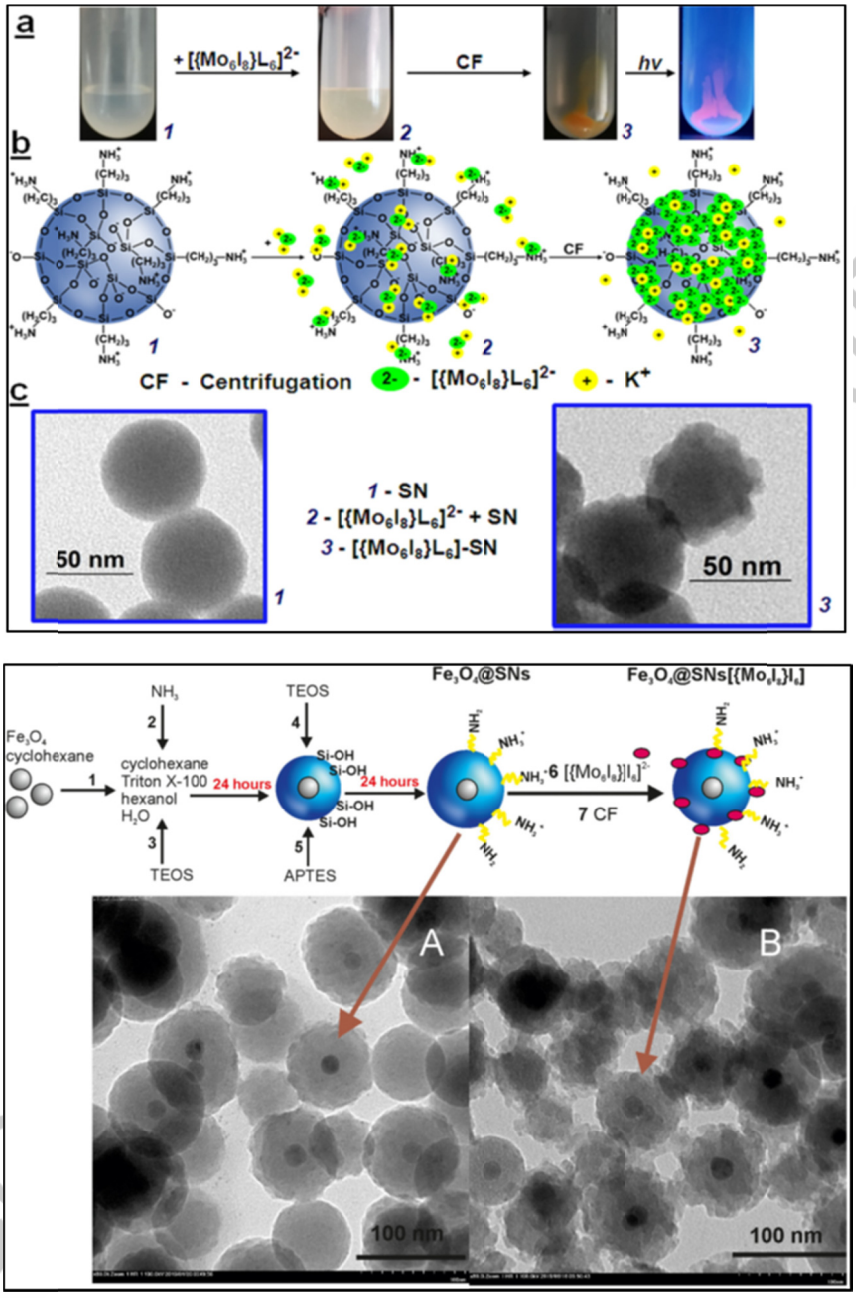

Figure 7. Upper: (a) Photos of silica nanoparticles in aqueous solution (1), silica nanoparticles in the cluster solutions (2) and assembled silica nanoparticles with clusters (3) before and after irradiation; (b) Schematic representation of self-assembly of the clusters complexes on silica surface; (c) TEM images of the silica nanoparticles and SiO_2@[{$Mo_6I^i_8$}L^a_6]. Adapted from 132 with permission of Elsevier. Lower: Schematically represented synthesis of Fe_3O_4@SiO_2@[{$Mo_6I^i_8$}L^a_6] and TEM images of Fe_3O_4@SiO_2 (A) and Fe_3O_4@SiO_2@[{$Mo_6I^i_8$}L^a_6] (B). Adapted from 139 with permission from Elsevier.

High uptake capacity of the clusters (8700 of $[\{Mo_6I^i_8\}I^a_6]^{2-}$ and 6500 of $[\{Mo_6I^i_8\}(CH_3COO)^a_6]^{2-}$ per each nanoparticle) was possible thanks to the ionic self-assembly and coordination bonds between the charged nanoclusters and ionic (amino- and siloxy-) groups at the silica (Figure 7 upper). Fedorenko *et al.* mixed the previous works by the combination of superparamagnetic iron oxides at the center of the silica nanocomposites and $[\{Mo_6I^i_8I^a_6]^{2-}$ cluster units at the surface within amino-decorated group (Figure 7 lower).

Interestingly, very recently, Elistratova *et al.* extended this process to water insoluble cluster salts $(Bu_4N)_2[\{Mo_6I^i_8\}L^a_6]$ (L = CF_3COO^- and $C_6F_5COO^-$) by using an additional layer of polyethylene imine (PEI) at the surface of the silica in order to significantly improve the colloid stability. [143] For the first time, this work highlighted the combination of pronounced PDT effect with high anticancer potential in the irradiation-free conditions using Mo_6 based silica nanocomposites. Khazieva *et al.* expanded this strategy to $[\{Re_6S^i_8\}(OH)^a_6]^{4-}$. [142] Most of these red-NIR luminescent nanocomposites could have applications in biotechnology field (*in vitro* bioimaging, cellular photosensitisation, PDT…). 234, 235] The strong potential of these nanocomposites as cellular bioimaging agent has been revealed by cellular internalizations and flow cytometry measurements. [123,124,132,139,142,143] Neaime *et al.* reported the first preparation of transferrin grafted silica nanoparticles loaded by $[\{Mo_6I^i_8\}(C_2F_5COO)^a_6]^{2-}$ metal atom clusters used for time-gated luminescence (TGL) bioimaging observation. [123] TGL imaging clearly showed that the conjugates accumulated around the nuclei upon internalization into living cells. Moreover, cellular imaging and pronounced PDT effects were observed, no matter, the localization of the cluster units (interfacial or encapsulation). [124,132]

To conclude on this part on 0D silica nanocomposites prepared by microemulsion process, we just mentioned that more "exotic" 0D silica nanocomposites β-$NaYF_4$:Yb:Er@$NaYF_4$@$[\{Mo_6Br^i_8\}Br^a_6]$@SiO_2 or ITO@$\{M_6Br^i_{12}\}$@SiO_2 (M = Nb, Ta) (ITO = indium tin oxide) were reported by Thangaraju *et al.* or Chen *et al.* respectively. [98,175] The latter case will be presented more in detail in the section related to films and coatings prepared by EPD for saving energy applications.

The microemulsion route is not the only way to prepare functional 0D silica nanocomposites and obviously the well-known "Stöber-Fink-Bohn" process was one of them. [236] The first example of homogeneous 0D nanocomposite prepared by this simple process was reported by Dechézelles *et al.* in 2010 and it was dedicated to the engineering of photonic colloidal crystals based on $[\{Mo_6Br^i_8\}Br^a_6]@SiO_2$ (25 layers of silica microparticles with a diameter = 330 nm) by using the Langmuir–Blodgett technique. [89] These photonic structures exhibit strong angle-dependent luminescent properties. An inhibition of the emission intensity from the light sources was observed in the spectral region of the stopband, which follows the Bragg-Snell law as the angle between the [111] direction and the incident beam was varied. Moreover, the incorporation of one or several planar defects (monolayer of silica microparticles with a diameter = 450 nm) within the periodic structures gives rise to the creation of a passband in the stopband. In the energy range of this passband, an increase of the emission intensity has been found. In the same year, Gao *et al.* reported the encapsulation of several positively charged phosphine-terminated rhenium (III) chalcogenide clusters ($[\{Re_6Se^i_8\}(Et_3P)^a_5I^a]I$, $[\{Re_6S^i_8\}(Et_3P)^a_5Br^a]Br$, $[\{Re_6Se^i_8\}(Bu_3P)^a_5I^a]I$, and $[\{Re_6S^i_8\}(Bu_3P)^a_5Br^a]Br$) in silica nanoparticles (10-20 nm) for singlet oxygen production and PDT applications. Surprisingly, the encapsulation was ineffective for neutral and anionic clusters. [90] Two years later, Kirakci *et al.* prepared singlet oxygen photoactive composite materials by incorporating $(Bu_4N)_2[\{Mo_6I^i_8\}(CF_3COO)^a_6]$ cluster compounds into silica particles with sizes about 10 nm or 500 nm. [47] Interestingly, the intensive luminescence of the smallest $[\{Mo_6I^i_8\}(CF_3COO)^a_6]@SiO_2$ nanoparticles was completely and effectively quenched by oxygen. In contrast, the bigger microparticles were not affected by oxygen, which suggested that a high fraction of nanoclusters is not accessible to oxygen because of the large size of the silica microparticles. The comparison of the photo-physical properties of this nanocluster with those of the archetypal complexes $[Ru(bpy)_3]^{2+}$ and $[Ir(ppy)_3]$ illustrated the relevance of this nanocomposites. The last case is related to the work performed by Vorotnikov *et al.* on the detailed investigation of silica microparticles (500 nm) incorporating of various quantities of $(Bu_4N)_2[\{Mo_6X^i_8\}(NO_3)^a_6]$ (X = Cl, Br, I) cluster

compounds. [133,191] These studies revealed that hydrolysis of the molybdenum cluster precursors during the "Stöber-Fink-Bohn" process strongly affects both morphology and photophysical parameters of the materials, especially at high loadings. Low loadings of the nanoclusters demonstrated the most promising set of properties (i.e., the highest photoluminescence quantum yields and efficient singlet oxygen generation) for cellular internalization of proteins, such as the HIV TAT protein (HIV: human immunodeficiency viruses; TAT: Trans-Activator of Transcription) and commercial protein delivery agents (e.g., Pierce™).

The two last examples of original chemical route to prepare 0D SiO_2 nanocomposite based on metal atom clusters are related to the work of Nguyen *et al.* [116] and de la Torre *et al.* [237] In the first work, commercial pseudocube hollow silica nanoparticles (HSNs) (SiliNax SPPN(b)), supplied from Nittetsu Mining Co., Ltd) were used and the $[\{Mo_6I^i_8\}X^a_6]^{2-}$ (X = Cl, C_2F_5COO) nanoclusters have been successfully embedded into the HSNs and/or deposited at their surface by a vacuum impregnation process (VIP) at room temperature (Figure 8). The HSNs were clearly filled by the Mo_6 nanoclusters as confirmed by HRTEM coupled energy-dispersive X-ray analysis (EDX), inductively coupled plasma atomic emission spectroscopy (ICP-AES) and Brunauer–Emmett–Teller (BET) analysis. The results of the UV-Vis and photoluminescence spectra demonstrated that the optical properties of the Mo_6 cluster-functionalized HSNs nanocomposites were still retained even when annealed at 200°C.

In the second example, de la Torre *et al.* used amino-decorated mesoporous silica nanoparticles MCM-41 as containers. They incorporated the hexanuclear molybdenum cluster $(Bu_4N)_2[Mo_6I_8(CH_3CO_2)_6$ by a simple electrostatic assembly. Basically, an aqueous solution of cluster units (0.035 M) containing Pluronic® F-127 (0.3 mM) was mixed with an aqueous suspension of APTES@MCM-41 (0.5 g L-1) (APTES: 3-Aminopropyl)triethoxysilane). The mixture was shaken for 10 min and then sonicated for 15 min. Finally functionalized @MCM-41 nanoparticles were separated by centrifugation at 9000 rpm, washed with water and dried under vacuum. The highly specific surface area of these nanoparticles (~1000 m^2/g) guarantees a very good dispersion of the nanocluster,

as corroborated by electron microscopy analysis. The activity of this new photosensitizer for PDT was tested in cancer cells and this nanocomposite exhibits a good activity against human cervical cancer (HeLa) cells whereas free cluster compound showed practically no photoactivity, probably due to poor cellular uptake and degradation inside the cell. [237]

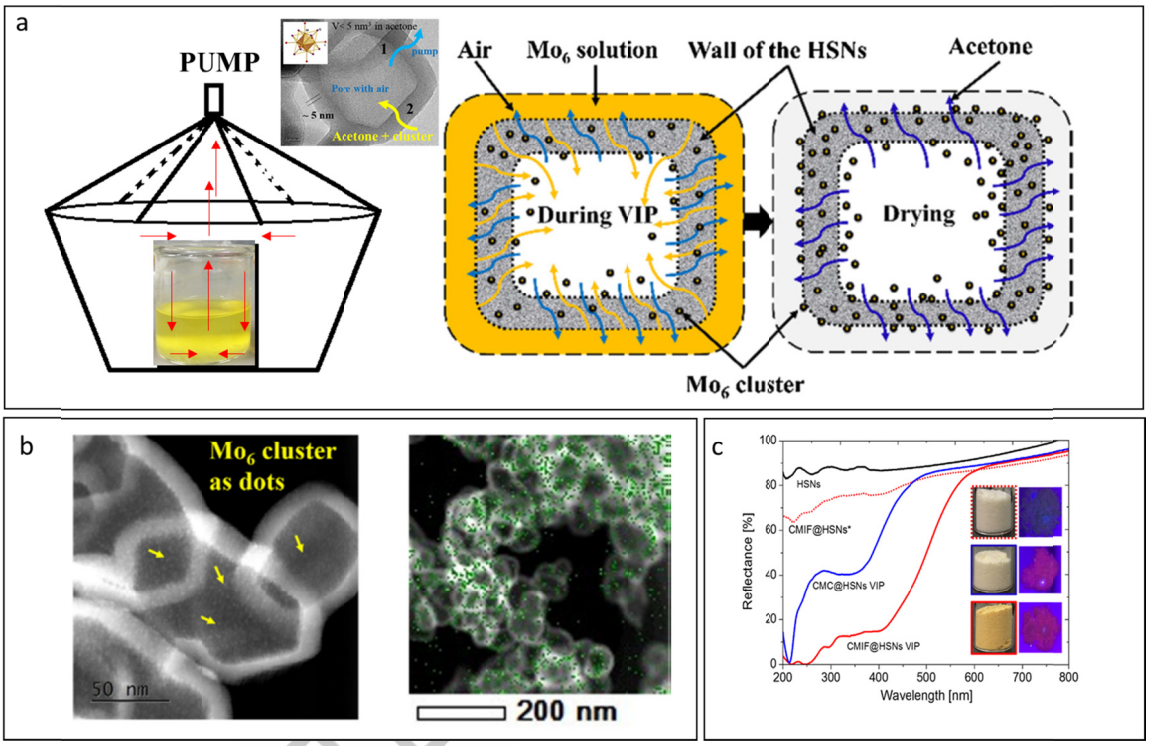

Figure 8. Upper: (a) Sketch of the vacuum impregnation process (VIP) and the possible movement of the air and the nanoclusters (b) STEM image of $[\{Mo_6I^i_8\}(C_2F_5COO)^a_6]$@HSNs and the overlapped EDX mapping image of the Mo element on the HSNs. (c) The UV-Vis reflectance spectra of: HSNs (black), HSNs mixed with $[\{Mo_6I^i_8\}(C_2F_5COO)^a_6]^{2-}$ without the VIP (red dot), $[\{Mo_6I^i_8\}Cl)^a_6]$@HSNs (blue) and $[\{Mo_6I^i_8](C_2F_5COO)^a_6]$@HSNs with the VIP (red line). Adapted from 116 with permission from Elsevier.

Finally, these studies suggested a potential application as insulation material prepared by efficient and very simple methods.

2.1.2 Nanocrystals-clusters assemblies: @ZnO, @TiO_2, @Au

Surprisingly, since 2008, only few 0D nanocomposites based on other oxides than SiO_2 were reported for optical (for instance, $(Bu_4N)_2[\{Mo_6Br^i_8\}Br^a_6]$@ZnO) or catalytic

($K_4[\{Re_6S_8\}(CN)_6]$-$Cu(OH)_2$@TiO_2) applications, this leaves the door opens to many experiments in the future. [84,87,111] In the first paper by Grasset *et al.*, the main idea was to induce synergetic optical effects between the semi-conductor nanocrystal and the nanoclusters. Indeed, the photoemission studies showed that $[\{Mo_6Br^i_8\}X_6]^{2-}$ cluster units (X = Br or OH) can efficiently interact with ZnO nanocrystals, not only in the colloidal solution, but also in solid-state conditions confirming an immobilization of the units on the ZnO surface. As reported above, $NaYF_4$, ITO and iron oxides nanocrystals were mixed with nanoclusters, but there are no clear synergetic effects between both components.

Very recently new nanocomposites emerged with gold nanoparticles as core and several studies demonstrated the synergetic effect of the association with Mo_6 nanoclusters as shells for plasmonic applications or photodynamic and photothermal therapies. [168,169,170] Novikova *et al.* demonstrated that a partial overlap of the photoemission spectrum of the $[\{Mo_6I_8\}L_6]^{2-}$ (L = NO^{3-} and p-toluenesulfonate) clusters and the surface plasmon resonance band of the spherical gold nanoparticles facilitated energy transfer between the both photoactive components. Specifically, by a careful control of the spacing between the cluster shell and the gold nanoparticle with an SiO_2 layer (21 nm), a significant increase in luminescence and photosensitizing properties of the nanocomposites was achieved. In parallel, the cluster complex facilitated energy conversion to heat by gold particles and hence increased the heating rate under laser irradiation. [168] These properties can be even improved by optimizing the aspect ratio of the gold nanorods. [169] Sciortino *et al.* show, very recently, that the plasmon resonance energy of gold nanoparticles (100 nm) can be tuned over a large area of the visible spectrum, from 2.4 to 1.6 eV, by changing the thickness of the $[\{Mo_6Br^i_8\}(NCS)^a_6]$ nanocluster shells between zero and 70 nm. Interestingly, the plasmonic response was performed at nanometer resolution on individual nanoparticles using electron energy-loss spectroscopy (EELS) directly inside a TEM. [170]

2.2 2D nanocomposites

The second illustration of the powder nanocomposites is related to layered materials (2D) as matrixes or supports (graphene-, layered hydroxides- and boron nitride(BN)-based

materials). All these materials are mainly interesting for their (photo)catalytic properties.

2.2.1 Graphene

In 2013, Barras *et al.* reported the first example of gold nanoparticles/$Na_2[\{Mo_6Br_8\}(N_3)_6]$ nanoclusters deposited on graphene oxide nanosheets (GONs) and its photocatalytic activity. [109] This nanocomposite exhibits a high photocatalytic activity for the degradation of organic molecules (ex: rhodamine B) under visible light irradiation. Nevertheless, the synthesis of this cluster compound with N_3 ligands is explosive and complicated to safely managed. In 2015, Kumar *et al.* replaced this unstable nanocluster by the very well known and safe $Cs_2[\{Mo_6Br^i_8\}Br^a_6]$ and $(Bu_4N)_2[\{Mo_6Br^i_8\}Br^a_6]$ nanocluster compounds. [112] The proof of the loading of these Mo_6 nanoclusters on GONs was probed by Fourier-transform infrared (FTIR) spectroscopy, X-ray photoelectron spectroscopy (XPS), HRTEM and EDX analysis. These new nanocomposites presented an activity for visible light induced photocatalytic reduction of carbon dioxide into methanol. One year later, very interestingly, Feliz *et al.* extended the catalytic activity of these nanocomposites to photocatalytic hydrogen evolution reaction (HER) from liquid water under homogeneous and heterogeneous conditions by using $(Bu_4N)_2[\{Mo_6Br^i_8\}F^a_6]$ nanocluster compound as starting precursors. [94] In this specific case, the catalytic activity of the $\{Mo_6Br^i_8\}^{4+}$ is enhanced by the *in situ* exchange of the apical F ligands by OH ligands and the generation of $[\{Mo_6Br^i_8\}F^a_{6-x}(OH)_x]^{2-}$ cluster units at the surface of the GONs. Nevertheless, it was observed that the covalent grafting of the nanoclusters on the surface of GONs limited the accessibility to the nanocluster active sites for the catalytic reaction and altered the lattice sp^2 structure of graphene, which results in defects and a loss of electronic properties. Feliz *et al.* proposed recently to solve this issue to use the $[\{Mo_6I^i_8\}(C_2F_5COO)^a_6]^{2-}$ cluster units and to add pyrene groups as counter cations of this cluster units as noncovalent interactions on the graphene surface. [115] The pyrene moieties act simultaneously as energy transmitters and as supramolecular linkers between the cluster anions and graphene. The production of green H_2 from sunlight is one of the most important targets for low-carbon energy production in the future in order to reduce the global warming and this beautiful

work including a supramolecular strategy opened up wide perspectives in terms of research prospects to design better nanoclusters/GONs nanocomposites for H_2 production. In parallel, Puche *et al.* demonstrated for the first time a successful water vapor photocatalytic reduction using $(Bu_4N)_2[\{Mo_6I^i_8\}(O_2C_2H_3)^a_6]$ cluster compound deposited on GO as catalysts. [119]

The production of green H_2 from sunlight is one of the most important targets for low-carbon energy production in the future in order to reduce the global warming and these works opened up wide perspectives in terms of research prospects to design better nanoclusters/GONs nanocomposites for H_2 production.

2.2.1 Layered hydroxides

During the last decade, there was a growing interest of the synthesis of heterostructured nanocomposites using layered hydroxides (monolayer = LHSs, double layer = LDHs) because of their unique two-dimensional (2D) lamellar structural features and properties for heterogeneous (photo)catalysis, water treatment, agriculture and biotechnology applications for instance. [238-242]

Regarding the layered hydroxide nanocomposites functionalized with octahedral metal atom clusters, there are only few examples, two were reported by Christiano *et al.* in the eighties [69,70] and the two others very recently by Ngyuen *et al.* [117,217] The first two examples were focused on the intercalation in Na^+-Montmorillonite of $\{M_6X_{12}\}^{n+}$ (M = Nb, Ta; n = 2-4) and $\{Mo_6Cl_8\}^{4+}$ cluster cores by ion exchange process. The nanoclusters have been converted to metal oxide pillared forms with potential utility for oxidation catalysis. [69,70] The third example was dedicated to the synthesis of a new zinc-aluminum layered double hydroxide (Zn_2Al-LDH)-based nanocomposite functionalized with the $[\{Mo_6Cl^i_8\}Cl^a_6]^{2-}$ cluster units. LDHs are composed by octahedral hydroxide layers occupied by divalent and trivalent metals with the general formula of $[M^{2+}_{1-x}M^{3+}_x(OH)_2]^{x+}[A^{n-}]_{x/n}\cdot mH_2O$ (x as the molar ratio $M^{2+}/(M^{2+}+M^{3+})$ in the range 0.2–0.33) (M^{2+} = Cu, Zn, Co, Mg, Cr…; M^{3+} = Al, Fe, Tb…). The metal hydroxide layers are positively charged and are neutralized by negatively organic or inorganic ions (A=NO_3^-,

CO_3^{2-}, SO_4^{2-}, F^-, Cl^- or alkyl anions…) accompanied by the absorption of the interlayer water molecules. Generally, these negatively charged molecules control the interspace between two metal hydroxide layers and can be exchanged by bigger molecules in order to expand it. [244] This strategy was used by Nguyen *et al.* by replacing NO^{3-} by n-dodecyl sulfate anions ($CH_3(CH_2)_{10}CH_2OSO_3^-$). [117] Indeed, the interlayer distance value, estimated by X-ray diffraction (XRD), for the starting LDH-1 is about 0.9 nm, which is too narrow to intercalate the cluster units with a size of 1.2 nm. This space is extended to 2.7 nm in the LDH-2 by the intercalation of n-dodecyl sulfate anions. Then, the $[\{Mo_6Cl^i_8\}Cl^a_6]^{2-}$ cluster units were simply introduced into the LDH-2 by an anion exchangeable method in dimethylformamide under ambient conditions (Figure 9). The addition of the nanoclusters induced an exfoliation, an interlayer expansion (up to 5 nm) and an amorphization of the LDH-2. Again, a part of the apical ligands of the nanoclusters are exchanged during the synthesis process and all the results support for the possible chemical bonding between the $[\{Mo_6Cl^i_8\}Cl^a_3(OH)^a_3]^{2-}$ or $[\{Mo_6Cl^i_8\}Cl^a_3(H_2O)^a(OH)^a_2]^{1-}$ anionic clusters or $[\{Mo_6Cl^i_8\}Cl^a_3(H_2O)^a_2(OH)^a]$ neutral cluster and the hydroxide of Zn-AL LDH-2. The efficiency of the degradation of the methylene blue was evaluated at more than 90 wt% after 2 h by using the Mo_6@LDH-2 nanocomposite with the existence of H_2O_2 as an optimal co-agent.

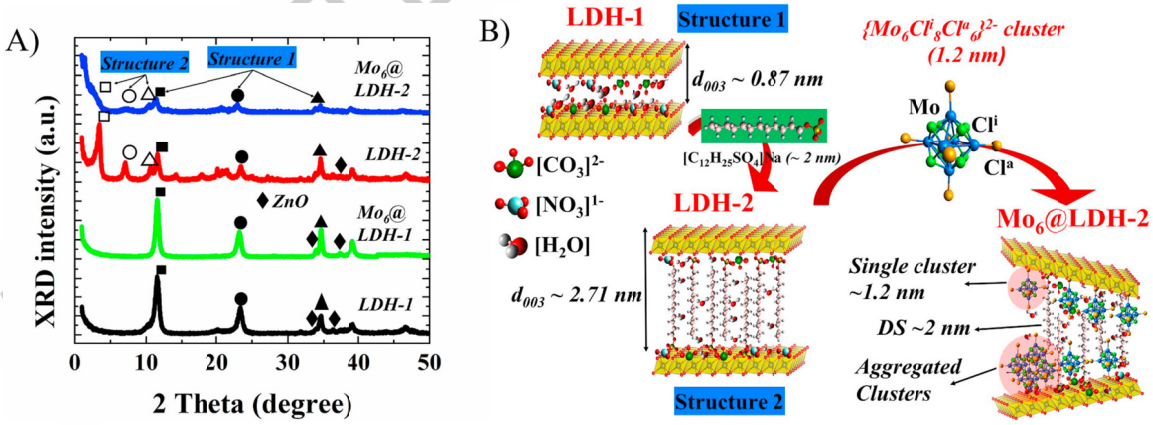

Figure 9. A) Powder-XRD patterns of LDH-1, Mo_6@LDH-1, LDH-2, Mo_6@LDH-2 with the indications of the planes of 003 (■), 006 (●), 009 (▲) and the lozenge symbol (♦) assigned for the ZnO phase. (B) Schematic of the process to fabricate the LDH and designed structure of its nanocomposite. Adapted from 117 with permission from Elsevier.

Very recently, a simplest one-pot synthesis was proposed by Nguyen *et al.* to prepare copper LHSs nanocomposites (noted Mo_6@CHN) mixed with $A_2[\{Mo_6X^i_8\}X^a_6]$ nanocluster compounds (A = Cs, Bu_4N; X = Cl, Br and I), the last example. [217] In this process, monoclinic copper hydroxynitrate (CHN), was fabricated in the presence of the nanoclusters by simply mixing an ethanolic solution of $Cu(NO_3)_2{\cdot}3H_2O$ and a solution of nanoclusters dispersed in acetone (Figure 10a), followed by thermal treatment at 80°C for 3h. The precipitate powder was collected by centrifugation and washing several times, then dried at 100°C. XRD and HRTEM analysis confirmed the presence of CHN, whereas photoluminescence and XPS study proved the existence of the integrity of the $\{Mo_6X^i_8\}^{4+}$ cluster cores even after the thermal and chemical treatments. Unlike Mo_6@Zn_2AL-LDH nanocomposites, the clusters do not fit between the layers but only at the surface in the case of Mo_6@CHN. The expected chemical formula of the Mo_6@CHN nanocomposites was estimated to be $[\{Mo_6X^i_8\}X^a_4(OH)^a_y(H_2O)^a_x]^{x-2}$@$[Cu_2(OH)_3NO_3]_7$. A high catalytic degradation rate of methylene blue after 30 minutes was reached by using the Mo_6@CHN/H_2O_2 systems. The reuse of the system was demonstrated up to 4 reaction cycles with an excellent efficiency (Figure 10b).

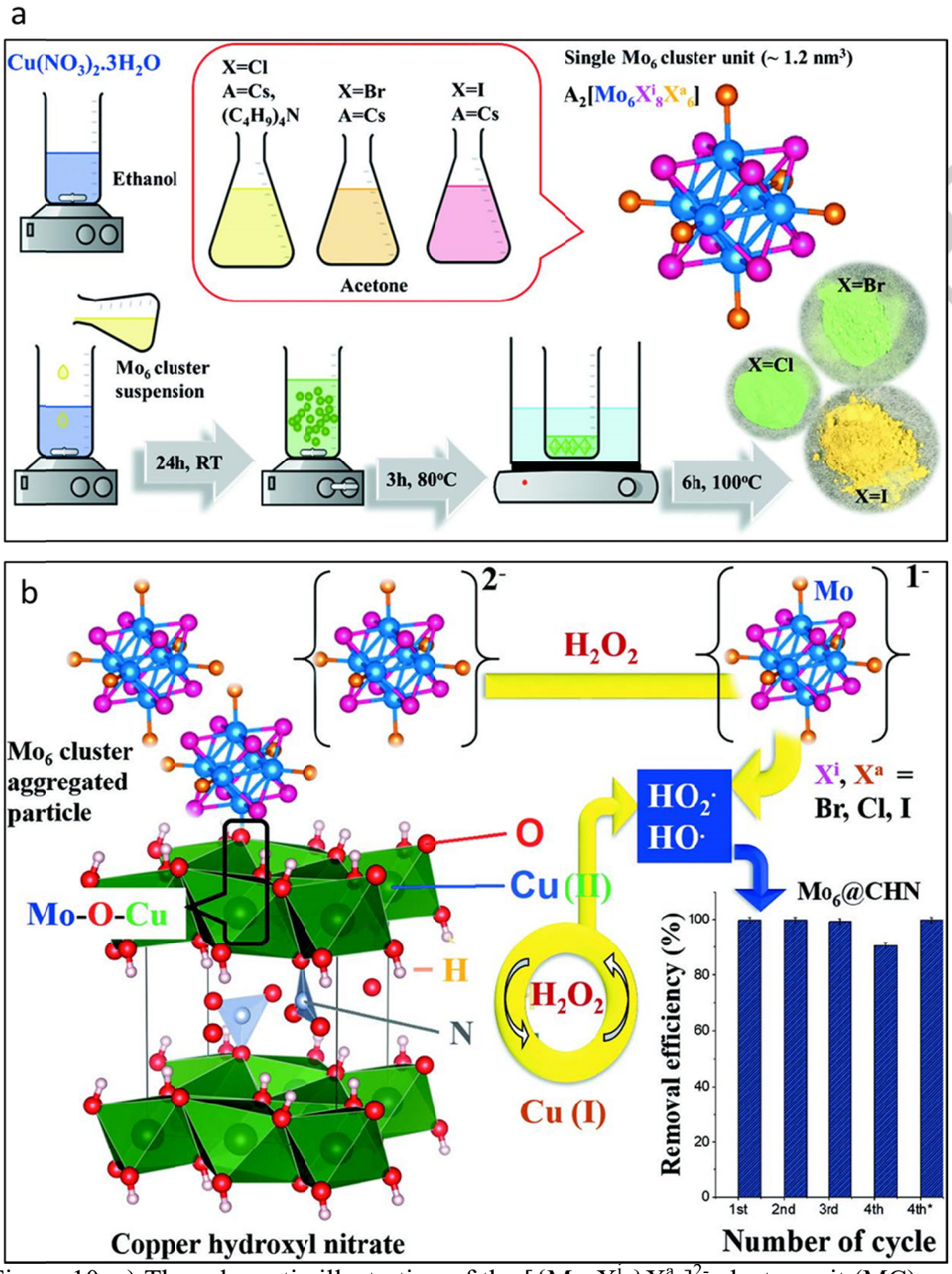

Figure 10. a) The schematic illustration of the $[\{Mo_6X^i_8\}X^a_6]^{2-}$ cluster unit (MC) and of the preparation of the Mo_6@CHN nanocomposites (images inside the circles are true photos of powders). b) Schematic of the interaction between the two components of the nanocomposite and the results of catalytic study in presence of H_2O_2. All the reactions were

performed for 2 h in the dark. Adapted from 217 with permission from Taylor and Francis.

2.2.3 h-BN

The last example of 2D materials is related to the preparation of nanocomposite based on hexamolybdenum nanoclusters and exfoliated hexagonal boron nitride (h-BN) nanosheets. [118] h-BN is known to have high thermal conductivity, stability toward high temperatures and aggressive chemical conditions (acids, bases, and oxidants) and some catalytic properties. The cluster deposition on the exfoliated h-BN nanosheet surface was obtained by their impregnation by a $(Bu_4N)_2[\{Mo_6I_8\}X^a_6]$ (X = I, NO_3) in acetone solution. Interestingly, again, the possibility to play with the apical ligands of the cluster units was used to control the interaction with the matrix. The cluster units with the more labile apical ligands, NO_3^-, gave the best results, because of the replacement of NO_3^- by OH and water molecules able to undergo in situ hydrolysis resulting in formation of an insoluble thin amorphous film of $[\{Mo_6I_8\}(H_2O)_2(OH)_4]\cdot yH_2O$ on a modified h-BN nanosheet surface.

To resume this section on 0D and 2D nanocomposites based on transition metal clusters, it was clearly demonstrated that if their potential is noticeably important, there is still a lot of room for new original systems. Indeed, nanocomposites based on silica matrix represent the vast majority of the examples reported to date for the 0D and the use of 2D materials as support for the metal atom clusters is apparently important for developing new (photo)catalysts. Indeed, these studies evidence that nanocomposites based on transition metal atom clusters are very promising new materials in many important catalytic fields like the elimination of pollutants or the production of green H_2 and other areas related to environmental protection. The choice of the matrix is very important, for example, inert and biocompatible silica is a good compromise for biotechnology applications, whereas more active matrix support (for instance copper hydroxynitrate, metal or semiconductor) are necessary for catalytic or photonic applications. One conclusion of these works is that the incorporation of metal atom clusters into matrix supports enhances their stability, their photoactivity and could improve their cellular uptake, compared to free clusters. Moreover, a novel 1D hybrid lead perovskite $[\{Re_6S_8\}(PzH)_6][Pb_3I_8(DMF)_2]\}\cdot 6(DMF)$ with

hexarhenium cluster cations has been synthesized recently by Ly *et al.* [167] This original study introduces a new class of nanocomposites and opens a promising path to materials with great potential for optoelectronic applications in photonic devices with broadband emission and stability. The maturity of this scientific field is still far from being reached.

3. Thin films and coatings

Thin films and coatings, with thickness ranging from nanometers to a few tens of micrometers are playing a very important and indispensable role in daily life with a global material market valued around USD 8000 million in 2020 and it is expected to reach USD 8500 million by the end of 2027 for end-user industries. [244] Nevertheless, as is known, main transition metal atom clusters compounds based on Nb_6, Mo_6, Ta_6, W_6, Re_6 are ceramic-like materials, [37-67] which clearly and strongly limit their application for thin films and coatings. In this review, conventional coating methods (dip coating, drop-casting, spin-coating…), which were applied for nanocomposite metal cluster-based films highly dispersed in a matrix, will be developed at the end of this section. We will first focus on the use of the EPD for the fabrication of pure octahedral cluster-based and nanocomposite thin films, which is a real breakthrough in this field. This well-known industrial technic was developed first for transition metal atom clusters in the International Research Laboratory "Laboratory for Innovative Key Materials and Structures" (IRL 3629 LINK) at the National Institute for Materials Science in Japan. [193] Similarly to the previous section several kinds of octahedral metal clusters were used with different positions of inner ligands; face-capped $[\{M_6L^i_8\}L^a_6]^{n-/+}$ and edge-bridged $[\{M_6L^i_{12}\}L^a_6]^{n-/+}$ cluster units. Both of them own the charge on the cluster units, a key point for the success of EPD.

3.1 EPD

EPD is an advanced technique for thin films and coatings due to its versatile and cost-effective process, simplicity, and the scaled-up possibility to large product volumes and sizes. In general, EPD acts as electrochemical equipment; an electric field is applied between two electrodes that force the charged particles to move toward the oppositely conductive electrodes, called electrophoresis. Then, the accumulation of the charged

particles by physical interaction will form a condensed layer on the surface of the electrodes, called deposition. EPD has been applied for metal oxide, traditional ceramic materials, and advanced materials with μm-sized or submicrometric (d > 100 nm), for example, functional ceramic coatings, porous materials, laminated ceramics, functionally graded materials, thin films, and nanostructured materials. [245-248]

To date, the EPD technique was developed for a variety of nano-architecture materials, including nanorods, nanowires, nanotubes, and nanosheets [249]. The approach of EPD on antibacterial coatings also attracted huge interest for biomedical applications with promising results [250]. Thanks to the driving force induced by the electrical field, highly concentrated colloidal solutions are not required (compared to conventional deposition process) and generally the deposition time is low, from tens of second to several tens of minutes. Nevertheless, the most interesting point of EPD is to fabricate pure metal cluster-based thin film with no matrix or binders that is limited or almost impossible to achieve from other methods.

3.1.1 EPD of $[\{Mo_6Br^i_8\}Br^a_6]^{2-}$ cluster units: the model case

In 2016, for the first time, Nguyen *et al.* revealed that an amorphous Mo_6 cluster-based thin film deposited on ITO-coated glass (ITO glass) could be successfully fabricated by using the EPD process at a low applied voltage (13 V) and very short deposition time (30 s) [193]. In this work, the dispersing medium of face-capped $[\{Mo_6Br^i_8\}Br^a_6]^{2-}$ cluster units, deposition time, and the applied voltage of EPD were preferably optimized to retain the chemical composition, octahedral structure as well as photostability.

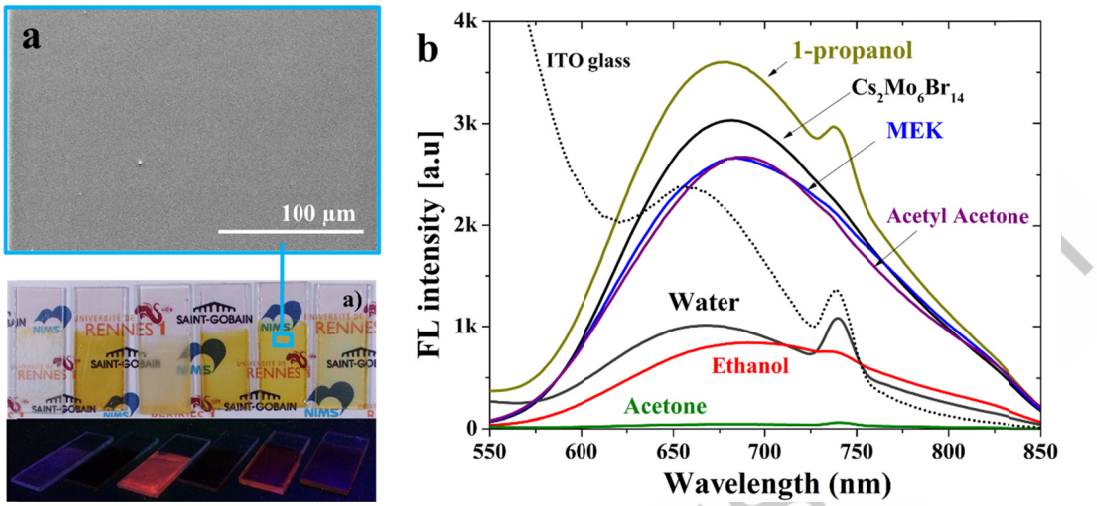

Figure 11. (a) SEM image of the surface of the Mo_6 film deposited from MEK, photos of the films deposited from (left to right) water, ethanol, 1-propanol, acetone, and MEK solutions at 15 V for 20 s and from acetylacetone solution at 50 V for 40 s (upper), respectively. Image of the luminescence of the cluster thin films irradiated at 324 nm wavelength (under). (b) Emission spectra excited at 370 nm of ITO glass, $Cs_2[\{Mo_6Br^i_8\}Br^a_6]$ compound, Mo_6 films. Adapted from 193 with permission from ECS.

Methyl ethyl ketone (MEK) was selected as the most suitable dispersing medium for the $Cs_2[\{Mo_6Br^i_8\}Br^a_6]$ cluster compound to obtain the homogeneous and transparent film (Figure 11a). Importantly, the luminescence of the Mo_6 clusters excited at 370 nm was retained in some cases (Figure 11b). Indeed, the solvent affects the dissociation of $[\{Mo_6Br^i_8\}Br^a_6]^{2-}$ anion and counter cation, and the hydrolysis reaction at the surface of the electrode during EPD. The hydroxyl group created during the EPD process by hydrolysis reaction increased the exchange of the apical ligands, resulting in modification of the optical properties. The unique and nanometer-size structure composed of metallic core and surrounding ligands contributed to the distinct EPD mechanism in comparison with other materials. In 2017, an EPD mechanism for this Mo_6 metal cluster-based film was proposed by Nguyen *et al.* [198] Complementary experimental technics (XRD, XRF, HRTEM, Electrospray ionization-mass spectrometry, SEM-EDX, XPS, IR…) clearly demonstrated that the microstructure of the films is heterogenous and dense (Figure 12). The most important part of the film is composed by an amorphous stacking of nanoclusters with the general formula, $[H_3O^+]_2[\{Mo_6Br^i_8\}Br^a_4(OH)_2]$. The closest part (few ten nanometers) to

the ITO glass substrate is enriched in Br anions and in aggregated nanoclusters based on the zero-charged clusters, $[Mo_6Br^{i}_8Br^{a}_4(H_2O)_2]$. The size of these Mo_6 zero-charged clusters was confirmed by TEM that showed many spherical nanoparticles of about 6 nm (Figure 12a). The role of the counter cations, inorganic (Cs^+) and organic $(N(n\text{-}C_4H_9)_4)^+$ compositions, was investigated to understand their effect on the dissolution of the cluster in MEK. Cs^+ cation was confirmed to be eliminated from the Mo_6 film by presenting Cs 3d region in the XPS spectrum (Figure 12b) while the disappearance of $(N(n\text{-}C_4H_9)_4)^+$ (TBA^+) cation was confirmed by FTIR spectrum. These counter-cations are mainly exchanged by H_3O^+ in the film. Regarding the cluster units' structure, the binding energy of Mo 3d was retained after EPD which meant the octahedral structure was stabilized (Figure 12c). Interestingly, the binding energy peak of Br apical ligands was reduced in Br 3d regions that explained the loss of two bromide apical ligands (Figure 12d). Moreover, the FTIR spectrum suggested the increase of the OH group in the EPD film. The Br/Mo atomic ratio in the film was sharply decreased during the first 10 s of the deposition and low voltages, then finally reached the value close to the theoretical index (2.33) at 40 s and 17 V (Figure 12f). Based on all these results, a scheme of the film suggested the heterogenous layer structure and hydrogen bonding interaction between the components was proposed (Figure 12g).

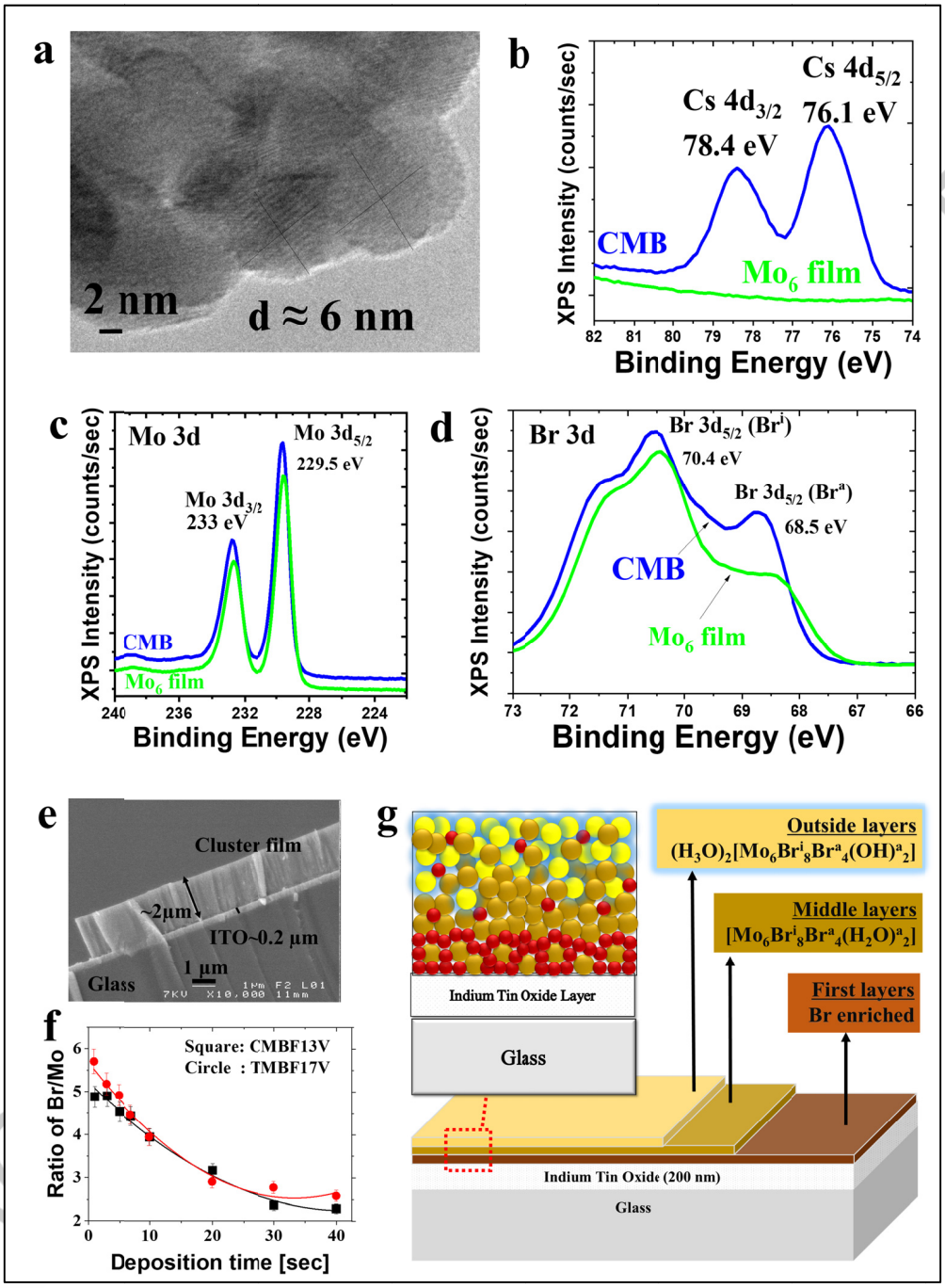

Figure 12. a) TEM image of the spherical Mo_6 cluster nanoparticles included in the Mo_6 film. The XPS spectra of (b) Cs 3d, (c) Mo 3d and (d) Br 3d region. e) SEM image of the cross-section of the Mo_6 film. f) XRF analysis versus deposited time. g) Schematic representation of the multilayered structure of the Mo_6 cluster thin film. Adapted from 198 with permission from ECS.

In summary, a mechanism of the Mo_6 film performance by using EPD was proposed: (i) the exchange of 2 Br apical ligands by OH^- or H_2O groups in solution, (ii) Cs^+ and TBA^+ cations are mainly replaced in the film by H_3O^+ to neutralize the negative charges of the Mo_6 nanoclusters at the electrode surface, and (iii) two kinds of clusters, i.e., $[Mo_6Br^i_8Br^a_4(H_2O)_2]$ and $[H_3O^+]_2[Mo_6Br^i_8Br^a_4(OH)_2]$, mainly composed the dense film (Figure 12e). Even though a slight modification of luminescent emission peak was recognized due to the change of the Mo_6 cluster network, the obtained EPD film showed high transmittance in the visible range and strong absorption in UV and NIR ranges. Stabilization of the thin film in air and moisture was an issue and free-cracking Mo_6 cluster thin film was prepared by the use of a top-coating Polydimethylsiloxane agent of the Mo_6 film. [95] These optimized parameters of EPD on the Mo_6 cluster motivated many achievements after that.

3.1.2 Sensor.

Very recently, the light-dependent ionic-electronic conduction on pure Mo_6 thin film prepared by EPD was demonstrated and studied by Harada *et al.* [153] The micron-size Mo_6 cluster film presented an ionic conductivity (Figure 13). Interestingly, this conductivity can be controlled and tuned by temperature and humidity. Activation energies at the relative humidities (RH) of 50 RH% and 80 RH% were estimated at 68 kJ/mol and 50 kJ/mol, respectively (Figures 13a and b). In addition, the H_3O^+ counter cations coordinate with the substituted OH- groups at the Br^a sites by hydrogen bonding, and many water molecules would be similarly linked by hydrogen bonds around it (Figure 13c). As the result, the existence of HO−H*−OH bridges between adjacent cluster units and activation energies seem to favor the vehicle diffusion model. [251] Moreover, the electronic conduction of the MC film greatly changes depending on the wavelength (from UV to red) and intensity of the irradiated light. The effect of photons on the electronic properties of ionic conductors at room or low temperature is a new and interesting research field. [251] These unique multi-sensing properties would present new possibilities for environmental sensor applications.

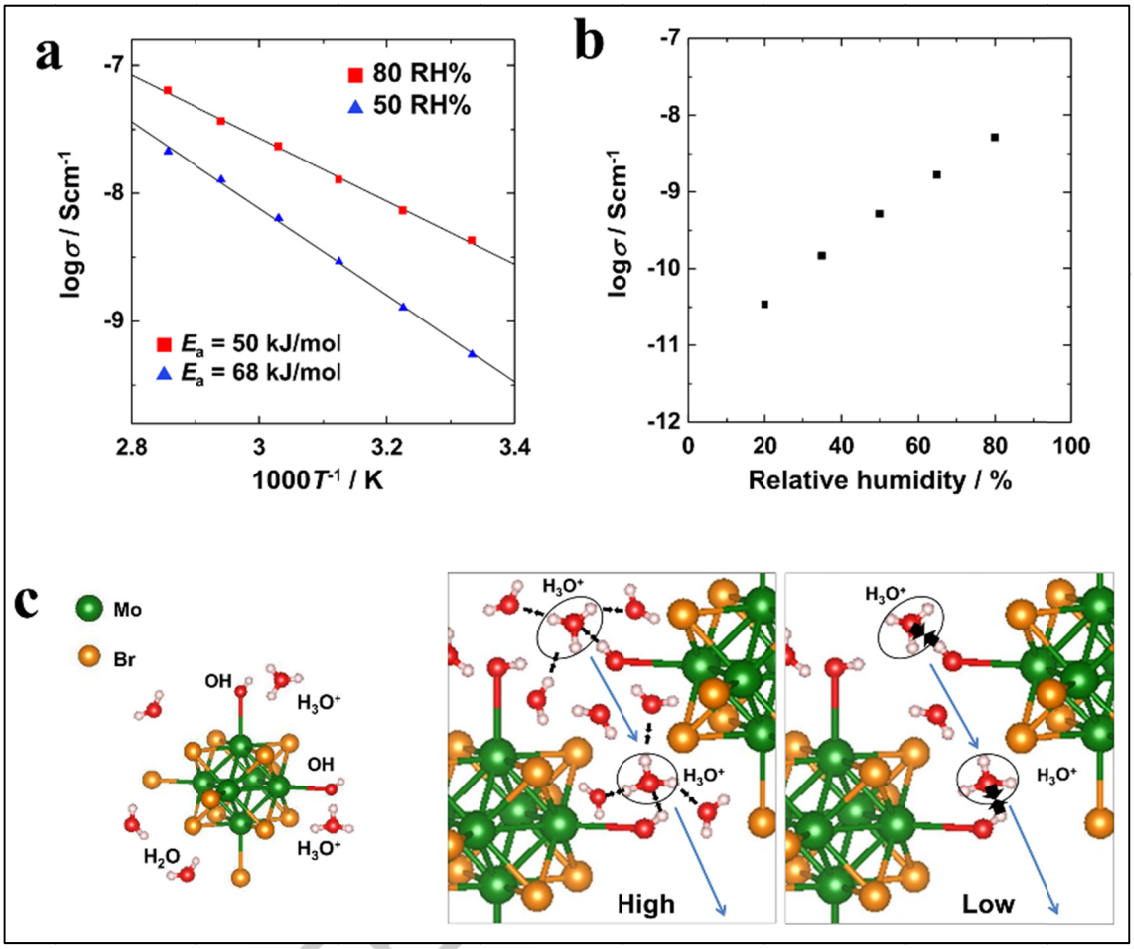

Figure 13. (a) Conduction properties of amorphous octahedral molybdenum cluster thin film. **(b)** Temperature dependences of conductivity for the cluster film due to differences in humidity. **(c)** Schematic illustration of octahedral molybdenum cluster in the film and structures postulated for the cluster films in high and low humidities. Adapted from 153 with permission from Springer Nature.

3.1.3 Absorber for solar cell: from DSSC to all-solid

The discovery of the possible deposition by EPD of pure molecular Mo_6 atom clusters opened the way to all-solid solar cells for photovoltaic applications. In the frame of the LINK project, Renaud *et al.* first reported the use of the iodide Mo_6 clusters as an inorganic absorber for dyed sensitive solar cells (DSSC). By using EPD, high-quality, mesoporous TiO_2 (n-type) photoanodes and NiO (p-type) photocathodes containing homogeneous, amorphous layers of the Mo_6 cluster were successfully prepared [99]. The use of EPD

greatly improved the homogeneity and the concentration of the Mo_6 absorber coated in porous photoelectrodes, compared to the classical soaking method (Figure 14). [93] The UV-Vis absorption characteristic of the Mo_6 cluster $(Mo_6I^i_8I^a_6)^{2-}$, one of the clusters exhibiting one of the strongest absorptions in visible light range, was retained after being deposited on both kinds of photoelectrodes (Figures 14a and b). The multilayer structure of the Mo_6 cluster-coated photoelectrode was confirmed in the SEM image with the deposition of the Mo_6 cluster on the surface and inside the pore (Figures 14c and d). For the photoelectrodes prepared by EPD, the photoconversion efficiency is clearly improved by 35–300 %, according to the type of electrolyte or semiconductor comparison with a soaking method (Figures 14e and f). Beyond the performance of the DSSC cells composed of the transition metal cluster, these promising results will open the new pathway for the investigation of photoelectronic applications, ranging from photoelectrochemical devices (PEC) to all solid solar cells. The future challenge in using the Mo_6 cluster as a non-toxic alternative in optoelectronic devices (stable under atmospheric conditions) is to optimize the band alignment between the cluster and the n-type transparent semiconducting oxides in order to favor an effective charge transfer.

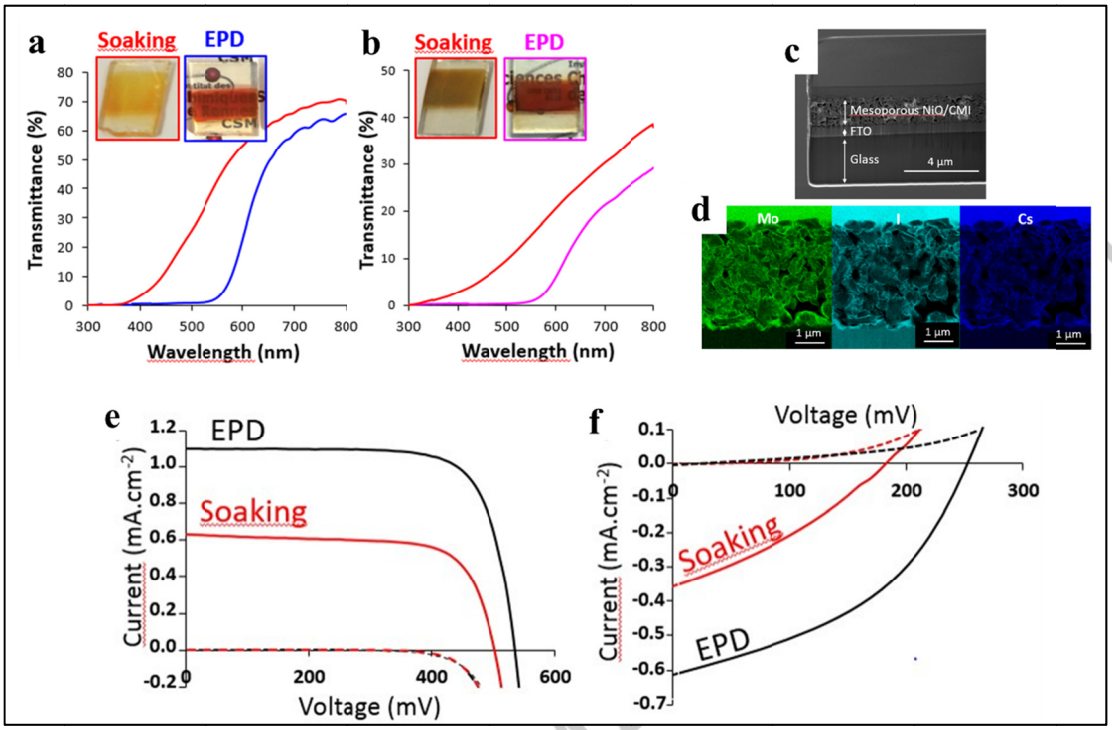

Figure 14. Comparison of the optical properties between (a) CMI@TiO_2@FTO and (b) films CMI@NiO@FTO prepared by EPD at 20 V and 15 V for 30 s respectively or soaking method (for 48h) from a CMI solution at 17 mM in acetone. (c) SEM image of a cross-section a CMI@NiO@FTO photoelectrode obtained at 10 V for 30 s and d) EDS analyses on the mesoporous NiO/CMI layer. Comparison of photoresponses in the dark (dash lines) and under$AM_{1.5}$ illumination (1000 $W.m^{-2}$, solid line) of photovoltaic cells prepared from (e) CMI@TiO_2@FTO and (f) CMI@NiO@FTO photoelectrodes colored by soaking method or by EPD during 30 s at 20 and 15 V respectively. The used electrolytes were the I^-/I_3^- and the cobalt complex CMI@TiO_2@FTO and CMI@NiO@FTO photoelectrodes respectively. Reproduced from 99 with permission from Elsevier.

In parallel, to these results on DSCC solar cells, Renaud *et al.* claimed, for the first time, the potential of the Mo_6 cluster-based nanoarchitectonic owning the characteristic as ambipolar materials [104]. Ambipolar material is known as new semiconducting compounds in which holes and electrons can intrinsically transport and transfer simultaneously [253,254]. In this unique case, the thin films of the aqua-complex-based compound $[\{Mo_6I_8^i\}I_4^a(H_2O)_2^a]\cdot xH_2O$ prepared by EPD was studied through an in-depth photoelectrochemical performance. The charge transport properties depended on the potential values in dark or under light and the behavior of the electrodes (n-type and p-type)

(Figure 15a). All electrodes (Fluorine doped tin oxide (FTO), MC film, MC pellet) were demonstrated a straight line with a positive slope characteristic of n-type conductivity, favoring electron transport in the MC compound (Figure 15b). The MC iodide absorber composed of the photoelectrode of the all-solid solar cell was measured the current-voltage characteristics in the dark and under AM1.5 illumination (1000 $W \cdot m^{-2}$) of this p-i-n junction (Figures 15c and d). The photoresponse demonstrated the hole and electron injection from the MC layer to semiconducting electrodes with the similar lifetime and opposite directions, a proof of ambipolar behavior. These charge carrier transports are possible to across the solar cell because of the full adequacy between the energy levels of each layer (Figure 15e). The nanoarchitectonic materials based on transition clusters open a potential in the field of photovoltaics for the collection of light and the generation of electron/hole pairs.

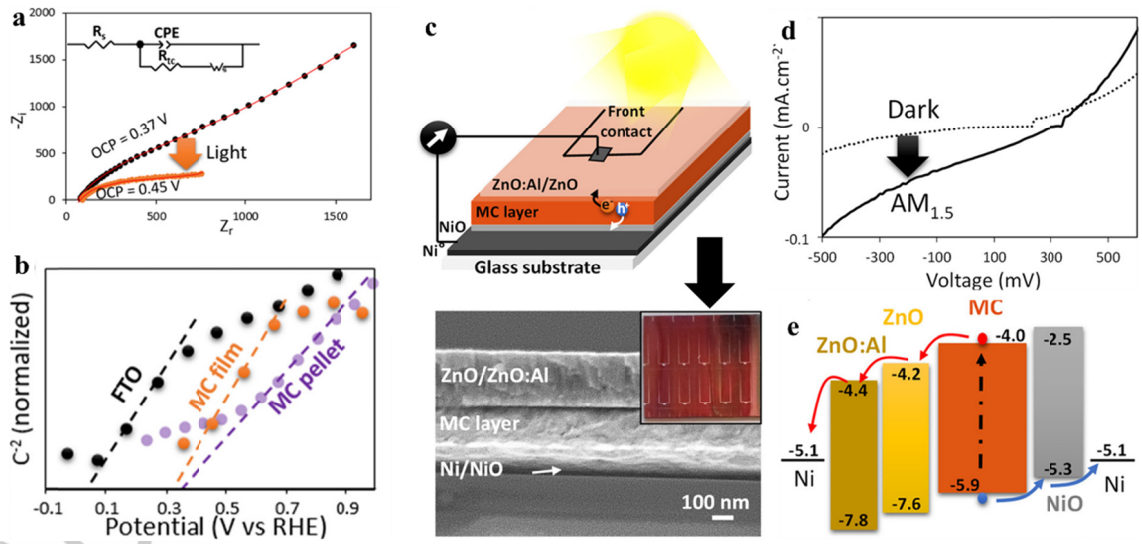

Figure 15. (a) Nyquist plots of the electrochemical circuit in the dark and under illumination at OCP and the equivalent circuit used to fit them. (b) Mott–Schottky plots for the MC film deposited on FTO, the FTO substrate, and the $Cs_2[\{Mo_6I_8^i\}I_6^a]$ dense pellet depicted vs RHE by using the formulae $V_{fb}(RHE) = V_{fb}(Ag/AgCl) + 0.059\ pH + V_{Ag/AgCl}(RHE)$. (c) MC-based all-solid solar Cell, (d) I(V) measurements in the dark and under AM1.5 Illumination, (e) energy levels of each layer on an absolute scale with respect to vacuum. Adapted with permission from 104. Copyright 2022 American Chemical Society.

3.1.4 Pathogenic bacterial biofilms

The last example of thin film prepared by EPD of pure Mo_6 nanoclusters is reporting the recent work of Kirakci *et al.* on very promising coating for mitigation of pathogenic bacterial biofilms under blue light. [138] They utilized EPD to prepare dense layers of the $Na_2[Mo_6I_8(OPOPh_2)_6]$ (1) and $[Mo_6I_8(OCOC_4H_8PPh_3)_6]$-$Br_4$ (2) clusters compounds deposited on ITO coated glass (Figure 16a). The MC layers showed high transparency and thickness of about 1 micron even though the morphology existed big particles (Figure 16b). The photoexcited MCs created singlet oxygen $O_2(^1\Delta_g)$ which was able to inactivate several pathogens. The study revealed that continuous irradiation of 460 nm light on the EPD film resulted in strong antibacterial properties on Gram-positive *Staphylococcus aureus* and *Enterococcus faecalis*, as well as, Gram-negative *Pseudomonas aeruginosa* and *Escherichia coli* bacterial strains (Figures 16d and e). Both layers displayed strong inhibition of the biofilm growth, and moreover, the film with the cluster 1 is also able to eradicate of matured biofilms, which is very interesting. These Mo_6 cluster-based photoactive layers are attractive for the design of antibacterial biofilm activated by visible light and reduce the harm of UV/blue light due to production of red light or oxygen sensing. The study of the electrophoretically photoactive MC film on the fight against infective microorganisms under blue light opens a new strategy for the mitigation of pathogenic bacterial biofilms.

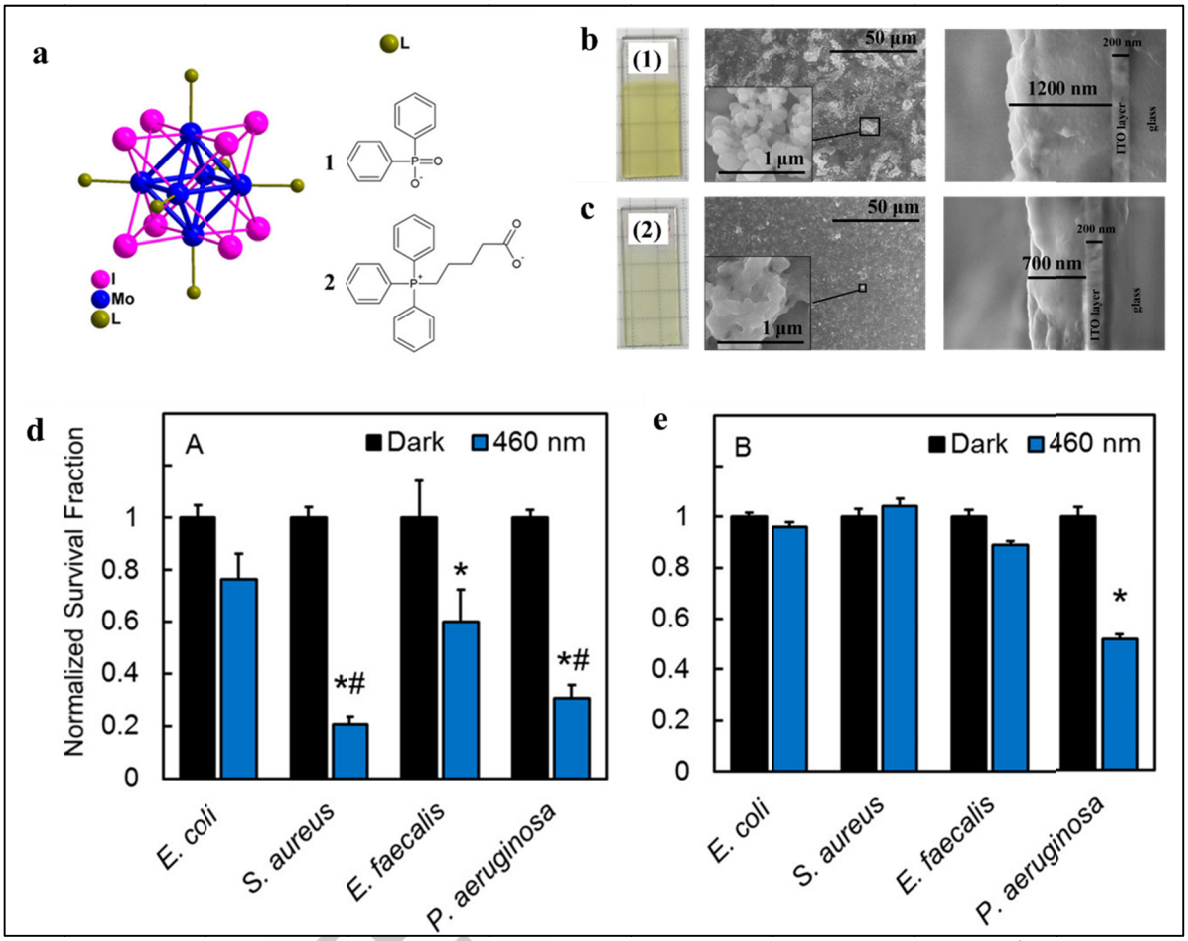

Figure 16. (a) Schematic representation of complexes $[Mo_6I_8(OPOPh_2)_6]^{2-}$ (1) and $[Mo_6I_8(OCOC_4H_8PPh_3)_6]^{4+}$ (2). Photographs of the 1/ITO glass (b) and 2/ITO (c) glass layers under visible light, surface morphology (middle), and cross-section (right) images. Eradication of matured biofilms on 1/ITO glass (d) and 2/ITO glass (e) after exposure to 460 nm light for 1 h (18 mW cm^{-2}). Notes: *significantly different from the respective dark control; and #significantly different from *E. coli* under 460 nm light. Adapted with permission from 138. Copyright 2020 American Chemical Society.

3.1.5 UV and NIR blocking transparent thin films for window application

Previous results demonstrated that EPD is the most relevant technique to prepare pure Mo_6 metal cluster-based thin film, however, for unknown reasons yet, it failed to be applied for some Mo_6 clusters containing for instance the distinctive characteristic of the apical ligand (Cl or $OCOC_2F_5$). In similar way, even if Ta_6 or Nb_6 nanoclusters could be deposited as a single component, their instability in air is too high to prepare stable pure functional films

(see for instance [96]). To overpass this problem, small amount of polymer was used as binders to support the dispersing ability of the clusters and their chemical stabilization. For instance, transparent films containing $[\{Mo_6I^i_8\}I^a_4(OCOC_2F_5)_2]^{2-}$ cluster unit and $[\{Nb_6X^i_8\}X^a_6]^{4-}$ (X = Cl, Br) cluster units were fabricated by using EPD with the support of poly(methyl methacrylate) (PMMA) as a stabilizing binder. Transparent thin films were obtained with thicknesses of about 1.5-micrometer. They exhibited strong absorption in range of UV and NIR light as well as high transparency in range of visible light (>60%), and an improved stability against moderate temperature and humidity conditions. [207] As these specific Mo_6 and Nb_6-based cluster units, a Ta_6-based cluster dispersed in MEK was successfully deposited on the ITO-coated glass by EPD as the first example. [96] However, the film quality was opaque with the existence of big particles. There were specific phenomena that needed to be clear in this original work. First, the green-colored $[\{Ta_6(Br)^i_{12}\}(H_2O)^a_6]^{2+}$ species was stable in water, however, it is failure to prepare film by EPD. Second, by using ketones (acetone or MEK) as a good dispersing medium for EPD, a brown Ta-based cluster film was successfully deposited on an anodic electrode as seen in figure 17a. This unwanted changing of color was simply explained by the oxidation of the clusters from $[\{Ta_6(Br)^i_{12}\}(H_2O)^a_6]^{2+}$ to brown-colored $[\{Ta_6(Br)^i_{12}\}(H_2O)^a_6]^{3+/4+}$ cluster units. Considering the kinetics of the oxidation and the necessity to used ketone as solvents for EPD, an investigation of the addition of water was carried out by Nguyen *et al.* Films containing green-colored $\{Ta_6(Br)^i_{12}(H_2O)^a_6\}^{2+}$ unit species were successfully fabricated with adding a small amount of water (Figure 17b). However, again it was impossible to maintain the green color for several days at room temperature in air due to the high reactivity of the Ta_6 cluster units. Finally, it was found that polyvinylpyrrolidone (PVP) was an excellent stabilizer of the green-colored $\{Ta_6(Br)^i_{12}(H_2O)^a_6\}^{2+}$ cluster species to obtain the homogeneous films and to improve their transparency using an optimized EPD process (Figures 17c and d). Films with a transparency upper than 60 % in the visible and strong absorption in the UV and NIR light ranges were obtained (Figure 17e). The efficiency in energy saving of these new UV-NIR filters was estimated by the determination of different figure of merit (FOM) values, such as T_{vis}, T_{sol} and T_{vis}/T_{sol} (T_{sol} = solar transmittance and

T_{vis} = visible transmittance), and the color coordinates (x, y, z and L*a*b). The T_{vis}/T_{sol} ratio of the Ta-based thin film is equal to 1.25 for the best films that is potential result for energy saving window-based applications.

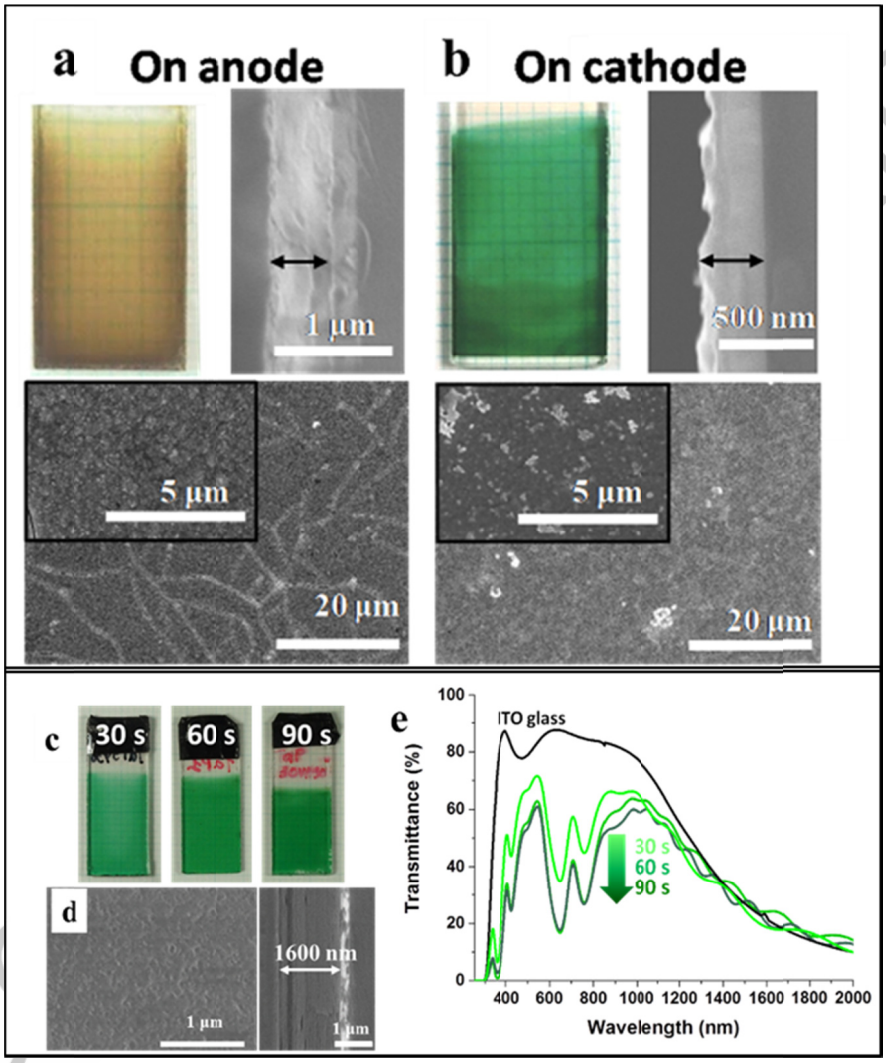

Figure 17. Photograph and SEM images of the cross section and surface of (a) the brown-Ta_6@ITO film (25 V and 60 s); (b) the green-Ta_6@ITO film (20 V and 60 s). (c) Photographs of 1x2.5 cm substrates and (d) SEM images of green-Ta_6@PVP@ITO films on 1 x 2.5 cm substrates prepared at 30 V and 30 s. e) UV-Vis-NIR transmission spectra of the ITO substrate and the green-Ta_6@PVP@ITO films on 1x2.5 cm substrates obtained at 30 V and 30 s, 60 s and 90 s. Reproduced from 96 with permission from the Royal Society of Chemistry.

As mentioned in the 0D SiO_2 nanocomposites section, Ta_6 and Nb_6 cluster units were

embedded into SiO_2 nanoparticles by reverse microemulsion method. [98,199] These 0D nanocomposite were used to prepare the first all inorganic film nanocomposites. HAADF-STEM images of ITO@Ta_6@SiO_2 NPs indicated a core-shell structure of about 76 nm averagely with the presence of discrete ITO nanoparticles occupied in the center. In addition, the Ta_6 cluster units were uniformly dispersed with a size of 1 nm in the whole SiO_2 shell. (Figure 18a). The elements (Si, O, In, Ta, and Br) were confirmed in the EDS spectrum that proved the successful synthesis of ITO@Ta_6@SiO_2 NPs (Figure 18b). Thanks to the negative zeta potential of ITO@Ta_6@SiO_2 NPs in acetone, EPD was successfully applied to fabricate the ITO@Ta_6@SiO_2 film with the relative thickness (0.9 to 1.5 microns) (Figure 18c). As expected, these ITO@Ta_6@SiO_2 films showed strong absorption in the UV light range with high transparency and the appearance of a band of 800 nm which indicates the improvement towards energy saving applications (Figure 19d). [98].

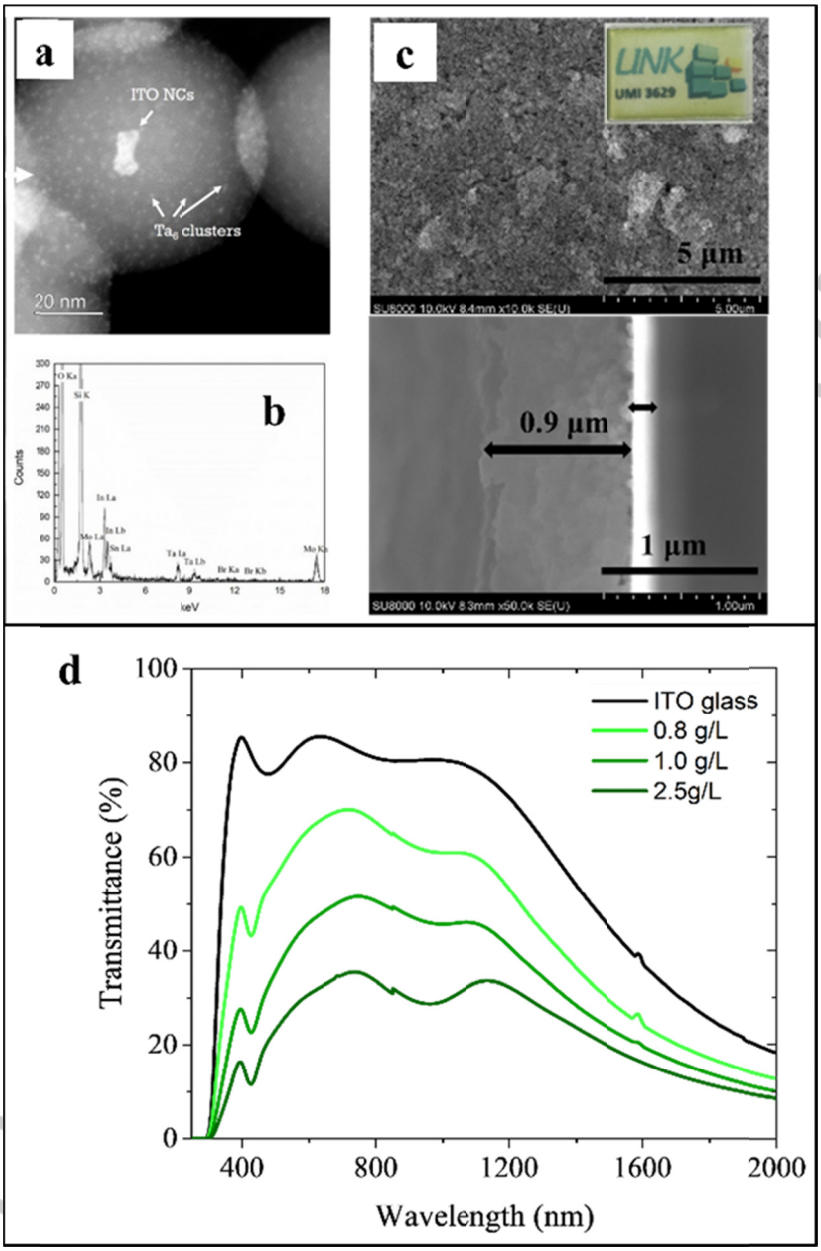

Figure 18. (a) high magnification of HAADF-STEM images of ITO@Ta_6@SiO_2 NPs; (b) EDS spectrum (point mode) of ITO@Ta_6@SiO_2 NPs revealing the coexistence of Si, O, In, Sn, Ta, Br elements. (c) Optical photographs and SEM micrographs, surface morphology and cross section of ITO@Nb_6@SiO_2 based films prepared from solution concentrations equal to 0.8 g/L and deposited by EPD at 20 V for 20 s. (d) Transmission UV-Vis-NIR spectra of the ITO@Nb_6@SiO_2 NPs-based films on the ITO-coated glass by varying the solution concentration (0.8; 1.0; and 2.5 g/L); the spectrum of the substrate is used as a reference. Reproduced from 98 with permission from the Royal Society of Chemistry.

3.1.6 Photodetector

Silica is not the only inorganic matrix available for preparing all inorganic nanocomposite thin films based on transition metal atom clusters. Very recently, Nguyen *et al.* demonstrated the possibility to use LDH matrix. [151]. By using EPD, a thin and transparent $Cs_2[Mo_6I^i_8I^a_6]$-functionalized LDH film (~ 3µm) was successfully prepared with a dense lamellar structure (Figure 19a). It was revealed that these films exhibited several interesting complementary properties, i.e., i) a red emission centered at the wavelength of 690 nm by UV-Vis light irradiation, ii) an anionic conductivity of about 10^{-6} $S.cm^{-1}$ with an activation energy (E_a) of about 1.08 eV, iii) a proper photocurrent response under UV-Vis light excitation ranging from 320 to 540 nm, and iv) a photocurrent response depending on the film thickness, temperature, and humidity (Figures 19 b and c). The remarkable point in this study is the determination of the relation between the photoresponse and the temperature or the humidity which has not been figured out, to the best of our knowledge, in previous reports about LDH-based materials. [255-258] The reproducibility and stabilization of the sample's photocurrent response were established. The excellent photoconductivity properties sensitizing with temperature and humidity obtained from the electrophoretic Mo_6-functionalized LDH films supported application potential for photo-humidity sensing and a photodetector.

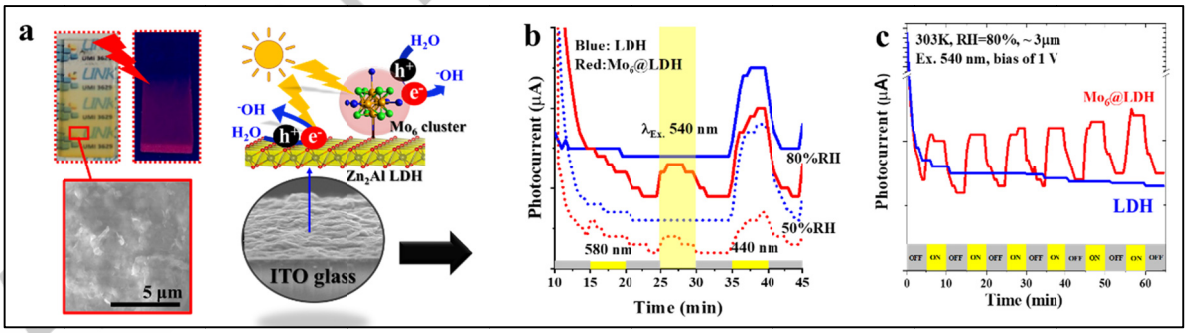

Figure 19. (a) Photographs of the UV-Vis irradiated films, the morphology (left) and cross-section (right) images of the thin film prepared by EPD. (b) The photocurrent controlled by on-off switching procedure under the illumination by different light wavelengths of the LDH and Mo_6@LDH films measured at RH of 50% and RH of 80 % and 303 K versus the time. (c) The repeatability of the photocurrent responses of the LDH and Mo_6@LDH films versus the on-off switching time with $\lambda_{ex.}$ = 540 nm. Adapted with permission from 151.

This section clearly shows that this field of research is really new and has very strong potential in key areas for the future (PV, mitigation of pathogenic, sensors). The use of EPD to fabricate thin films based on clusters of transition metals is a real breakthrough. Considering the importance of the activity on thin films in the economy and the already active use of EPD in industry, we can imagine that this strong potential will be materialized by innovations very soon.

3.2 CSD processes

As explain in the previous section, EPD can be used for the fabrication of pure octahedral cluster-based and nanocomposite thin films with no matrix or binders thanks to the charge on cluster units. In parallel, more conventional coating methods such as spin-coating, dip-coating or drop-casting are also efficiently employed despite the ceramic-like aspect of metallic clusters synthesized by solid-state chemistry. Indeed, as already mentioned molecular MC can be solubilized in many solvents which facilitates their coating process. Furthermore, the advantage of such process lies in the fact that it is possible to modify the chemistry, i.e., the ligand nature or the VEC before the deposition. The main issue is to control these parameters during all the shaping process.

Depending on the application or the property that needs to be enhanced, MC can simply be associated with a binder [80,92,144,105-107] to facilitate the chemical solution deposition (CSD) process or it can be part of a more elaborate devices including several layers, [107, 156,160] ink, [187] polymer dispersed liquid crystal, [101] quantum dots and nanocrystals [102,171,192] or DSSC electrodes.[93, 97]

3.2.1 Photonic and photovoltaic devices

Thanks to their high phosphorescent properties, Mo_6 and Re_6 nanoclusters are actively used for optical thin film and coating devices. Indeed, the development of luminescent thin films and coatings free of heavy metal or rare earth elements is an important issue for environmental reasons and energy efficiency. The first examples of such hybrid

nanocomposites were reported in 2013. [156,171] Aubert *et al.*, first reported a ZnO-$Cs_2[\{Mo_6Br_8\}Br_6]$@PVP film with an average thickness of 3 µm. [171] The properties of such films were improved later by Truong *et al.* by replacing the bromine nanoclusters by a more efficient, $Cs_2[\{Mo_6I_8\}(OOC_2F_5)_6]$. [192] Interestingly, in these similar processes, nanocomposite colloids of ZnO nanocrystals and Mo_6 nanocluster compounds were prepared by very simple and low-cost solution chemistry including PVP as matrix. The resulting solutions have been used to fabricate highly transparent and tunable luminescent films free of heavy metals or rare earth elements. The luminescence properties of the later system are highly tunable (from yellow to red emission) and the emission wavelength is strongly dependent on the ratios between ZnO and CMIF amounts and the excitation wavelength. In parallel, in 2013, Zhao *et al.* prepared novel transparent luminescent solar concentrators devices composed of phosphorescent Mo_6 chloride nanoclusters. [92] The near-perfect absorption cutoff at the edge of the visible spectrum (430 nm) and the massive Stokes shift to the near-infrared (800 nm) of these nanoclusters allows for efficient and selective harvesting of ultraviolet (UV) photons, improved reabsorption efficiency and non-tinted transparency in the visible spectrum. Since, these pioneer works, excellent results were obtained by several groups in the world for light emitting devices [156, 160] or transparent luminescent solar concentrators. [101, 102]

3.2.2 UV and NIR blocking transparent thin films for window application

Previous section mentions that Nb_6 or Ta_6 nanoclusters could be deposited by EPD technique but it needs more steps than with Mo_6. Their instability in air has to be considered by using a binder. Recent studies focus on the chemistry of niobium and tantalum clusters from an experimental and a theoretical aspect. [61,106] It helps to understand some mechanisms and properties of the cluster units $[\{M_6X^i_{12}\}L^a_6]^{n-/+}$ (M = Nb, Ta ; X= Cl, Br ; L = X, H_2O ; $2 \leq n \leq 4$) in the solid-state and in solution. Ta_6 clusters show a strong absorption in UV, whereas Nb_6 clusters present a great absorption in NIR (Figure 20b). Starting from this advancement, heterometallic clusters, i.e. $[\{Nb_{6-x}Ta_xX^i_{12}\}L^a_6]^{n-/+}$ ($1 \leq x \leq 5$) have been synthesized and studied. Their UV and NIR blocking capacity were

evaluated according to their VEC. [105, 106]

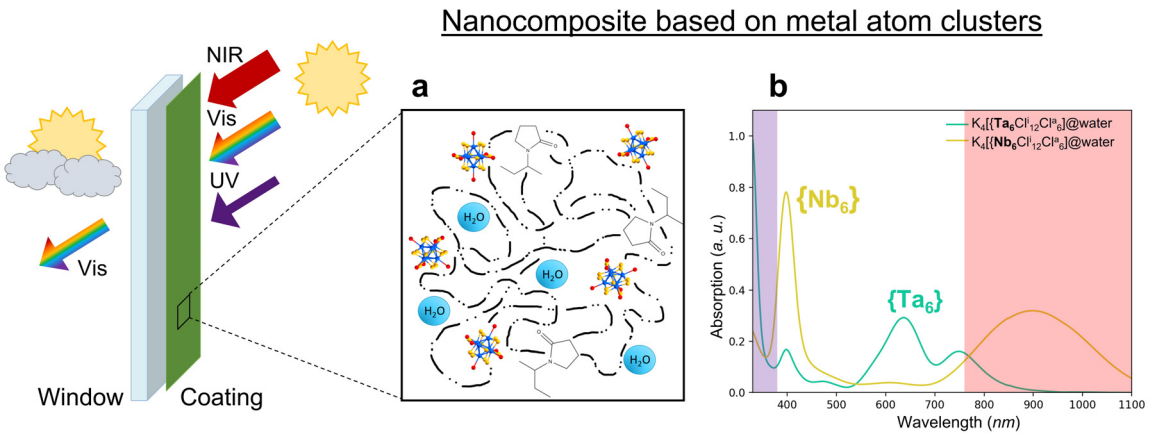

Figure 20. (a) Sketch of the nanocomposite based on metal atom clusters $[\{M_6X^i_{12}\}X^a_6]^{4-}$. (b) UV-Vis absorption spectra of $K_4[\{M_6Cl^i_{12}\}Cl^a_6]$ (M = Nb, Ta) in water. Reproduced from 107 with permission from Taylor and Francis.

$[\{Nb_{6-x}Ta_xX^i_{12}\}H_2O]^{2+}$ (X = Cl, Br) cluster units are stable in water and can be then integrated in organic (PVP) or hybrid (SiO_2-PEG) matrix by drop-casting or Mayer rod coating process in a reproducible way (Figure 21a). These matrices agree with a solar application (transparency, cost, implementation), can be shaped with a thickness of a few tens of micrometers (Figure 21) and are prepared in aqueous solution, without extra steps. Furthermore, it is possible to control the VEC and so, the optical properties of the cluster units from their solubilization to their integration into the matrixes. Experimental and theoretical studies highlight which oxidation state of the integrated cluster units should be selected for a solar control application. Nb_6 and hetero-metallic Nb_5Ta clusters show higher NIR shielding at VEC 16 whereas Ta_6 clusters need to be oxidized to VEC 15 to absorb in the NIR region. However, VEC 14 has to be avoided for homo and heterometallic clusters because of their low UV and NIR absorption. Based on their electrochemical potential in water, SnX_2 (X = Cl, Br) (Figure 21b) and $Fe(NO_3)_3$ have been used during the process to keep Nb_6 and Nb_5Ta clusters at VEC 16 or to oxidized Ta_6 clusters to VEC 15 respectively. Optical properties were maintained throughout the process and evaluated for the obtained nanocomposites.

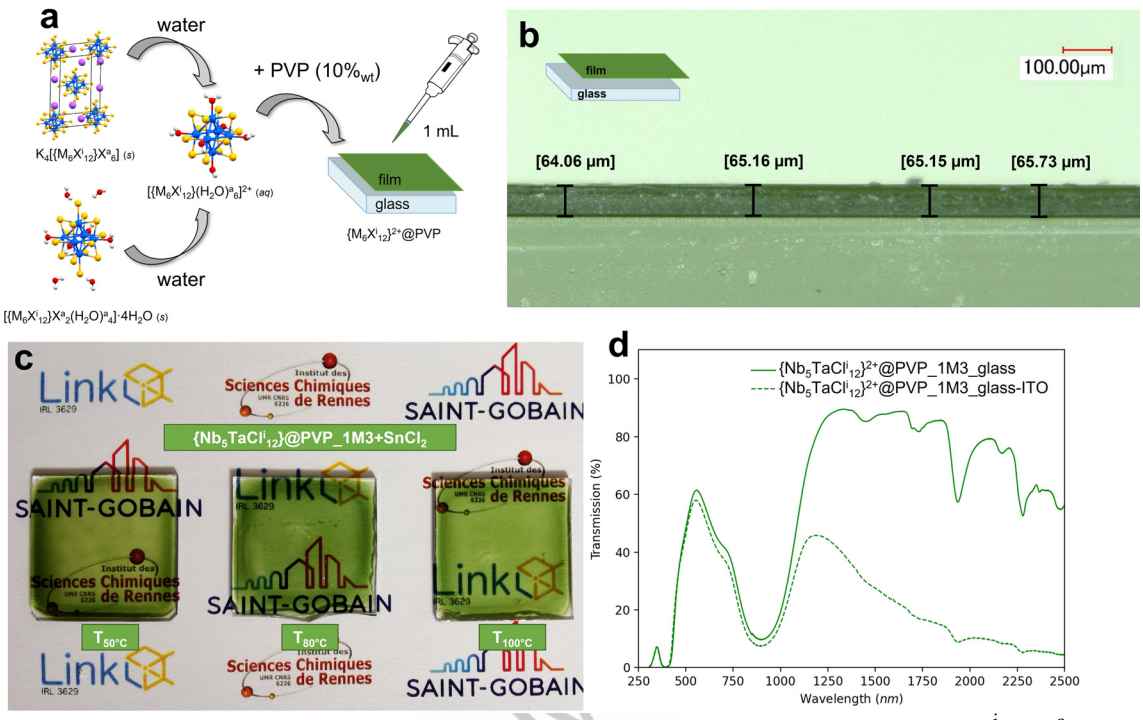

Figure 21. (a) Sketch of the PVP film preparation from $K_4[\{M_6X^i_{12}\}X^a_6]$ or $[\{M_6X^i_{12}\}X^a_2(H_2O)_4]\cdot 4H_2O$. (b) Digital microscope picture of the cross section of a $\{M_6X^i_{12}\}$@PVP nanocomposite film on a glass substrate. (c) Picture of the nanocomposite films after obtained from the $\{Nb_5TaCl^i_{12}\}^{2+}$ (VEC 16) cluster core reduced by $SnCl_2$ in PVP and after a thermal treatment (T = 50, 80 and 100°C) during 18 hours. (d) UV-Vis transmission spectra of $\{Nb_5TaCl^i_{12}\}$@PVP (VEC 16) on glass and ITO glass substrate. Reproduced from 105 and 107 with permission from MDPI and Taylor and Francis.

As well as for films obtained by EPD, FOM values (T_{vis}, T_{sol}, T_{vis}/T_{sol}, S_{NIR}) and color coordinates were measured for films obtained by CSD process. $\{Nb_6X^i_{12}\}$ (VEC = 16) and $\{Ta_6X^i_{12}\}$ (VEC = 15) cluster cores show similar values of T_{vis}/T_{sol} (1.27-1.29) when integrated in PVP films on a glass substrate. The highest values were reached with $\{Nb_5TaX^i_{12}\}$ (1.30-1.33) and even higher by including an ITO layer (1.73) (Figure 21c). Indeed, the NIR shielding of clusters mainly absorb between 700 and 1100 nm, whereas NIR reflection of ITO is above 1200 nm. Their association allow to get rid of almost all the NIR solar radiation and to obtain excellent T_{vis}/T_{sol} and S_{NIR} values. By comparison, a perfect solar control material can be simulated with a film that transmits 90% of visible

light, and absorbs 100% of UV (200–400 nm) and NIR (780–2500 nm). Its T_{vis}/T_{sol} ratio would be 1.85.

4. Conclusions

It has been clearly demonstrated that the remarkable properties of the octahedral transition metal atom clusters can be largely preserved and enhanced in the form of nanocomposites. Introduction to various Nb_6, Mo_6, Ta_6, W_6, Re_6 molecular nanoclusters in nanocomposites with two-dimensional, one-dimensional and zero-dimensional morphologies has been presented in this review paper. Matrices ranging from organic polymers to inorganic layered oxides can be used and adapted to the targeted applications. The clear potential and synergetic effects of these nanocomposites for biotechnology applications, PV, solar control, catalytic, photonic and sensor applications was strongly demonstrated. Indeed, the incorporation of metal atom clusters into matrix supports enhances their stability, their photoactivity and could improve their cellular uptake for biotechnologies, compared to free clusters. This review also provides a basic level of understanding how nanocomposites are characterized and processed using different technics and methods. As a new strategy, the electrophoretic deposition process appears to be very efficient to fabricate highly transparent, homogeneous and functional nanocomposite thin films and coatings.

Of course, this field of research is quite young and new challenges and opportunities using transition metal clusters as building blocks for multifunctional nanocomposites are numerous. This field can be extended to the use of other transition metal clusters, such as titanium, vanadium, copper, zirconium or event heterometallic systems as already started by Lebastard *et al.*. [105, 107, 258-263] This family of nanoclusters is extremely rich and could be even probably enriched by using machine learning methods. [264-266] Controlled self-assembly of nanoclusters could play a key role in customizing advanced functional materials via collective and synergetic properties between neighbored building blocks. [267] As briefly mentioned in the introduction, the condensation and dimensionality of the metal atom clusters influence strongly the electronic properties and an association with an adequate matrix could generate new nanocomposites. For instance, the mixing of MCs with

semiconductor nanocrystals could also be very interesting for photovoltaic applications. Moreover, to increase the dimensionality of the metal atom clusters could be very interesting in terms of thermal stability for instance, which is still a weak point for the molecular nanoclusters.

Furthermore, recently, calculations suggested that Nb_6 or Ta_6 clusters could be used for new material design, for instance as cations in hybrid organic-inorganic perovskites, as a substitute for toxic Pb. Indeed, band gaps, band alignment, and hydrogen adsorption calculations show that the designed cluster-based hybrid perovskites have potential as intermediate-band materials for photovoltaics, and as photocatalysts for the hydrogen evolution reaction. [268] Another possibility is to use these transition metal atom clusters as precursors for the discovery of new compounds and nanocomposites like nitrides, carbides, borides, sulfides or alloys. [269-273] The field of possibilities is open to everyone and the adventure of the nanocomposites based on metal atom clusters has only just begun.

Acknowledgments

The authors are grateful to T. Aubert, W. Chen, B. Dierre, F. Dorson, M. Dubernet, K. Harada, O. Makrygenni, C. Neaime, N. Nerambourg, N. Saito, F. Sciortino and G. Truong, who made a part of their internship, PhD or postdoc work on the "nanocomposites based on MC" research project. The authors deeply thank Dr. Y. Matsui, T. Takei from NIMS and M. C. Derouet, M. V. Dorcet, M. F. Gouttefangeas, Ms V. Le Cam and M. S. Paofai from Rennes Univ. (UR1) for their technical assistance support. The authors thank Prof. Y. Bando, Prof. H. Haneda, Prof. K. Kimoto, Dr. Y. Matsushita, Prof. T. Mori, Dr. N. Shirahata from NIMS and MANA-NIMS, Prof. S. Ravaine from Bordeaux Univ., Prof. K. Lang and Dr. K. Kiracki from the Institute of Inorganic Chemistry of the Czech Academy of Sciences, Dr M. Matsuda from Kumamoto Univ., Ms C. Comby-Zerbino, Dr. L. MacAleese, F. Chirot, P. Dugourd from Lyon Univ., Dr. S. Jobic and F. Odobel from Nantes Univ. and Dr. M. Amela-Cortes, Dr. F. Cabello-Hurtado, Dr. K. Costuas, Dr. P. Lemoine, Dr. Y. Molard from UR1 or CNRS for very fruitful discussion and collaborations. Some part of the experiments was performed on ScanMAT, UAR 2025 CNRS-UR1. This UAR received a financial support from the European Union through the European Regional Development Fund (ERDF), the Département d'Ille et Vilaine, Rennes Métropole and Région Bretagne (2015-2020 CPER project SCANMAT). The major part of the studies was carried out as a part of the France-Japan International Collaboration Framework (IRL3629

LINK). The authors wish to thank Mr. D. Lechevalier, Dr. M. Kono and Ms A. Shigemura of Saint-Gobain KK (Tokyo, Japan) and Dr. D. Berthebaud of CNRS for their significant support involved in LINK and related activities. A part of the works presented in this review has been financially supported by Saint-Gobain, NIMS, UR1, CNRS, JSPS, Region Bretagne and ANR (CLUSTOP-11-BS08-013-01; CLIMATE- 17-CE09-0018).

References

1) Blumstein A, Etude des polymerization en couche adsorbée. *Bull. Soc. Chim. Fr.* 1961:899–905.
2) Gorsse S, Hutchinson C, Gouné M, et al. Additive manufacturing of metals: a brief review of the characteristic microstructures and properties of steels, Ti-6Al-4V and high-entropy alloys. *Sci. Technol. Adv. Mater.* 2017;18(1):584–610.
3) Fu S, Sun Z, Huang P, et al. Some basic aspects of polymer nanocomposites: A critical review. *Nano Mater. Sci.* 2019;1:2–30.
4) Omanović-Mikličanin E, Badnjević A, Kazlagić A, et al. Nanocomposites: a brief review. *Health Technol.* 2020;10:51–59.
5) Liu R, Duaya J, Bok Lee S. Heterogeneous nanostructured electrode materials for electrochemical energy storage. *Chem. Commun.* 2011;47:1384–1404.
6) Aono M, Ariga K. The way to nanoarchitectonics and the way of nanoarchitectonics. *Adv. Mater.* 2016;28:989–992.
7) Ariga K, Nishikawa M, Mori T, et al. Self-assembly as a key player for materials nanoarchitectonics. *Sci. Technol. Adv. Mater.* 2019;20:51–95.
8) Ariga K, Fakhrullin R, Materials nanoarchitectonics from atom to living cell: A method for everything. *Bull. Chem. Soc. Jpn.* 2022;95:774–795.
9) Hu W, Shi J, Lv W, et al. Regulation of stem cell fate and function by using bioactive materials with nanoarchitectonics for regenerative medicine. *Sci. Technol. Adv. Mater.* 2022;23(1):393–412.
10) Chen G, Singh SK, Takeyasu K, et al. Versatile nanoarchitectonics of Pt with morphology control of oxygen reduction reaction catalysts. *Sci. Technol. Adv. Mater.* 2022;23(1):413–423.
11) Shen X, Song J, Sevencan C, et al. Bio-interactive nanoarchitectonics with two-dimensional materials and environments. *Sci. Technol. Adv. Mater.* 2022;23(1):199–224.
12) Park HJ, Shin DJ, Yu J. Categorization of quantum dots, clusters, nanoclusters, and nanodots. *J. Chem. Educ.* 2021;98:703−709.
13) Breitscheidel B, Zieder J, Schubert U. Metal complexes in inorganic matrixes. 7. Nanometer-sized, uniform metal particles in a silica matrix by sol-gel processing of metal complexes. *Chem. Mater.* 1991;3(3):559–566.
14) Gacoin T, Chaput F, Boilot JP. Complexed metal clusters in organically modified oxide matrices. *Chem. Mater.* 1993;5:1150–1156.
15) Shang L, Dong SJ, Nienhaus GU. Ultra-small fluorescent metal nanoclusters: Synthesis and biological applications. *Nano Today.* 2011;6:401–418.

16) Sun HT, Sakka Y. Luminescent metal nanoclusters: controlled synthesis and functional applications. *Sci. Technol. Adv. Mater.* 2014;15:014205.
17) Chakraborty I, Pradeep T. Atomically precise clusters of noble metals: Emerging link between atoms and nanoparticles. *Chem. Rev.* 2017;117:8208−8271.
18) Fu F, Dedieu A, Wang W, et al. Stabilization of a new nanocomposite family by reduction of gold nanoclusters with electron-reservoir complexes. *Chem. Commun.* 2019:55:10277–10280.
19) Su Y, Xue T, Liu Y, et al. Luminescent metal nanoclusters for biomedical applications. *Nano Research*. 2019;12:1251–1265.
20) Doud EA, Voevodin A, Hochuli TJ, et al. Superatoms in materials science. *Nature Rev. Mater.* 2020;5(5):371–387.
21) Zhang Y, Feng N, Zhoua S, et al. Fluorescent nanocomposites based on gold nanoclusters for metal ion detection and white light emitting diodes. *Nanoscale.* 2021;13:4140–4150.
22) Hasegawa S, Tsukuda T. Exploring novel catalysis using polymer-stabilized metal clusters *Bull. Chem. Soc. Jpn.* 2021;94:1036–1044.
23) Kawawaki T, Shimizu N, Mitomi Y, et al. Supported, ∼1-nm-Sized platinum clusters: controlled preparation and enhanced catalytic activity. *Bull. Chem. Soc. Jpn.* 2021;94:2853–2870.
24) Chen T, Lin H, Cao Y, et al. Interactions of Metal Nanoclusters with Light: Fundamentals and applications. *Adv. Mater.* 2021;2103918.
25) Seong H, Efremov V, Park G, et al. Atomically precise gold nanoclusters as model catalysts for identifying active sites for electroreduction of CO_2. *Angew. Chem. Int. Ed.* 2021;60:14563–14570.
26) Huang JH, Si Y, Dong XY, et al. Symmetry breaking of atomically precise fullerene-like metal nanoclusters. *J. Am. Chem. Soc.* 2021;143(32):12439–12444.
27) Qian S, Wang Z, Zuo Z, et al. Engineering luminescent metal nanoclusters for sensing applications. *Coord. Chem. Rev.* 2022;451:214268.
28) Masuda S, Takano S, Yamazoe S, et al. Synthesis of active, robust and cationic Au_{25} cluster catalysts on double metal hydroxide by long-term oxidative aging of $Au_{25}(SR)_{18}$. *Nanoscale.* 2022;14:3031–3039.
29) Cordier S, Dorson F, Grasset F. Novel nanomaterials based on inorganic molybdenum octahedral clusters. *J. Clust. Sci.* 2009;20:9–21.
30) Aubert T, Grasset F, Mornet S, et al. Functional silica nanoparticles synthesized by water-in-oil microemulsion processes. *J. Colloid Interface Sci.* 2010;341(2):201–208.
31) Cordier S, Molard Y, Brylev KA, et al. Advances in the engineering of near infrared emitting liquid crystals and copolymers, extended porous frameworks, theranostic tools and molecular junctions using tailored Re_6 cluster building blocks. *J. Clust. Sci.* 2014;26(1):53–81.
32) Cordier S, Grasset F, Molard Y, et al. Inorganic molybdenum octahedral nanosized cluster units, versatile functional building block for nanoarchitectonics. *J. Inorg. Organomet. Polym. Mater.* 2015;25(2);189–204.

33) Molard Y, Clustomesogens: liquid crystalline hybrid nanomaterials containing functional metal nanoclusters. *Acc. Chem. Res.* 2016;49:1514–1523.
34) Nguyen TKN, Renaud A, Dierre B. Extended study on electrophoretic deposition process of inorganic octahedral metal clusters: advanced multifunctional transparent nanocomposite thin films. *Bull. Chem. Soc. Jpn.* 2018;91:1763–1774.
35) Xie J, Wang L, Anderson JS. Heavy chalcogenide-transition metal clusters as coordination polymer nodes. *Chem. Sci.* 2020;11:8350–8372
36) Verger A, Brandhonneur N, Molard Y, et al. From molecules to nanovectors: Current state of the art and applications of photosensitizers in photodynamic therapy. *Int. J. Pharm.* 2021;604:120763.
37) Cotton, F.A. Metal *Atom Clusters in Oxide Systems*. *Inorg. Chem.* 1964;3:1217–1220.
38) Selby HD, Zheng Z. New directions of cluster chemistry – the story of the $[Re_6(\mu_3\text{-}Se)_8]_{2+}$ clusters. *Comments Inorg. Chem.* 2005;26(1-2):75–102.
39) Perrin A, Perrin C. The molybdenum and rhenium octahedral cluster chalcohalides in solid-state chemistry: From condensed to discrete cluster units. *C. R. Chim.* 2012;15(9):815–836.
40) Fedorov V. Metal clusters. As they were born in Siberia. *J. Clust. Sci.* 2015;26(1):3–15.
41) Lemoine P, Halet JF, Cordier S. Ligated transition metal clusters in solid-state chemistry: The legacy of Marcel Sergent (Ed.: J.-F. Halet), Structure and Bonding, (Series ed.: D. M. P. Mingos), Springer International Publishing, 2019;180:143–190.
42) Chevrel R, Sergent M, Prigent J. Sur de nouvelles phases sulfurées ternaires du molybdène. *J. Solid State Chem.* 1071;3:515–519.
43) Zhou T, Lenoir B, Colin M, et al. Promising thermoelectric properties in AgxMo9Se11 compounds ($3.4 \leq x \leq 3.9$). *Appl. Phys. Lett.* 2011;98:162106
44) Aurbach D, Lu Z, Schechter A, Prototype systems for rechargeable magnesium batteries. *Nature* 2000;407:724–727.
45) Cario L, Vaju C, Corraze B, et al. Electric-field-induced resistive switching in a family of mott insulators: Towards a new class of RRAM memories. *Adv. Mater.* 2010;22:5193–5197.
46) Sokolov MN, Mihailov MA, Peresypkina EV, Highly luminescent complexes $[Mo_6X_8(n\text{-}C_3F_7COO)_6]^{2-}$ (X = Br, I). *Dalton Trans.* 2011;40(24):6375– 6377.
47) Kirakci K, Kubát P, Dušek M, et al. A highly luminescent hexanuclear molybdenum cluster - a promising candidate toward photoactive materials. *Eur. J. Inorg. Chem.* 2012;8(19):3107– 3111.
48) Costuas K, Garreau A, Bulou A, et al. Combined theoretical and time-resolved photoluminescence investigations of $[Mo_6Br^i_8Br^a_6]^{2-}$ metal cluster units: evidence of dual emission. *Phys Chem Chem Phys.* 2015;17:28574–28585.
49) Dierre B, Costuas K, Dumait N, et al. Mo_6 cluster-based compounds for energy conversion applications: comparative study of photoluminescence and cathodoluminescence, *Sci. Technol. Adv. Mater.* 217;18(1):458–466.

50) Evtushok DV, Melnikov AR, Vorotnikova NA, et al. A comparative study of optical properties and X-ray induced luminescence of octahedral molybdenum and tungsten cluster complexes. *Dalton Trans.* 2017;46(35):11738–11747.
51) Ivanov AA, Konovalov DI, Pozmogova TN, et al. Water-soluble Re_6-clusters with aromatic phosphine ligands – from synthesis to potential biomedical applications. *Inorg. Chem. Front.* 2019;6:882–892.
52) Marchuk MV, Vorotnikova NA, Vorotnikov YA, et al; Optical property trends in a family of $\{Mo_6I_8\}$ aquahydroxo complexes. *Dalton Trans.* 2021;50:8794–8802.
53) McCarley RE, Hughes BG, Cotton FA, et al. The two-electron oxidation of metal atom cluster species of the type $[M_6X_{12}]^{2+}$. *Inorg. Chem.* 1965;*4:*1491–1492.
54) Espenson JH, McCarley RE. Oxidation of tantalum cluster ions. *J. Am. Chem. Soc.* 1966;*88:*1063–1064.
55) Fan PD, Deglmann P, Ahlrichs R. Electron counts for face-bridged octahedral transition metal clusters. *Chem. Eur. J.* 2002;8:1059–1067.
56) Ramirez-Tagle R, Arratia-Perez R. Electronic structure and molecular properties of the $[Mo_6X_8L_6]^{2-}$; X = Cl, Br, I; L = F, Cl, Br, I clusters. *Chem. Phys. Lett.* 2008;460(4–6):438–441.
57) Gray TG. Divergent electronic structures of isoelectronic metalloclusters: tungsten(II) halides and rhenium(III) chalcogenide halides. *Chem. - A Eur. J.* 2009;5(11):2581–2593.
58) Schott E, Zarate X, Alvarado-Soto L, et al. Effect over the electronic structure by changing the core metals from Mo to W in a family of $[Mo_{6-n}W_nCl_8F_6]^{2-}$ (n = 0–6) clusters. *Polyhedron.* 2013;65:98–101.
59) Saito N, Cordier S, Lemoine P, et al. Lattice and valence electronic structures of crystalline octahedral molybdenum halide clusters-based compounds, $Cs_2[Mo_6X_{14}]$ (X = Cl, Br, I), studied by density functional theory calculations. *Inorg. Chem.* 2017;56:6234–6243.
60) Kirakci K, Demel J, Hynek J, et al. Phosphinate apical ligands – a route to water-stable octahedral molybdenum cluster complex. *Inorg. Chem.* 2019;58:16546–16552.
61) Wilmet M, Lebastard C, Sciortino F, et al. Revisiting properties of edge-bridged bromide tantalum clusters in the solid-state, in solution and vice versa: an intertwined experimental and modelling approach. *Dalton Trans.* 2021;50:8002.
62) Novikova ED, Gassan ED, Ivanov AA, et al. Neutral Mo_6Q_8-clusters with terminal phosphane ligands – a route to water-soluble molecular units of Chevrel phases. *New J. Chem.* 2022;46:2218–2223.
63) Long JR, McCarty LS, Holm RH. A solid-state route to molecular clusters: access to the solution chemistry of $[Re_6Q_8]^{2+}$ (Q = S, Se) core-containing clusters via dimensional reduction. *J. Am. Chem. Soc.* 1996;118:4603–4616
64) Kirakci K, Cordier S, Perrin, C. Synthesis and characterization of $Cs_2Mo_6X_{14}$ (X = Br or I) hexamolybdenum cluster halides: Efficient Mo_6 cluster precursors for solution chemistry syntheses. *Z. Anorg. Allg. Chem.* 2005;631:411−416.
65) Piedra-Garza LF, Kockerling M Straightforward synthesis and structure of a new starting material for niobium cluster phases: $[Nb_6Cli_{12}(CH_3OH)^a{}_4Cl^a{}_2]\cdot 6CH_3OH$.

Inorg. Chem. 2006;45:8829−8831.
66) Shamshurin MV, Mikhaylov MA, Sukhikh T, et al. Octahedral $\{Ta_6I_{12}\}$ Clusters. *Inorg. Chem.* 2019;58:9028−9035.
67) Schröder F, Köckerling M. Improved access through ball milling: Octahedral Ta_6 cluster alkoxides with weakly coordinating cations and a rare example of an electron-poor Ta_6 cluster *Z. Anorg. Allg. Chem.* 2021;647:1625.
68) Grasset F, Dorson F, Cordier S, et al. Water-in-Oil microemulsion preparation and characterization of $Cs_2[Mo_6X_{14}]@SiO_2$ phosphor nanoparticles based on transition metal clusters (X = Cl, Br, and I). *Adv. Mater.* 2008;20:143–148.
69) Christiano SP, Wang J, Pinnavaia TJ. Intercalation of niobium and tantalum $M_6C1_{12}^{n+}$ cluster cations in Montmorillonite: A new route to pillared clays. *Inorg. Chem.* 1985;24(8),1223–1227.
70) Christiano SP, Pinnavaia TJ. Intercalation in Montmorillonite of molybdenum cations containing the Mo_6Cl_8 cluster core. *J. Solid State Chem.* 1986; 64, 232–239.
71) Newsham MD. Excited-state properties of transition-metal complexes in solution and the solid state; Thesis, Ph.D. Dissertation, Michigan State University, 1988.
72) Robinson LM, Lu H, Hupp JT, et al. Nature of the interaction and photophysical properties of $[Mo_6Cl^i_8(SO_3CF_3)^a_6]^{2-}$ and $[Mo_6Cl^i_8Cl^a_6]^{2-}$ on silica gel. *Chem. Mater.* 1995;7(1):43–49.
73) Jackson JA, Newsham MD, Worsham C, et al. Efficient singlet oxygen generation from polymers derivatized with hexanuclear molybdenum clusters. *Chem. Mater.* 1996;8:558–564.
74) Robinson LM, Shriver DF. Synthesis and photophysical properties of polymer-bound hexanuclear molybdenum clusters. *J. Coord. Chem.* 1996;37:119–129.
75) Ghosh RN, Baker GL, Ruud C, et al. Fiber-optic oxygen sensor using molybdenum chloride cluster luminescence. *Appl. Phys. Lett.* 1999;75(19):2885–2887.
76) Prokopuk N, Weinert CS, Siska DP, et al. Hydrogen-bonded hexamolybdenum clusters: formation of inorganic–organic networks. *Angew. Chem.* 2000;39(18):3312-3315.
77) Roland BK, Carter C, Zheng Z. Routes to metallodendrimers of the $[Re_6(\mu_3\text{-}Se)_8]^{2+}$ core-containing clusters. *J. Am. Chem. Soc.* 2002;124:6234–6235.
78) Selby HD, Orto P, Zheng Z. Supramolecular arrays of the $[Re_6(\mu_3\text{-}Se)_8]^{2+}$ core-containing clusters mediated by transition metal ions, *Polyhedron*. 2003;22:2999–3008
79) Roland BK, Flora WH, Carducci MD, et al. An inorganic-organic hybrid composite featuring metal-chalcogenide clusters. J. Cluster Sci. 2003;14:449-458.
80) Osborn DJ, Baker GL, Ghosh RN. Mo_6Cl_{12}-incorporated sol-gel for oxygen sensing applications. *J. Sol-Gel Sci. Technol.* 2005;36(1):5–10.
81) Roland BK, Flora WH, Selby HD, et al. Dendritic arrays of $[Re_6(\mu_3\text{-}Se)_8]^{2+}$ core-containing clusters: exploratory synthesis and electrochemical studies. *J. Am. Chem. Soc.* 2006;128(20):6620–6625.
82) Méry D, Plault L, Ornelas C, et al. From simple monopyridine clusters $[Mo_6Br_{13}(Py\text{-}R)][n\text{-}Bu_4N]$ and hexapyridine clusters $[Mo_6X_8(Py\text{-}R)_6][OSO_2CF_3]_4$ (X = Br or I) to cluster-cored organometallic stars, dendrons, and dendrimers. *Inorg.*

Chem. 2006;45(3):1156–1167.
83) Perruchas S, Flores S, Jousselme B, et al. [W_6S_8] octahedral tungsten clusters functionalized with thiophene derivatives: toward polymerizable building blocks. *Inorg. Chem.* 2007;46(21):8976–8987.
84) Grasset F, Molard Y, Cordier S, et al. When "metal atom clusters" meet ZnO nanocrystals: A $((n\text{-}C_4H_9)_4N)_2Mo_6Br_{14}$@ZnO hybrid. *Adv. Mater.* 2008;*20:*1710–1715.
85) Grasset F, Roullier V, Marchi-Artzner V, et al. Synthesis and characterization of magnetic-fluorescent composite colloidal nanostructure. *Proceeding 2nd IEEE International Nanoelectronics Conference* 2008;1023–1027.
86) Grasset F, Dorson F, Molard Y, et al. One-pot synthesis and characterizations of bi-functional phosphor–magnetic @SiO_2 nanoparticles: controlled and structured association of Mo_6 cluster units and γ-Fe_2O_3 nanocrystals. *Chem. Commun.* 2008;39:4729.
87) Grasset F, Cordier S, Molard Y, et al. Design of new M@ZnO nanocolloids: synthesis and shaping. *Int. J. Nanotechnol.* 2008;5(6-8):708–721.
88) Aubert T, Ledneva AY, Grasset F, et al. Synthesis and characterization of $A_4[Re_6Q_8L_6]$@SiO_2 red-emitting silica nanoparticles based on Re_6 metal atom clusters (A = Cs or K, Q = S or Se, and L = OH or CN). *Langmuir.* 2010;26(23):18512–18518.
89) Dechézelles JF, Aubert T, Grasset F, et al. Fine tuning of emission through the engineering of colloidal crystals. *Phys. Chem. Chem. Phys.* 2010;12(38):11993–11999.
90) Gao L, Peay MA, Gray TG. Encapsulation of phosphine-terminated rhenium(III) chalcogenide clusters in silica nanoparticles. *Chem. Mater.* 2010;22:6240–6245.
91) Dybtsev D, Serre C, Schmitz B, Influence of $[Mo_6Br_8F_6]^{2-}$ cluster unit inclusion within the mesoporous solid MIL-101 on hydrogen storage performance. *Langmuir.* 2010;26(13):11283–11290.
92) Zhao Y, Lunt R.R. transparent luminescent solar concentrators for large-area solar windows enabled by massive stokes-shift nanocluster phosphors. *Adv. Energy Mater.* 2013;3:1143−1148.
93) Renaud A, Grasset F, Dierre B, et al. Inorganic molybdenum clusters as light-harvester in all inorganic solar cells: A proof of concept. *ChemistrySelect.* 2016;1(10):2284–2289.
94) Feliz M, Puche M, Atienzar P, et al. In situ generation of active molybdenum octahedral clusters for photocatalytic hydrogen production from water. *Chem. Sus. Chem.* 2016;*9:1*963–1971.
95) Nguyen TKN, Dierre B, Grasset F, et al. Electrophoretic coating of octahedral molybdenum metal clusters for UV/NIR light screening. *Coatings.* 2017;7(8):114.
96) Nguyen TKN, Renaud A, Wilmet M, et al. New ultra-violet and near-infrared blocking filters for energy saving applications: Fabrication of tantalum metal atom cluster-based nanocomposite thin films by electrophoretic deposition. *J. Mater. Chem. C.* 2017;5:10477–10484.
97) Renaud A, Wilmet M, Truong TG, et al. Transparent tantalum cluster-based UV and

IR blocking electrochromic devices. *J. Mater. Chem. C.* 2017;5(32):8160–8168.
98) Chen W, Nguyen TKN, Wilmet M, et al. ITO@SiO_2 and ITO@{M_6Br_{12}}@SiO_2 (M = Nb, Ta) nanocomposite films for ultraviolet-near infrared shielding. *Nanoscale Adv.* 2019;1:3693–3698.
99) Renaud A, Nguyen TKN, Grasset F, et al. Preparation by electrophoretic deposition of molybdenum iodide cluster-based functional nanostructured photoelectrodes for solar cells. *Electrochim. Acta.* 2019;317:737−745.
100) Lunt RR, Zhao Y. Transparent luminescent solar Concentrators for integrated Solar windows. United State patent US10439090B2. 2019
101) Khlifi S, Bigeon J, Amela-Cortes M, et al. Switchable two-dimensional waveguiding abilities of luminescent hybrid nanocomposites for active solar concentrators. *ACS Appl. Mater. Interfaces.* 2020;12(12):14400–14407.
102) Choi J, Kim K, Kim SJ. Quantum dot assisted luminescent hexarhenium cluster dye for a transparent luminescent solar concentrator. *Sci. Rep.* 2021;11:13833.
103) Yang C, Sheng W, Moemeni M, et al. Ultraviolet and near-infrared dual-band selective-harvesting transparent luminescent solar concentrators. *Adv. Energy Mater.* 2021;11:2003581.
104) Renaud A, Jouan PY, Dumait N, et al. Evidence of the ambipolar behavior of Mo_6 cluster iodides in all-inorganic solar cells: a new example of nanoarchitectonic concept, *ACS Appl. Mater. Interfaces* 2022;14(1):1347–1354.
105) Lebastard C, Wilmet M, Cordier S, et al. Controlling the deposition process of nanocomposites based on {$Nb_{6-x}Ta_xX^i_{12}$} octahedral cluster building blocks (X^i = Cl, Br; $1 \leq x \leq 6$) for UV-NIR blockers coating applications. *Nanomaterials*. 2022; 12:2052.
106) Lebastard C, Wilmet W, Cordier S, et al. Nanoarchitectonics of glass coatings for near-infrared shielding: From solid-state cluster-based niobium chlorides to the shaping of nanocomposite films. *ACS Appl. Mater. Interfaces*. 2022;14:21116–21130
107) Lebastard C, Wilmet M, Cordier S, et al. High performance {Nb_5TaX_{12}}@PVP (X = Cl, Br) cluster-based nanocomposites coatings for solar glazing applications. *Sci. Technol. Adv. Mater.* 2022; 10.1080/14686996.2022.2105659
108) Choi J, Nguyen D, Gi E, et al. A highly efficient and transparent luminescent solar concentrator based on a nanosized metal cluster luminophore anchored on polymers. *J. Mater. Chem. C*. 2022;10:4402–4410.
109) Barras A Das MR, Devarapalli RR, et al. One-pot synthesis of gold nanoparticle/molybdenum cluster/graphene oxide nanocomposite and its photocatalytic activity. *Appl. Catal. B.* 2013;130-131:270–276.
110) Kumar S, Khatri OP, Cordier S, et al. Graphene oxide supported molybdenum cluster: First heterogenized homogeneous catalyst for the synthesis of dimethylcarbonate from CO_2 and methanol. *Chem. - Eur. J.* 2015;21(8):3488–3494.
111) Kumar P, Naumov NG, Boukherroub R, et al; Octahedral rhenium $K_4[Re_6S_8(CN)_6]$ and $Cu(OH)_2$ cluster modified TiO_2 for the photoreduction of CO_2

under visible light irradiation. *Appl. Catalysis A: General.* 2015;499:32–38.
112) Kumar P, Mungse HP, Cordier S, et al. Hexamolybdenum clusters supported on graphene oxide: Visible-light induced photocatalytic reduction of carbon dioxide into methanol. *Carbon.* 2015;94:91–100.
113) Bůžek D, Hynek J, Kučeráková M, et al. Mo^{II} cluster complex-based coordination polymer as an efficient heterogeneous catalyst in the Suzuki–Miyaura coupling reaction. *Eur. J. Inorg. Chem.* 2016;28:4668–4673.
114) Arnau del Valle C, Felip-León C, Angulo-Pachón CA, et al. photoactive hexanuclear molybdenum nanoclusters embedded in molecular organogels. *Inorg. Chem.* 2019;58:8900–8905.
115) Feliz M, Atienzar P, Amela-Cortés M, et al. Supramolecular anchoring of octahedral molybdenum clusters onto graphene and their synergies in photocatalytic water reduction. Inorg. Chem. 2019;58(22):15443–15454.
116) Nguyen TKN, Grasset F, Cordier S, et al. Preparation and characterization of hollow silica nanocomposite functionalized with UV absorbable molybdenum cluster. *Adv. Powder Technol.* 2020;31(2):895–903.
117) Nguyen TKN, Matsui Y, Shirahata N, et al. Zn-Al layered double hydroxide-based nanocomposite functionalized with an octahedral molybdenum cluster exhibiting prominent photoactive and oxidation properties. *Appl Clay Sci.* 2020;196:105765.
118) Ivanova MN, Vorotnikov YA, Plotnikova EE, et al. Hexamolybdenum clusters supported on exfoliated h-BN nanosheets for photocatalytic water purification. *Inorg. Chem.* 2020;59(9):6439–6448.
119) Puche M, García-Aboal R, Mikhaylov MA, et al. Enhanced photocatalytic activity and stability in hydrogen evolution of Mo_6 iodide clusters supported on graphene oxide. *Nanomaterials.* 2020;10(7):1259.
120) Aubert T, Cabello-Hurtado F, Esnault MA, et al. Extended investigations on luminescent $Cs_2[Mo_6Br_{14}]@SiO_2$ nanoparticles: physico-structural characterizations and toxicity studies. *J. Phys. Chem. C.* 2013;117(39):20154–20163.
121) Aubert T, Nerambourg N, Neaime C, et al. Multi-functional silica nanoparticles based on metal atom clusters: from design to toxicological studies. *Key Eng. Mater.* 2014;617:179–183.
122) Vorotnikova NA, Efremova OA, Tsygankova AR, et al. Characterization and cytotoxicity studies of thiol-modified polystyrene microbeads doped with $[\{Mo_6X_8\}(NO_3)_6]^{2-}$ (X = Cl, Br, I). *Polym. Adv. Technol.* 2016;27(7):922–928.
123) Neaime C, Amela-Cortes M, Grasset F, et al. Time-gated luminescence bioimaging with new luminescent nanocolloids based on $[Mo_6I_8(C_2F_5COO)_6]^{2-}$ metal atom clusters. *Phys. Chem. Chem. Phys.* 2016;18(43):30166-30173.
124) Solovieva AO, Vorotnikov YA, Trifonova KE, et al. Cellular internalisation, bioimaging and dark and photodynamic cytotoxicity of silica nanoparticles doped by $\{Mo_6I_8\}^{4+}$ metal clusters *J. Mater. Chem. B.* 2016;4(28):4839–4846.
125) Cabello-Hurtado F, Lozano-Baena MD, Neaime C, et al. Studies on plant cell toxicity of luminescent silica nanoparticles ($Cs_2[Mo_6Br_{14}]@SiO_2$) and its constitutive components *J. Nanoparticle Res.* 2016;18:3.

126) Beltran A, Mikhailov M, Sokolov MN, et al. A photobleaching resistant polymer supported hexanuclear molybdenum iodide cluster for photocatalytic oxygenations and photodynamic inactivation of staphylococcus aureus. *J. Mater. Chem. B.* 2016;4:5975–5979.
127) Cheplakova AM, Solovieva AO, Pozmogova TN, et al. Nanosized mesoporous metal–organic framework MIL-101 as a nanocarrier for photoactive hexamolybdenum cluster compounds. *J. Inorg. Biochem.* 2017; 166:100–107.
128) Felip-León C, Arnau del Valle C, Pérez-Laguna V, et al. Superior performance of macroporous over gel type polystyrene as a support for the development of photo-bactericidal materials. *J. Mater. Chem. B*. 2017;5:6058–6064.
129) Elistratova JG, Brylev KA, Solovieva AO, et al. Supporting effect of polyethylenimine on hexarhenium hydroxo cluster complex for cellular imaging applications. *J. Photochem. Photobiol. A: Chem.* 2017;340:46–52.
130) Pellen-Mussi P, Tricot-Doleux S, Neaime C, et al. Evaluation of functional SiO_2 nanoparticles toxicity by a 3D culture model. *J. Nanosci. Nanotechnol.* 2018;18(5): 3148–3157.
131) Brandhonneur N, Hatahet T, Amela-Cortes M, et al. Molybdenum cluster loaded PLGA nanoparticles: An innovative theranostic approach for the treatment of ovarian cancer. *Eur. J. Pharm. Biopharm.* 2018;125:95–105.
132) Elistratova J, Mukhametshina A, Kholin K, et al. Interfacial uploading of luminescent hexamolybdenum cluster units onto amino-decorated silica nanoparticles as new design of nanomaterial for cellular imaging and photodynamic therapy. *J. Colloid Interface Sci.* 2019;538:387–396.
133) Vorotnikov YA, Pozmogova TN, Solovieva AO, et al. Luminescent silica mesoparticles for protein transduction. *Mater. Sci. Eng. C.* 2019 ;96 :530–538.
134) Vorotnikova NA, Alekseev AY, Vorotnikov YA, et al. Octahedral molybdenum cluster as a photoactive antimicrobial additive to a fluoroplastic. Mater. Sci. Eng. C. 2019;105:110150.
135) Vorotnikov YA, Novikova ED, Solovieva AO, et al. Single-domain antibody C7b for address delivery of nanoparticles to HER2-positive cancers. *Nanoscale.* 2020;12:21885–21894.
136) Dollo G, Boucaud Y, Amela-Cortes M, et al. PLGA nanoparticles embedding molybdenum cluster salts: Influence of chemical composition on physico-chemical properties, encapsulation efficiencies, colloidal stabilities and in vitro release. *Int. J. Pharm.* 2020;576:119025.
137) López-López N, Muñoz Resta I, de Llanos R, et al. Photodynamic inactivation of staphylococcus aureus biofilms using a hexanuclear molybdenum complex embedded in transparent polyhema hydrogels. *ACS Biomater. Sci. Eng.* 2020;6(12):6995–7003.
138) Kirakci K, Nguyen TKN, Grasset F, et al. Electrophoretically deposited layers of octahedral molybdenum cluster complexes: a promising coating for mitigation of pathogenic bacterial biofilms under blue light. *ACS Appl Mater Interfaces.* 2020;12(47):52492–52499.
139) Fedorenko S, Elistratova J, Stepanov A, et al. ROS-generation and cellular

uptake behavior of amino-silica nanoparticles arisen from their uploading by both iron-oxides and hexamolybdenum clusters. *Mater. Sci. Eng. C.* 2020;117:111305

140) Khlifi S, Taupier G, Amela-Cortes M, et al. Expanding the toolbox of octahedral molybdenum clusters and nanocomposites made thereof: evidence of two-photon absorption induced NIR emission and singlet oxygen production. *Inorg. Chem.* 2021;60(8):5446–5451.

141) Brandhonneur N, Boucaud Y, Verger A, et al. Molybdenum cluster loaded PLGA nanoparticles as efficient tools against epithelial ovarian cancer. *Int. J. Pharm.* 2021;592:120079.

142) Khazieva A, Kholin K, Nizameev I, et al. Surface modification of silica nanoparticles by hexarhenium anionic cluster complexes for pH-sensing and staining of cell nuclei. *J. Colloid Interface Sci.* 2021;594:759–769.

143) Elistratova JG, Mikhaylov MA, Sukhikh TS, et al. Anticancer potential of hexamolybdenum clusters $[\{Mo_6I_8\}(L)_6]^{2-}$ (L = $CF3COO^-$ and $C6F5COO^-$) incorporated into different nanoparticulate forms. *J. Mol. Liq.* 2021;343:117601.

144) Vorotnikova NA, Bardin VA, Vorotnikov YA, et al. Heterogeneous photoactive antimicrobial coatings based on a fluoroplastic doped with an octahedral molybdenum cluster compound. *Dalton Trans.* 2021;50:8467–8475.

145) Faizullin BA, Strelnik ID, Dayanova IR, et al. Structure impact on photodynamic therapy and cellular contrasting functions of colloids constructed from dimeric Au(I) complex and hexamolybdenum clusters. Mater. Sci. & Eng. C. 2021;128,112355.

146) Baker GL, Ghosh RN, Osborn DJ. Sol-gel encapsulated hexanuclear clusters for oxygen sensing by optical techniques. United States patent US7858380B2. 2010.

147) Ghosh RN, Askeland PA, Kramer S, et al. Optical dissolved oxygen sensor utilizing molybdenum chloride cluster phosphorescence. *Appl. Phys. Lett.* 2011;98(22): 221103.

148) Elistratova J, Mikhailov M, Burilov V, et al. Supramolecular assemblies of triblock copolymers with hexanuclear molybdenum clusters for sensing antibiotics in aqueous solutions via energy transfer. *RSC Adv.* 2014;4:27922–27930.

149) Ghosh RN, Loloee R, Askeland PA, et al. Optical sensor and sensing system for oxygen monitoring in fluids using molybdenum cluster phosphorescence. United States patent US2014/0017127A1. 2014.

150) Litvinova YM, Gayfulin YM, Kovalenko KA, et al. Multifunctional metal–organic frameworks based on redox-active rhenium octahedral clusters. *Inorg. Chem.* 2018;57:2072–2084.

151) Nguyen TKN, Dumait N, Grasset F, et al. Zn−Al layered double hydroxide film functionalized by a luminescent octahedral molybdenum cluster: ultraviolet−Visible photoconductivity response. *ACS Appl Mater Interfaces*. 2020;12:40495–40509.

152) Uchikoshi T, Nguyen TKN, Harada K, et al. Molybdenum cluster film-containing element, sensor, device, and method for measuring temperature, humidity, and light using them. Japanese patent A00486JP01. 2021

153) Nguyen TKN, Harada K, Grasset F, et al. Light-dependent ionic-electronic conduction in amorphous octahedral molybdenum cluster thin film. *NPG Asia.* 2022; 14:21.
154) Molard Y, Ledneva A, Amela-Cortes M, et al. Ionically self-assembled clustomesogen with switchable magnetic/luminescence properties containing $[Re_6Se8(CN)_6]^{n-}$ (n = 3, 4) anionic clusters. *Chem. Mater.* 2011;23:5122–5130.
155) Nerambourg N, Aubert T, Neaime C, et al. Multifunctional hybrid silica nanoparticles based on $[Mo_6Br_{14}]^{2-}$ phosphorescent nanosized clusters, magnetic γ-Fe_2O_3 and plasmonic gold nanoparticles. *J. Colloid Interface Sci.* 2014;424:132–140.
156) Lunt RR, Kuttipillai PS. Nanocluster based light emitting device. United States patent US2015/0069366A1. 2015.
157) Prévôt M, Amela-Cortes M, Manna SK, et al. Design and integration in electro-optic devices of highly efficient and robust red-nir phosphorescent nematic hybrid liquid crystals containing $[Mo_6I_8(OCOC_nF_{2n+1})_6]^{2-}$(n= 1, 2, 3) nanoclusters. *Adv. Funct. Mater.* 2015;25:4966–4975.
158) Wood SM, Prevot M, Amela-Cortes M, et al. Polarized phosphorescence of isotropic and metal-based clustomesogens dispersed into chiral nematic liquid crystalline films. *Adv. Opt. Mater.* 2015;3(10):1368–1372.
159) Prévôt M, Amela-Cortes M, Manna SK, et al. Electroswitchable red-NIR luminescence of ionic clustomesogen containing nematic liquid crystalline devices. *J. Mater. Chem. C. 2015;*3:5152–5161.
160) Kuttipillai PS, Zhao Y, Traverse CJ, et al. Phosphorescent nanocluster light-emitting diodes. *Adv Mater.* 2016;28(2):320–326.
161) Huby N, Bigeon J, Lagneaux Q, et al. Facile design of red-emitting waveguides using hybrid nanocomposites made of inorganic clusters dispersed in SU8 photoresist host. *Opt. Mater.* 2016;52:196–202.
162) Bigeon J, Huby N, Amela-Cortes M, et al. Efficient active waveguiding properties of Mo_6 nano-cluster-doped polymer nanotubes. *Nanotechnology.* 2016;27(25):255201.
163) Kuttipillai PS, Yang C, Chen P, et al. Enhanced electroluminescence efficiency in metal halide nanocluster based light emitting diodes through apical halide exchange. *ACS Appl. Energy Mater.* 2018;1(8):3587–3592.
164) Ferreira Molina E, Martins de Jesus NA, Paofai S, et al; When a red–NIR-emissive $Cs_2[Mo_6Br_{14}]$ interacts with an active diureasil–peo matrix: design of tunable and white-light-emitting hybrid material. *Chem. - Eur. J.* 2019;25(67):15248–15251.
165) Khlifi S, Fournier Le Ray N, Paofai S, et al. Self-erasable inkless imprinting using a dual emitting hybrid organic-inorganic material. *Mater. Today.* 2020;35:34–41.
166) Khlifi S, Bigeon J, Amela-Cortes M, et al. Poly(dimethylsiloxane) functionalized with complementary organic and inorganic emitters for the design of white emissive waveguides. *J. Mater. Chem. C.* 2021;9(22):7094–7102.

167) Ly GT, Choi J, Kim Y, et al. One-dimensional lead iodide hybrid stabilized by inorganic hexarhenium cluster cations as a new broadband emitter, *RSC Adv*. 2021;11(40):24580–24587.
168) Novikova ED, Vorotnikov YA, Nikolaev NA, et al. Synergetic effect of Mo_6 clusters and gold nanoparticles on the photophysical properties of both components. *Chem. Eur. J.* 2021;27:2818–2825.
169) Novikova ED, Vorotnikov YA, Nikolaev NA, et al. The role of gold nanoparticles' aspect ratio in plasmon-enhanced luminescence and the singlet oxygen generation rate of Mo_6 clusters. *Chem. Commun.* 2021;57:7770–7773.
170) Sciortino F, Cretu O, Karanikolas V, et al. Surface plasmon tunability of core-shell Au@Mo_6 nanoparticles by shell thickness modification. *J. Phys. Chem. Let.* 2022;13:2150−2157.
171) Aubert T, Nerambourg N, Saito N, et al. Tunable Visible emission of luminescent hybrid nanoparticles incorporating two complementary luminophores: ZnO nanocrystals and $[Mo_6Br_{14}]^{2-}$ nanosized cluster units. *Part. Part. Syst. Charact.* 2013;30(1):90-95.
172) Molard Y, Dorson F, Brylev KA, et al. Red-NIR luminescent hybrid poly(methyl methacrylate) containing covalently linked octahedral rhenium metallic clusters. *Chem. - Eur. J.* 2010;16(19):5613–5619
173) Molard Y, Dorson F, Cîrcu V, et al. Clustomesogens: Liquid crystal materials containing transition‐metal clusters. *Angew. Chem. Int. Ed.*, 2010;49:3351–3355.
174) Mocanu AS, Amela-Cortes M, Molard Y, et al. Liquid crystal properties resulting from synergetic effects between non-mesogenic organic molecules and a one nanometre sized octahedral transition metal cluster. *Chem. Commun.* 2011;47:2056–2058.
175) Thangaraju D, Gredin P, Mortier M, et al. Enhanced infrared emission characteristics of multifunctional β-$NaYF_4$:Yb:Er@$NaYF_4$@$Cs_2[Mo_6Br_{14}]$@SiO_2 core-shell nanostructures. ISIEM 2013 Conferences, 2013.
176) Molard Y, Labbé C, Cardin J, et al. Sensitization of Er^{3+} infrared photoluminescence embedded in a hybrid organic‐inorganic copolymer containing octahedral molybdenum clusters. *Adv. Funct. Mater.* 2013;23(38):4821–4825.
177) Golubeva ND, Adamenko OA, Boiko GN, et al. Synthesis, structure, and properties of new hybrid nanocomposites containing the $[Mo_6(\mu_3\text{-}Cl)_8]^{4+}$. *Inorg. Mater*. 2014;0(3):306–313.
178) Amela-Cortes M, Garreau A, Cordier S, et al. Deep red luminescent hybrid copolymer materials with high transition metal cluster content. *J. Mater. Chem. C.* 2014;2(8):1545–1552.
179) Amela-Cortes M, Cordier S, Naumov NG, et al. Hexacyano octahedral metallic clusters as versatile building blocks in the design of extended polymeric framework and clustomesogens. *J. Mater. Chem. C.* 2014;2:9813–9823.
180) Efremova OA, Brylev KA, Kozlova O, et al. Polymerisable octahedral rhenium cluster complexes as precursors for photo/electroluminescent polymers. *J. Mater. Chem. C.* 2014;2(40):8630–8638.

181) Efremova OA, Shestopalov MA, Chirtsova NA, et al. A highly emissive inorganic hexamolybdenum cluster complex as a handy precursor for the preparation of new luminescent materials. *Dalton Trans.* 2014;43:6021–6025.
182) Neaime C, Nerambourg N, Aubert T, et al. Magnetic and fluorescent hybrid silica nanoparticles based on the co-encapsulation of γ-Fe_2O_3 nanocristals and $[Mo_6Br_{14}]^{2-}$ luminescent nanosized clusters by water-in-oil microemulsion. *Key Eng. Mater.* 2014; 617:174–178.
183) Amela-Cortes M, Paofai S, Cordier S, et al. Tuned red NIR phosphorescence of polyurethane hybrid composites embedding metallic nanoclusters for oxygen sensing *Chem. Commun.* 2015;51(38):8177–8180.
184) Cîrcu V, Molard Y, Amela-Cortes M, et al. From mesomorphic phosphine oxide to clustomesogens containing molybdenum and tungsten octahedral cluster cores *Angewandte Chem. Int. Ed.* 2015 ;54:10921.
185) Nayak SK, Amela-Cortes M, Roiland C, et al. From metallic cluster-based ceramics to nematic hybrid liquid crystals: a double supramolecular approach. *Chem. Commun.* 2015;51:3774–3777.
186) El Osta R, Demont A, Audebrand N, et al. Supramolecular frameworks built up from red-phosphorescent trans-Re_6 cluster building blocks: one pot synthesis, crystal structures, and DFT investigations. *Z. Anorg. Allg. Chem.*, 2015;641(6):1156–1163.
187) Robin M, Kuai W, Amela-Cortes M, et al. Epoxy based ink as versatile material for inkjet-printed devices. *ACS Appl. Mater. Interfaces*. 2015;7(39):21975–21984
188) Efremova OA, Brylev KA, Vorotnikov YA, et al. Photoluminescent materials based on PMMA and a highly-emissive octahedral molybdenum metal cluster complex. *J. Mater. Chem. C.* 2016;4(3):497–503.
189) Nayak SK, Amela-Cortes M, Neidhardt MM, et al. Phosphorescent columnar hybrid materials containing polyionic inorganic nanoclusters. *Chem. Commun.* 2016 ;52:3127–3130.
190) Amela-Cortes M, Molard Y, Paofai S, et al. Versatility of the ionic assembling method to design highly luminescent PMMA nanocomposites containing $[M_6Q^i_8L^a_6]_{n-}$ octahedral nano-building blocks. *Dalton Trans.* 2016;45:237–245.
191) Vorotnikov YA, Efremova OA, Vorotnikova NA, et al. On the synthesis and characterisation of luminescent hybrid particles: Mo_6 metal cluster complex/SiO_2. *RSC Adv.* 2016;6(49):43367–43375.
192) Truong TG, Dierre B, Grasset F, et al. Visible tunable lighting system based on polymer composites embedding ZnO and metallic clusters: from colloids to thin films. *Sci. Technol. Adv. Mater.* 2016;17:443-453.
193) Nguyen TKN, Grasset F, Dierre B, et al. Fabrication of transparent thin film of octahedral molybdenum metal clusters by electrophoretic deposition. *ECS J. Solid State Sci. Technol.* 2016;5:R178–R186.
194) Svezhentseva EV, Solovieva AO, Vorotnikov YA, et al. Water-soluble hybrid materials based on $\{Mo_6X_8\}^{4+}$ (X = Cl, Br, I) cluster complexes and sodium

polystyrene sulfonate. *New J. Chem.* 2017;41:1670–1676.
195) Vorotnikova NA, Edeleva MV, Kurskaya OG, et al. One-pot Synthesis of $\{Mo_6I_8\}^{4+}$-doped Polystyrene Microspheres via a Free Radical Dispersion Copolymerisation Reaction. *Polym. Int.* 2017;66(12):1906–1912.
196) Evtushok DV, Vorotnikova NA, Logvinenko VA, et al. Luminescent coordination polymers based on Ca^{2+} and octahedral cluster anions $[\{M_6Cl^i_8\}Cl^a_6]^{2-}$ (M = Mo, W): synthesis and thermal stability studies. *New J. Chem.* 2017;41(24):14855–14861.
197) Moussawi MA, Leclerc-Laronze N, Floquet S, et al. Polyoxometalate, cationic cluster, and γ-cyclodextrin: from primary interactions to supramolecular hybrid materials. *J. Am. Chem. Soc.* 2017;139(36):12793–12803.
198) Nguyen TKN, Dierre B, Grasset F, et al. Formation mechanism of transparent Mo_6 metal atom cluster film prepared by electrophoretic deposition. *J. Electrochem. Soc.* 2017;164:D412–D418.
199) Chen W, Wilmet M, Truong TG, et al. Embedding hexanuclear tantalum bromide cluster $\{Ta_6Br_{12}\}$ into SiO_2 nanoparticles by reverse microemulsion method. *Heliyon.* 2018;4(6):e00654.
200) Ivanov AA, Falaise C, Abramov PA, et al. Host-guest binding hierarchy within redox- and luminescence-responsive supramolecular self-assembly based on chalcogenide clusters and γ-cyclodextrin. *Chem.- A Eur. J.* 2018;24(51):13467–13478.
201) Camerel F, Kinloch F, Jeannin O, et al. Ionic columnar clustomesogens: associations between anionic hexanuclear rhenium clusters and liquid crystalline triphenylene tethered imidazoliums. *Dalton Trans.*, 2018;47:10884–10896.
202) Gandubert A, Amela-Cortes M, Nayak SK, et al. Tailoring the self-assembling abilities of functional hybrid nanomaterials: from rod-like to disk-like clustomesogens based on a luminescent $\{Mo_6Br_8\}^{4+}$ inorganic cluster core. *J. Mater. Chem. C.* 2018;6:2556–2564.
203) Guy K, Ehni P, Paofai S, et al. Lord of the Crowns: A new precious in the kingdom of clustomesogens. *Angewandte Chem.* 2018;130:11866–11696.
204) Abramov PA, Ivanov AA, Shestopalov MA, et al. Supramolecular adduct of γ-Cyclodextrin and $[\{Re_6Q_8\}(H_2O)_6]^{2+}$ (Q=S, Se). *J. Clust. Sci.* 2018;29(1):9–13.
205) Robin M, Dumait N, Amela-Cortes M, et al. Direct Integration of red-NIR emissive ceramic-like $A_nM_6X^i_8X^a_6$ metal cluster salts in organic copolymers using supramolecular interactions. *Chem. - A Eur. J.* 2018 ;24(19):4825–4829.
206) Volostnykh MV, Mikhaylov MA, Sinelshchikova AA, et al. Hybrid organic–inorganic supramolecular systems based on a pyridine end-decorated molybdenum(II) halide cluster and zinc(ii) porphyrinate. *Dalton Trans.* 2019;48:1835–1842.
207) Nguyen TKN, Dubernet M, Matsui Y, et al. Transparent functional nanocomposite films based on octahedral metal clusters: synthesis by electrophoretic deposition process and characterization. *R. Soc. Open Sci.* 2019;6:181647.
208) Litvinova YM, Gayfulin YM, Brylev KA, et al. Metal–organic frameworks

with solvent-free lanthanide coordination environments: synthesis from aqueous ethanol solutions. *CrystEngComm*, 2020;22:7935–7943.
209) Falaise C, Ivanov AA, Molard Y, et al. From supramolecular to solid-state chemistry: crystal engineering of luminescent materials by trapping molecular clusters in an aluminium-based host matrix. *Mater. Horizons.* 2020;7:2399–2406.
210) Ivanov AA, Falaise C, Shmakova AA, et al. Cyclodextrin-assisted hierarchical aggregation of Dawson-type polyoxometalate in the presence of $\{Re_6Se_8\}$ based clusters. *Inorg. Chem.* 2020;59(16):11396–11406.
211) Hummel T, Dutczak D, Alekseev AY, et al. Photodynamic properties of tungsten iodide clusters incorporated into silicone: $A_2[M_6I_8L_6]$@silicone. *RSC Adv.* 2020;10(37):22257–22263.
212) Falaise C, Khlifi S, Bauduin P, et al. "Host in host" supramolecular core–shell type systems based on giant ring-shaped polyoxometalates. *Angewandte Chem. Int. Ed.* 2021;60(25):14146–14153.
213) Audebrand N, Demont A, El Osta R, et al. Supramolecular frameworks based on rhenium clusters using the synthons approach. *Molecules.* 2021;26(9):2662.
214) Konovalov DI, Ivanov AA, Vorotnikov YA, et al. Self-assembled microporous M-HOFs based on an octahedral rhenium cluster with benzimidazole. *Inorg. Chem.* 2021;60(19):14687–14696.
215) Litvinova YM; Gayfulin YM, Samsonenko DG, et al. Coordination polymers based on rhenium octahedral chalcocyanide cluster $[Re_6Se_8(CN)_6]^{4-}$ and lanthanide ions solvated with dimethylformamide. *Inorg. Chim. Acta*. 2021;528:120597
216) Liang Y, Sokolov MN, Mikhaylov MA, et al. A 3D electropolymerized thin film based on an isoporphyrin and on a pyridine end-decorated molybdenum(II) halide cluster: Photoelectrochemical and impedance properties. *Electrochim. Acta.* 2021;388:138493.
217) Nguyen TKN, Bourgès C, Naka T, et al. Synthesis of novel hexamolybdenum cluster-functionalized copper hydroxide nanocomposites and its catalytic activity for organic molecule degradation. *Sci. Technol. Adv. Mater.* 2021;22(1):758–771.
218) Zhang MQ, Grasset F, Dumait N, et al. Effect of sulfurization process on octahedral molybdenum cluster from Mo_6 cluster to MoS_2 nanosheet. Key Eng. Mater. 2021;904:334–338.
219) Ebert M, Carrasco I, Dumait N, et al. Joint venture of metal cluster and amphiphilic cationic minidendron resulting in near infrared emissive lamellar ionic liquid crystals. *Chem. – A Eur. J.* 2022;28:e202103446.
220) Sciortino F, Cretu O, Karanikolas V, et al. surface plasmon tunability of core-shell Au@Mo_6 nanoparticles by shell thickness modification. *J. Phys. Chem. Let.* 2022;13:2150−2157
221) José-Yacamán M, Rendón L, Arenas L, et al. Maya Blue Paint: An Ancient Nanostructured Material. *Science* 1996;273(5272):223–225.
222) Wang J, Hussain Shah Z, Zhang S, et al. Silica-based nanocomposites via

reverse microemulsions: classifications, preparations, and applications, Nanoscale 2014;6(9):4418–4437.
223) Ow H, Larson DR, Srivastava M, et al. Bright and stable core-shell fluorescent silica nanoparticles. *Nano Lett.* 2005;5(1): 113-117.
224) Vivero-Escoto JL, Huxford-Phillips RC, Lin W. Silica-based nanoprobes for biomedical imaging and theranostic applications. *Chem. Soc. Rev.* 2012;41:2673–2685.
225) Caltagirone C, Bettoschi A, Garau A, et al. Silica-based nanoparticles: a versatile tool for the development of efficient imaging agents. *Chem. Soc. Rev.* 2015;44:4645–4671.
226) Singh P, Srivastava S, Kumar Singh S. Nanosilica: Recent progress in synthesis, functionalization, biocompatibility, and biomedical applications. *ACS Biomater. Sci. Eng.* 2019;5:4882−4898.
227) Li Z, Mu Y, Peng C, et al. Understanding the mechanisms of silica nanoparticles for nanomedicine. *WIREs Nanomed. Nanobiotechnol.* 2021;13:e1658.
228) Lowe J, Stock D, Jap B, et al. Crystal structure of the 20S proteasome from the archaeon T. acidophilum at 3.4 A resolution. *Science*. 1995;268:533–539.
229) Cramer P, Bushnell DA, Fu J, et al. Architecture of RNA polymerase II and implications for the transcription mechanism. *Science*. 2000;288:640–649.
230) Ferreira KN, Iverson TM, Maghlaoui K, et al. Architecture of the photosynthetic oxygen-evolving center. *Science*. 2004;43:1831–1839.
231) Mullan BF, Madsen MT, Messerle L, et al. X-ray attenuation coefficients of high-atomic-number, hexanuclear transition metal cluster compounds: a new paradigm for radiographic contrast agents. *Acad. Radiol.* 2000;7:254–259.
232) Grasset F, Labhsetwar N, Li D, et al. Synthesis and magnetic characterization of zinc ferrite nanoparticles with different environments: Powder, colloidal solution, and zinc ferrite-silica core-shell nanoparticles. *Langmuir*. 2002;18:8209–8216.
233) El Mendili Y, Bardeau JF, Randrianantoandro N, et al. Structural behavior of laser-irradiated γ-Fe_2O_3 nanocrystals dispersed in porous silica matrix : γ-Fe_2O_3 to α-Fe_2O_3 phase transition and formation of ε-Fe_2O_3. *Sci. Technol. Adv. Mater.* 2016;17(1):597–609.
234) Zhang KY, Yu Q, Wei H, et al. Long-lived emissive probes for time-resolved photoluminescence bioimaging and biosensing. *Chem. Rev.* 2018;118:1770−1839.
235) Liu P, Mu X, Zhang XD, et al. The near-infrared-II fluorophores and advanced microscopy technologies development and application in bioimaging. *Bioconjugate Chem.* 2020;31:260−275.
236) Stöber W, Fink A, Bohn E. Controlled growth of monodisperse silica spheres in the micron size range. *J. Colloid Interface Sci.* 1968;26:62–69.
237) de la Torre C, Gavara R, García-Fernández A, et al. Enhancement of photoactivity and cellular uptake of $(Bu_4N)_2[Mo_6I_8(CH_3COO)_6]$ complex by loading on porous MCM-41 support. Photodynamic studies as an anticancer agent. *Biomater. Adv.* 2022:213057.

238) Chubar N, Gilmour R, Gerda V, et al. Layered double hydroxides as the next generation inorganic anion exchangers: Synthetic methods versus applicability. *Adv. Colloid Inter. Sci.* 2017;245:62–80.
239) Wu MJ, Wu JZ, Zhang J, et al. A review on fabricating heterostructures from layered double hydroxides for enhanced photocatalytic activities. *Catal. Sci. Technol.* 2018;8:1207–1228.
240) Rocha MG, Nakagaki S, Ucoski GM, et al. Comparison between catalytic activities of two zinc layered hydroxide salts in brilliant green organic dye bleaching. J Colloid Inter Sci. 2019;541:425–433.
241) Yang Z, Zhang C, Zeng G, et al. Design and engineering of layered double hydroxide based catalysts for water depollution by advanced oxidation processes: a review. *J. Mater. Chem. A*. 2020;8:4141–4173
242) Zobir SAM, Ali A, Adzmi F, et al. A review on nanopesticides for plant protection synthesized using the supramolecular chemistry of layered hydroxide hosts. *Biology.* 2021;10(11):1077.
243) Ahmed AAA, Talib ZA, Hussein MZ. Influence of sodium dodecyl sulfate concentration on the photocatalytic activity and dielectric properties of intercalated sodium dodecyl sulfate into Zn–Cd–Al layered double hydroxide. *Mater. Res. Bull.* 2015;62:122–131.
244) https://www.mordorintelligence.com/industry-reports/thin-film-material-market
245) Corni I, Ryan MP, Boccaccini AR, Electrophoretic deposition: From traditional ceramics to nanotechnology. *J. Eur. Ceram. Soc.* 2008;28:1353–1367.
246) Y. Sakka, T. Uchikoshi, Forming and microstructure control of ceramics by electrophoretic deposition. KONA Powder Part. J. 2010;28:74–90.
247) Pascall AJ, Qian F, Wang G, et al. Light-directed electrophoretic deposition: a new additive manufacturing technique for arbitrarily patterned 3D composites. *Adv. Mater.* 2014;26:2252–2256.
248) Hu S, Li W, Finklea F et al. A review of electrophoretic deposition of metal oxides and its application in solid oxide fuel cells. *Adv. Colloid Interface Sci.* 2020;276:102102.
249) Rehman MAU, Chen Q, Braem A, et al. Electrophoretic deposition of carbon nanotubes: recent progress and remaining challenges. *Int. Mater. Rev.* 2021;66(8):533–562.
250) Hadzhieva Z, Boccaccini AR. Recent developments in electrophoretic deposition (EPD) of antibacterial coatings for biomedical applications - A review. *Curr. Opin. Biomed. Eng.* 2022;21:100367.
251) Kreuer K D, Rabenau A, Weppner W, Vehicle Mechanism, A New Model for the Interpretation of the Conductivity of Fast Proton Conductors. *Angew. Chem. Int. Ed. Engl.* 1982;21:208-209.
252) Kim GY, Senocrate A, Yang TY, et al. Large tunable photo effect on ion conduction in halide perovskites and implications for photodecomposition. *Nat. Mater.* 2018;17:445–449.
253) Bisri S Z, Piliego C, Gao J, et al. Outlook and Emerging Semiconducting

Materials for Ambipolar Transistors. Adv. Mater. 2014;26:1176−1199.
254) Chen L, Léger Y, Loget G, et al. Epitaxial III–V/Si vertical heterostructures with hybrid 2D-semimetal/semiconductor ambipolar and photoactive properties. *Adv. Sci.* 2022;9:2101661
255) Jeon CW, Lee SS, Park I.K, Flexible Visible-Blind Ultraviolet Photodetectors Based on znal- Layered Double Hydroxide Nanosheet Scroll. *ACS Appl. Mater. Interfaces*. 2019;11:35138−35145.
256) Wang X, Ning X, Shao Q, et al. ZnFeAl-layered double hydroxides/tio$_2$ composites as photoanodes for photocathodic protection of 304 stainless steel. *Sci. Rep.* 2018;8:4116-4124.
257) Ding P, Luo F, Wang P, et al. Photo-induced charge kinetic acceleration in ultrathin layered double hydroxide nanosheets boosts the oxygen evolution reaction. *J. Mater. Chem. A*. 2020;8:1105–1112.
258) Kirakci K, Fejfarová K, Martinčík J, et al. Tetranuclear copper(I) iodide complexes: A new class of X-ray phosphors. *Inorg. Chem.* 2017;56:4609–4614.
259) Thefioux Y, Cordier M, Massuyeau F, et al. Polymorphic copper iodide anions: Luminescence thermochromism and mechanochromism of $(PPh_4)_2[Cu_2I_4]$. *Inorg. Chem.* 2020;59(8):5768–5780.
260) Perruchas S. Molecular copper iodide clusters: a distinguishing family of mechanochromic luminescent compounds. *Dalton Trans.* 2021;50(35):12031–12044.
261) Zheng HW, Yang DD, Liang QF, et al. A diamond-like cuprous coordination polymer based on the $[Cu_8I_6]^{2+}$ cluster with multistimuli-responsive luminescence and iodine adsorption behaviour. *J. Mater. Chem. C.* 2022;10:3901–3907.
262) Guthrie DH, Corbett JD. Two zirconium iodide clusters. Hexazirconium dodecaiodide (Zr_6I_{12}) and cesium hexazirconium tetradecaiodide ($CsZr_6I_{14}$). *Inorg. Chem.*1982;21:3290–3295.
263) Xue ZZ, Meng XD, Li XY, et al. Luminescent thermochromism and white-light emission of a 3D $[Ag_4Br_6]$ cluster-based coordination framework with both Adamantane-like node and linker. *Inorg. Chem.* 2021;60(7):4375–4379.
264) Jäger MOJ, Morooka EV, Federici Canova F, et al. Machine learning hydrogen adsorption on nanoclusters through structural descriptors. NPJ Comput. Mater. 2018;4:37.
265) Zeni C, Rossi K, Glielmo A, et al., Building machine learning force fields for nanoclusters. J. Chem. Phys. 2018;148:241739.
266) Li J, Chen T, Lim K, et al. Deep learning accelerated gold nanocluster synthesis. Adv. Intell. Syst. 2019;1:1900029.
267) Wu Z, Yao Q, Zang S, et al. Directed self-assembly of ultrasmall metal nanoclusters. ACS Mater. Lett. 2019;1:237−248.
268) N Seriani. An ab-initio study of clusters as building blocks for crystals: from Prussian blue analogues to hybrid perovskites. Phys. Status Solidi B. 2022; 10.1002/pssb.202200045.
269) Guy K, Tessier F, Kaper H, et al. Original synthesis of molybdenum nitrides

using metal cluster compounds as precursors for heterogeneous catalysis applications. Chem. Mater. 2020;32(14):6026–6034.
270) Guy K. « Synthèse de carbures et de nitrures d'éléments de transition à partir de clusters métalliques : applications en catalyse hétérogène », http://www.theses.fr/2020REN1S090, Thesis Rennes 1 Univ. 2020.
271) Zhang M, Grasset F, Dumait N, et al. Effect of sulfurization process on octahedral molybdenum cluster: From Mo_6 cluster to MoS_2 nanosheet. Key Eng. Mater. 2021;904:334–338.
272) Higashino S, Miyake M, Fujii H, et al. Electrodeposition of Al-W alloy films in a 1-ethyl-3-methyl-imidazolium chloride-$AlCl_3$ ionic liquid containing W_6Cl_{12}. J. Electrochem. Soc. 2017;164(4):D120–D125.
273) Higashino S, Takeuchi Y, Miyake M, et al. Tungsten(II) chloride hydrates with high solubility in chloroaluminate ionic liquids for the electrodeposition of Al–W alloy films. J. Electroanal. Chem. 2022;912:116238.

Figure captions

Figure 1: Schematic representation of $[\{M_6L^i_{12}\}L^a_6]^{n-/+}$ (M = Nb, Ta) and $[\{M_6L^i_8\}L^a_6]^{n-/+}$ (M = Mo, W, Re) molecular cluster units. Apical ligands (L^a) and inner ligands (L^i).

Figure 2: The illustration of the applications of $[\{Mo_6L^i_8\}^a_6]^{n-/+}$ and $[\{Ta_6L^i_{12}\}^a_6]^{n-/+}$ molecular cluster units.

Figure 3: a) Optical microscopy image of $[\{Mo_6X^i_8\}X^a_6]@SiO_2$ (X = Cl, Br, I) nanocomposites (powder between two plates of glass under irradiation at λ_{exc} = 546 nm). b) Scanning electron microscope (SEM) images of $[\{Mo_6X^i_8\}X^a_6]@SiO_2$ 0D homogeneous nanocomposites. c) Z-contrast high-angle annular dark field scanning transmission electron microscopy (HAADF-STEM) mode image of two adjacent $[\{Mo_6X^i_8\}X^a_6]@SiO_2$ nanoparticles. Adapted from 68 with permission from Wiley.

Figure 4: Multifunctional nanoparticles with complex architectures. Adapted from 32 with permission from Springer.

Figure 5. Optical microscope images using λ_{exc} = 405 nm of dispersed nanoparticles under a magnetic field (1.5 T) showing the growth of a nanoparticles layer along the wall of a cell as a function of time. Adapted from 86 with permission from the Royal Society of Chemistry.

Figure 6. High resolution transmission electron microscopy (HRTEM) images of (a) 6 nm, (b) 10.5 nm, (c) 15 nm (scale bar = 20 nm) γFe_2O_3 nanoparticles and the corresponding d, e and f $[[\{Mo_6X^i_8\}X^a_6]\text{-}\gamma Fe_2O_3]@SiO_2$ 0D nanocomposites (scale bar = 100 nm). g) TEM image of $[[\{Mo_6X^i_8\}X^a_6]\text{-}\gamma Fe_2O_3]@SiO_2@Au$. h) zoom. Adapted from 155 with permission from Elsevier.

Figure 7. Upper: (a) Photos of silica nanoparticles in aqueous solution (1), silica nanoparticles in the cluster solutions (2) and assembled silica nanoparticles with clusters (3) before and after irradiation; (b) Schematic representation of self-assembly of the clusters complexes on silica surface; (c) TEM images of the silica nanoparticles and SiO_2@[{$Mo_6I^i_8$}L^a_6]. Adapted from 132 with permission of Elsevier. Lower: Schematically represented synthesis of Fe_3O_4@SiO_2@[{$Mo_6I^i_8$}L^a_6] and TEM images of Fe_3O_4@SiO_2 (A) and Fe_3O_4@SiO_2@[{$Mo_6I^i_8$}L^a_6] (B). Adapted from 139 with permission from Elsevier.

Figure 8. Upper: (a) Sketch of the vacuum impregnation process (VIP) and the possible movement of the air and the nanoclusters (b) STEM image of [{$Mo_6I^i_8$}$(C_2F_5COO)^a_6$]@HSNs and the overlapped EDX mapping image of the Mo element on the HSNs. (c) The UV-Vis reflectance spectra of: HSNs (black), HSNs mixed with [{$Mo_6I^i_8$}$(C_2F_5COO)^a_6]^{2-}$ without the VIP (red dot), [{$Mo_6I^i_8$}$Cl)^a_6$]@HSNs (blue) and [{$Mo_6I^i_8$}$(C_2F_5COO)^a_6$]@HSNs with the VIP (red line). Adapted from 116 with permission from Elsevier.

Figure 9. A) Powder-XRD patterns of LDH-1, Mo_6@LDH-1, LDH-2, Mo_6@LDH-2 with the indications of the planes of 003 (■), 006 (●), 009 (▲) and the lozenge symbol (♦) assigned for the ZnO phase. (B) Schematic of the process to fabricate the LDH and designed structure of its nanocomposite. Adapted from 117 with permission from Elsevier.

Figure 10. a) The schematic illustration of the [{$Mo_6X^i_8$}$X^a_6]^{2-}$ cluster unit (MC) and of the preparation of the Mo_6@CHN nanocomposites (images inside the circles are true photos of powders). b) Schematic of the interaction between the two components of the nanocomposite and the results of catalytic study in presence of H_2O_2. All the reactions were performed for 2 h in the dark. Adapted from 217 with permission from Taylor and Francis.

Figure 11. (a) SEM image of the surface of the Mo_6 film deposited from MEK, photos of the films deposited from (left to right) water, ethanol, 1-propanol, acetone, and MEK solutions at 15 V for 20 s and from acetylacetone solution at 50 V for 40 s (upper), respectively. Image of the luminescence of the cluster thin films irradiated at 324 nm wavelength (under). (b) Emission spectra excited at 370 nm of ITO glass, Cs_2[{$Mo_6Br^i_8$}Br^a_6] compound, Mo_6 films. Adapted from 193 with permission from ECS.

Figure 12. a) TEM image of the spherical Mo_6 cluster nanoparticles included in the Mo_6 film. The XPS spectra of (b) Cs 3d, (c) Mo 3d and (d) Br 3d region. e) SEM image of the cross-section of the Mo_6 film. f) XRF analysis versus deposited time. g) Schematic representation of the multilayered structure of the Mo_6 cluster thin film. Adapted from 198 with permission from ECS.

Figure 13. (a) Conduction properties of amorphous octahedral molybdenum cluster thin film. **(b)** Temperature dependences of conductivity for the cluster film due to differences in humidity. **(c)** Schematic illustration of octahedral molybdenum cluster in the film and structures postulated for the cluster films in high and low humidities. Adapted from 153

with permission from Springer Nature.

Figure 14. Comparison of the optical properties between (a) CMI@TiO_2@FTO and (b) films CMI@NiO@FTO prepared by EPD at 20 V and 15 V for 30 s respectively or soaking method (for 48h) from a CMI solution at 17 mM in acetone. (c) SEM image of a cross-section a CMI@NiO@FTO photoelectrode obtained at 10 V for 30 s and d) EDS analyses on the mesoporous NiO/CMI layer. Comparison of photoresponses in the dark (dash lines) and under$AM_{1.5}$ illumination (1000 $W.m^{-2}$, solid line) of photovoltaic cells prepared from (e) CMI@TiO_2@FTO and (f) CMI@NiO@FTO photoelectrodes colored by soaking method or by EPD during 30 s at 20 and 15 V respectively. The used electrolytes were the I^-/I_3^- and the cobalt complex CMI@TiO_2@FTO and CMI@NiO@FTO photoelectrodes respectively. Reproduced from 99 with permission from Elsevier.

Figure 15. (a) Nyquist plots of the electrochemical circuit in the dark and under illumination at OCP and the equivalent circuit used to fit them. (b) Mott–Schottky plots for the MC film deposited on FTO, the FTO substrate, and the $Cs_2[\{Mo_6I_8^i\}I_6^a]$ dense pellet depicted vs RHE by using the formulae $V_{fb}(RHE) = V_{fb}(Ag/AgCl) + 0.059\ pH + V_{Ag/AgCl}(RHE)$. (c) MC-based all-solid solar Cell, (d) I(V) measurements in the dark and under AM1.5 Illumination, (e) energy levels of each layer on an absolute scale with respect to vacuum. Adapted with permission from 104. Copyright 2022 American Chemical Society.

Figure 16. (a) Schematic representation of complexes $[Mo_6I_8(OPOPh_2)_6]^{2-}$ (1) and $[Mo_6I_8(OCOC_4H_8PPh_3)_6]^{4+}$ (2). Photographs of the 1/ITO glass (b) and 2/ITO (c) glass layers under visible light, surface morphology (middle), and cross-section (right) images. Eradication of matured biofilms on 1/ITO glass (d) and 2/ITO glass (e) after exposure to 460 nm light for 1 h (18 mW cm^{-2}). Notes: *significantly different from the respective dark control; and #significantly different from *E. coli* under 460 nm light. Adapted with permission from 138. Copyright 2020 American Chemical Society.

Figure 17. Photograph and SEM images of the cross section and surface of (a) the brown-Ta_6@ITO film (25 V and 60 s); (b) the green-Ta_6@ITO film (20 V and 60 s). (c) Photographs of 1x2.5 cm substrates and (d) SEM images of green-Ta_6@PVP@ITO films on 1 x 2.5 cm substrates prepared at 30 V and 30 s. e) UV-vis-NIR transmission spectra of the ITO substrate and the green-Ta_6@PVP@ITO films on 1x2.5 cm substrates obtained at 30 V and 30 s, 60 s and 90 s. Reproduced from 96 with permission from the Royal Society of Chemistry.

Figure 18. (a) high magnification of HAADF-STEM images of ITO@Ta_6@SiO_2 NPs; (b) EDS spectrum (point mode) of ITO@Ta_6@SiO_2 NPs revealing the coexistence of Si, O, In, Sn, Ta, Br elements. (c) Optical photographs and SEM micrographs, surface morphology and cross section of ITO@Nb_6@SiO_2 based films prepared from solution concentrations equal to 0.8 g/L and deposited by EPD at 20 V for 20 s. (d) Transmission UV-Vis-NIR spectra of the ITO@Nb_6@SiO_2 NPs-based films on the ITO-coated glass by varying the

solution concentration (0.8; 1.0; and 2.5 g/L); the spectrum of the substrate is used as a reference. Reproduced from 98 with permission from the Royal Society of Chemistry.

Figure 19. (a) Photographs of the UV-Vis irradiated films, the morphology (left) and cross-section (right) images of the thin film prepared by EPD. (b) The photocurrent controlled by on-off switching procedure under the illumination by different light wavelengths of the LDH and Mo_6@LDH films measured at RH of 50% and RH of 80 % and 303 K versus the time. (c) The repeatability of the photocurrent responses of the LDH and Mo_6@LDH films versus the on-off switching time with $\lambda_{ex.}$ = 540 nm. Adapted with permission from 151. Copyright 2020 American Chemical Society.

Figure 20. (a) Sketch of the nanocomposite based on metal atom clusters $[\{M_6X^i_{12}\}X^a_6]^{4-}$. (b) UV-Vis absorption spectra of $K_4[\{M_6Cl^i_{12}\}Cl^a_6]$ (M = Nb, Ta) in water. Reproduced from 107 with permission from Taylor and Francis.

Figure 21. (a) Sketch of the PVP film preparation from $K_4[\{M_6X^i_{12}\}X^a_6]$ or $[\{M_6X^i_{12}\}X^a_2(H_2O)_4]\cdot 4H_2O$. (b) Digital microscope picture of the cross section of a $\{M_6X^i_{12}\}$@PVP nanocomposite film on a glass substrate. (c) Picture of the nanocomposite films after obtained from the $\{Nb_5TaCl^i_{12}\}^{2+}$ (VEC 16) cluster core reduced by $SnCl_2$ in PVP and after a thermal treatment (T = 50, 80 and 100°C) during 18 hours. (d) UV-Vis transmission spectra of $\{Nb_5TaCl^i_{12}\}$@PVP (VEC 16) on glass and ITO glass substrate. Reproduced from 105 and 107 with permission from MDPI and Taylor and Francis.

Ngan T. K. Nguyen

Dr. Ngan T. K. Nguyen received her Master's degree in Physical Chemistry in 2013 from University of Science, Vietnam National University Ho Chi Minh City. In 2015, she started her Ph.D. course as a junior researcher at National Institute for Materials Science (NIMS), Japan, and received her Ph.D. degree from Hokkaido University in 2018 with the research focusing on thin films and nanocomposites based on the metal atom cluster (MC) as part of the France-Japan International Research Laboratory (IRL3629 LINK). Then, she got a postdoc position at NIMS and continued to work on the "nanocomposites based on MC" project. In 2021, she won an ICYS Research Fellowship, and continues developing the

application of nanocomposites based on MC.
https://samurai.nims.go.jp/profiles/nguyen_thikimngan

Clément Lebastard

Dr. Clément Lebastard is currently a Research Fellow of the Japan Society for Promotion of Science (JSPS) at the National Institute for Materials Science (NIMS). He received a Ph.D. in Materials Science in the ISCR laboratory at Rennes University (France) in 2021. His research interests focused on the elaboration of functional nanomaterials and nanocomposites for energy related applications such as solar control and solar cells applications.

Maxence Wilmet

https://www.linkedin.com/in/maxence-wilmet-8278b191/

Noée Dumait

https://iscr.univ-rennes1.fr/noee-dumait

Adèle Renaud

After a Ph.D degree received in 2013 from the University of Nantes and postdoctoral fellowships at Arizona State University (USA) and at the University of Rennes 1, Adèle Renaud joined the team « Chimie du Solide et Matériaux » (CSM) of the Rennes Institute of Chemical Sciences (University of Rennes 1) as an associate professor in 2017. She is an expert in the preparation of functional nanostructured electrodes by solution chemistry and the characterization of opto- and photo-electronic properties via optical and electrochemical measurements.
https://iscr.univ-rennes1.fr/adele-renaud

Stéphane Cordier

https://iscr.univ-rennes1.fr/stephane-cordier

Naoki Ohashi

https://samurai.nims.go.jp/profiles/ohashi_naoki?locale=ja

Tetsuo Uchikoshi

Dr. Tetsuo Uchikoshi is a group leader and a co-director of the LINK Center at NIMS, a visiting professor at Hokkaido University and a part-time lecturer at Hosei University. He received his B.S. in metallurgical engineering (in 1986) and Ph.D. in Materials Science (in 1994) from Waseda University. He joined the National Research Institute for Metals (NRIM), the predecessor of NIMS, as a researcher. After spending years as a senior researcher, a principal researcher, and a chief researcher, he has been a group leader of the Fine Particles Engineering Group at NIMS since 2011. He worked as a visiting researcher under the guidance of Prof. P. S. Nicholson at McMaster University in Canada in 1997–1998 and a visiting professor at Kumamoto University in 2009–2012. He has held the title

of Fellow of the Ceramics Society of Japan since 2016.
https://samurai.nims.go.jp/profiles/uchikoshi_tetsuo?locale=en

Fabien Grasset

Dr. Fabien Grasset received his Ph. D. degree in 1998 from the University of Bordeaux I in the field of solid-state chemistry and material science at the ICMCB laboratory. In 2000–2001, he was a postdoc researcher at NIMS and widened his research to nanomaterials and colloidal science. After 13 years' experience as associate professor at the University of Rennes 1, he joined the CNRS as director of research in 2014. He was co-director of the IRL 3629 LINK project until 2019, a joint international laboratory between NIMS, Saint-Gobain and CNRS based at Tsukuba, Japan. He is currently working at the UMR 6226 ISCR at Rennes in the team CSM, France. Since 2006, his main research topic focused on functional nanomaterials and nanocomposites based on metal atom clusters or oxides.
https://iscr.univ-rennes1.fr/fabien-grasset

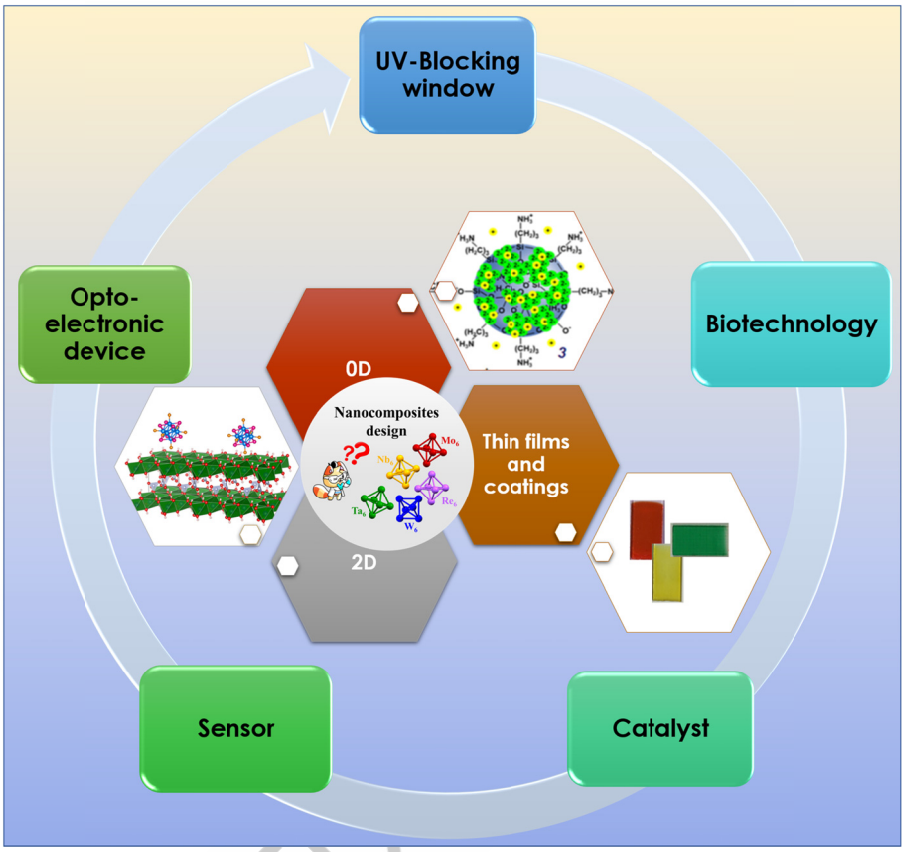

Graphical abstract